Supplementary Information for

Stable radical versus reversible σ-bond formation of (porphyrinyl)dicyanomethyl radicals

B. Adinarayana,[a] Daiki Shimizu,[a] Ko Furukawa,[b] and Atsuhiro Osuka[a]*

[a]Department of Chemistry, Graduate School of Science, Kyoto University, Sakyo-ku, Kyoto 606-8502, Japan.

[b]Center for Instrumental Analysis, Niigata University, Nishi-ku, Niigata 950-2181, Japan.

Contents

1. General Information:

Reagents and materials for the synthesis were purchased from commercial suppliers (reagent grade quality) and were used without further purification unless stated. The main precursor *meso*-bromoporphyrin **4**, *meso*,*β*,*β'*-trichloroporphyrin **5**, *meso*,*β*-dihaloporphyrins (**6**,**7**) and *β*-bromoporphyrin **16**, *β*,*β'*-dihaloporphyrins **17-19** were synthesized according to the reported procedures. [S1,2] Silica gel column chromatography was performed on Wako-gel C300 unless otherwise noted. Alumina column chromatography was performed on Sumitomo γ-Alumina KCG-1525W (Blockmann grade II). Thin-layer chromatography was carried out on aluminium sheets coated with silica gel 60 F254 (Merck 5554). High-resolution atmospheric-pressure-chemical-ionization time-of-flight mass spectrometry (HR-APCI-TOFMS) was recorded on a BRUKER micrOTOF model using positive mode. The NMR solvent $CDCl_3$ was purified by passing through a short pad of aluminum oxide prior to use. ^1H, and ^{13}C NMR spectra were recorded on a JEOL ECA600 spectrometer, and chemical shifts were reported in ppm (δ scale) relative to internal standards $CHCl_3$ (δ = 7.26 ppm for ^1H, 77.23 ppm for ^{13}C). UV/Visible absorption spectra were recorded on a Shimadzu UV-3600 spectrometer. Single crystal X-ray diffraction analysis data were collected at –180 °C with a Rigaku XtaLAB P200 by using graphite monochromated Cu-Kα radiation (λ = 1.54187 Å). The structures were solved by direct methods (SHELXT) and refined with full-matrix least square technique (SHELXL-2014/7).[S3] EPR spectra were recorded on a Bruker E500 spectrometer at Institute for Molecular Science, Okazaki, Japan. SQUID measurements were conducted by using a Quantum Design MPMS-2 system in Research Center for Low Temperature and Materials Sciences, Kyoto University. Redox potentials were measured by the cyclic voltammetry and differential pulse voltammetry method on an ALS660 electrochemical analyzer model. DFT calculations were performed using the Gaussian 09 program package at (U)B3LYP/6-311G* level.[S4]

2. Synthesis and spectral characterization:

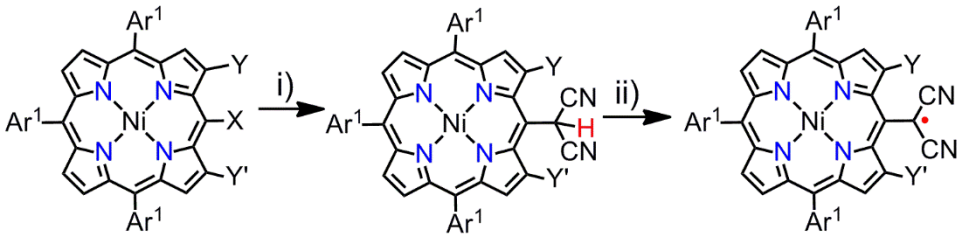

4 (X = Br, Y, Y' = H)
5 (X = Cl, Y, Y' = Cl)
6 (X = Cl, Y = Br, Y' = H)
7 (X = Cl, Y = I, Y' = H)
Ar^1 = 3,5-di-*tert*-butylphenyl

8 (Y, Y' = H, 65%)
9 (Y, Y' = Cl, 68%)
10 (Y = Br, Y' = H, 70%)
11 (Y = I, Y' = H, 69%)
Ar^1 = 3,5-di-*tert*-butylphenyl

12 (Y, Y' = H, 70%)
13 (Y, Y' = Cl, 70%)
14 (Y = Br, Y' = H, 65%)
15 (Y = I, Y' = H, 63%)
Ar^1 = 3,5-di-*tert*-butylphenyl

Scheme S1. Synthesis of **8**-**15**. (i) 10 equiv. malononitrile, 10 equiv. NaH, DMI, 60 °C, 1 h. (ii) 200 equiv. PbO_2, CH_2Cl_2, rt, 2 h.

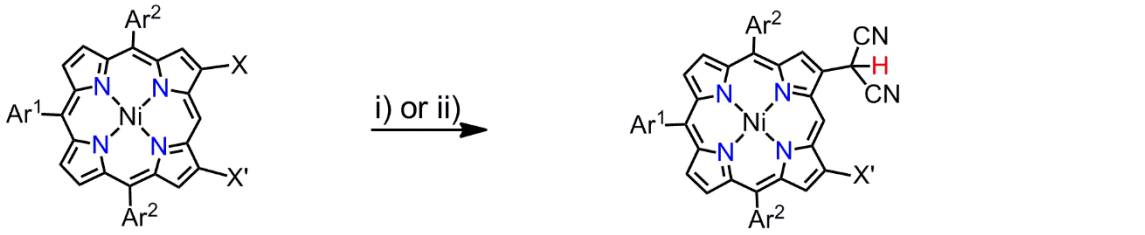

16 (X = Br, X' = H, Ar^1, Ar^2 = 3,5-di-*tert*-butylphenyl)
17 (X,X' = Br, Ar^1, Ar^2 = 3,5-di-*tert*-butylphenyl)
18 (X,X' = I, Ar^1, Ar^2 = 3,5-di-*tert*-butylphenyl)
19 (X,X' = I, Ar^1 = 3,5-di-*tert*-butylphenyl, Ar^2 = mesityl)

20 (X' = H, Ar^1, Ar^2 = 3,5-di-*tert*-butylphenyl, 74%)
21 (X' = Br, Ar^1, Ar^2 = 3,5-di-*tert*-butylphenyl, 68%)
22 (X' = I, Ar^1, Ar^2 = 3,5-di-*tert*-butylphenyl, 74%)
23 (X' = I, Ar^1 = 3,5-di-*tert*-butylphenyl, Ar^2 = mesityl, 78%)

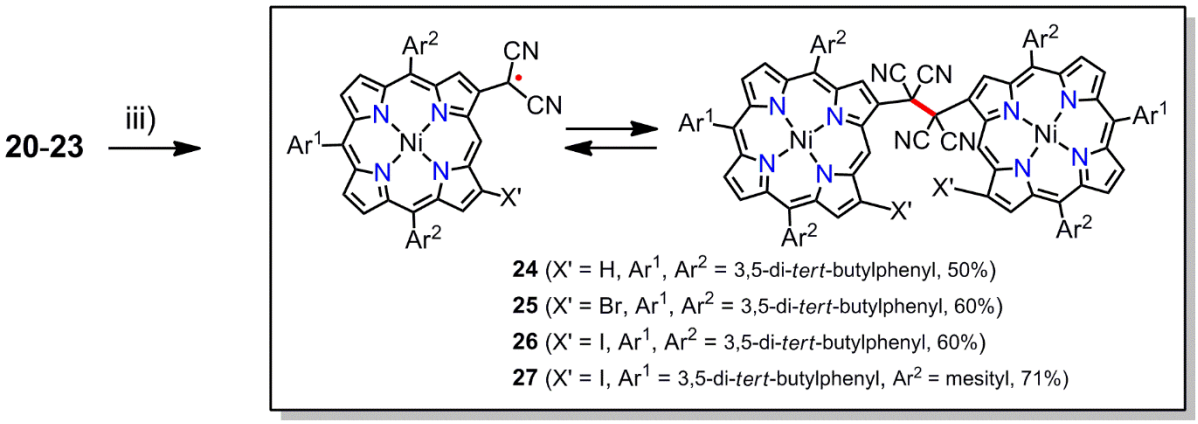

24 (X' = H, Ar^1, Ar^2 = 3,5-di-*tert*-butylphenyl, 50%)
25 (X' = Br, Ar^1, Ar^2 = 3,5-di-*tert*-butylphenyl, 60%)
26 (X' = I, Ar^1, Ar^2 = 3,5-di-*tert*-butylphenyl, 60%)
27 (X' = I, Ar^1 = 3,5-di-*tert*-butylphenyl, Ar^2 = mesityl, 71%)

Scheme S2. Synthesis of **20**-**27**. For Synthesis of **20** (i) 5 equiv. malononitrile, 8 equiv. NaH, DME, $Pd(PPh_3)_4$ (20 mol%), 80 °C, 2 h. For synthesis of **21**-**23** (ii) 10 equiv. malononitrile, 10 equiv. NaH, DMI, 100 °C, 6 h. (iii) 200 equiv. PbO_2, CH_2Cl_2, rt, 2 h.

2a. General procedure for the synthesis of 8-11:

A 25 ml Schlenk tube was loaded with *meso*-halogenated porphyrins **8-11** (20 mg), malononitrile (10 eq) and sodium hydride (60% in oil, 10eq), which was kept under N_2 atmosphere. The mixture was dissolved in dry 1,3-dimethyl-2-imidazolidinone (DMI) (3 mL), and the resulting solution was stirred at 60 °C for 1 h. After the completion of the reaction, the mixture was quenched with 1M HCL aq. and the resulting crude mixture was filtered. The precipitate was collected and further purified by column chromatography using silica gel (C300, in CH_2Cl_2:*n*-hexane:Et_2O 1:3:1) to afford target molecules in 66-70% yield.

Synthesis of 8:

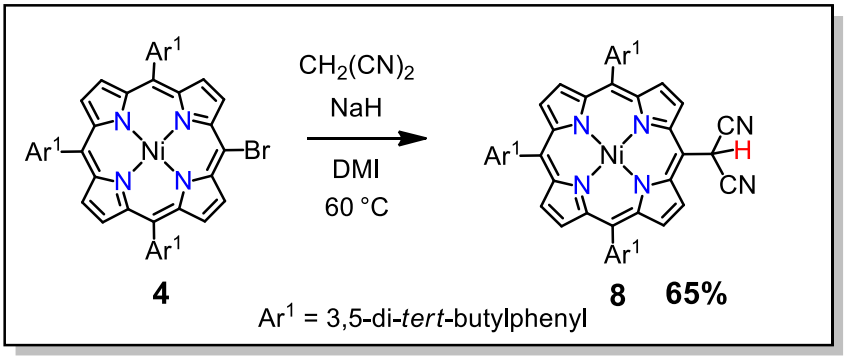

According to the general procedure, starting from *meso*-bromoporphyrin **4** (20 mg, 0.02 mmol), malononitrile (13.2 mg, 0.20 mmol) and sodium hydride (60% in oil, 8 mg, 0.20 mmol) the compound **8** was synthesized and purified by column chromatography using silica gel (C300, in CH_2Cl_2:*n*-hexane:Et_2O 1:3:1) to afford target molecule **8** in 65% yield (13 mg, 0.013 mmol).

^{1}H NMR (600 MHz, $CDCl_3$); δ/ppm = 9.35 (d, J = 4.9 Hz, 2H, β), 8.97 (d, J = 4.9 Hz, 2H, β), 8.78 (m, 4H, β), 7.83 (m, 6H, *meso*-Ar), 7.76 (m, 2H), 7.73 (m, 1H, *meso*-Ar), 7.01 (s, 1H, *meso*-$CH(CN)_2$), 1.49 (s, 36H, *t*Bu) and 1.46 (s, 18H, *t*Bu). ^{13}C NMR (151 MHz, $CDCl_3$); δ/ppm = 149.46, 149.36, 143.84, 143.22, 142.66, 140.17, 139.32, 139.22, 135.47, 133.77, 133.22, 128.84, 128.71, 127.25, 121.77, 121.68, 121.62, 113.91, 35.21, 35.18, 31.86 and 31.83. HR-APCI-TOFMS: *m*/*z* calcd for $[C_{65}H_{72}N_6{}^{58}Ni]^+$ = 994.5172; found = 994.5180 ($[M]^+$); UV-Vis (CH_2Cl_2): λ_{max}(nm) ($\varepsilon\times10^5$ [$M^{-1}cm^{-1}$]) = 418 (2.02), 534 (0.15), 568 (0.07).

Synthesis of 9:

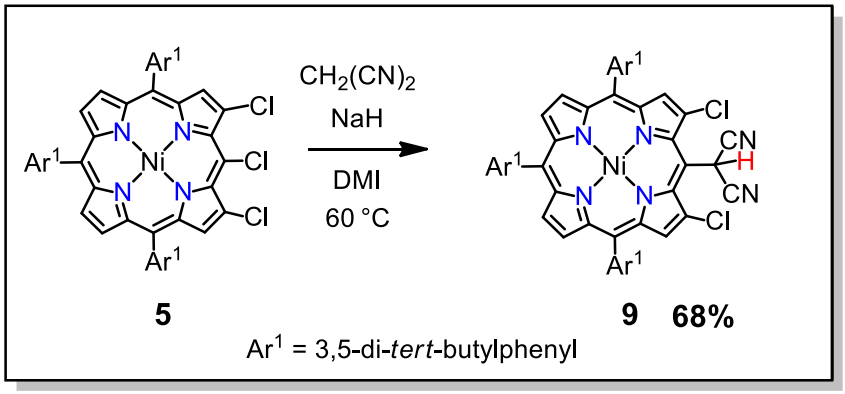

According the general procedure, starting from *meso*,*β*,*β'*-trichloroporphyrin **5** (20 mg, 0.019 mmol), malononitrile (12.5 mg, 0.19 mmol) and sodium hydride (60% in oil, 7.6 mg, 0.19 mmol) the compound **9** was synthesized and purified by column chromatography using silica gel (C300, in CH_2Cl_2:*n*-hexane:Et_2O 1:3:1) to afford target molecule **9** in 68% yield (14 mg, 0.013 mmol).

^{1}H NMR (600 MHz, $CDCl_3$); δ/ppm = 8.75 (s, 2H, *β*), 8.71 (d, J = 4.9 Hz, 2H, *β*), 8.67 (d, J = 4.9 Hz, 2H, *β*), 7.75 (d, J = 1.8 Hz, 2H, *meso*-Ar), 7.74 (t, J = 1.8 Hz, 2H, *meso*-Ar), 7.72 (d, J = 1.8 Hz, 4H, *meso*-Ar), 7.71 (s, 1H, *meso*-Ar), 7.37 (s, 1H, *meso*-$CH(CN)_2$), 1.47 (s, 36H, *t*Bu) and 1.45 (s, 18H, *t*Bu). ^{13}C NMR (151 MHz, $CDCl_3$); δ/ppm = 149.79, 149.67, 143.53, 143.20, 138.49, 138.31, 135.36, 134.68, 133.86, 128.58, 128.53, 122.22, 121.97, 121.44, 113.12, 35.23, 31.86, 31.85 and 31.82. HR-APCI-TOFMS: *m*/*z* calcd for $[C_{65}H_{70}Cl_2N_6{}^{58}Ni]^+$ = 1062.4392; found = 1062.4363 ($[M]^+$); UV-Vis (CH_2Cl_2): λ_{max}(nm) ($\varepsilon\times10^5$ $[M^{-1}cm^{-1}]$) = 428 (1.78), 551 (0.15), 591 (0.08).

Synthesis of 10:

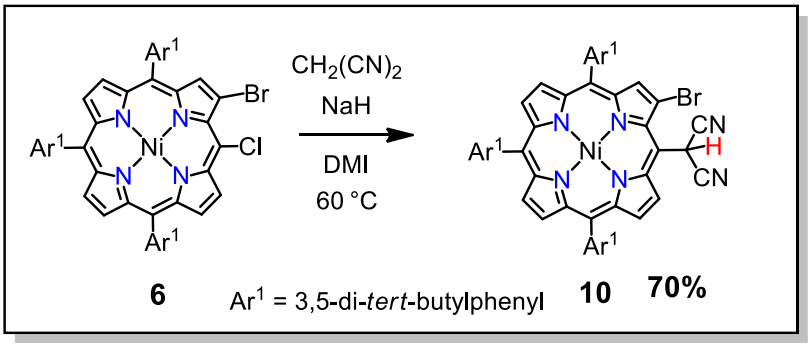

According the general procedure, starting from *meso*-chloro,*β*-bromoporphyrin **6** (20 mg, 0.019 mmol), malononitrile (12.5 mg, 0.19 mmol) and sodium hydride (60% in oil, 7.6 mg, 0.19 mmol) the compound **10** was synthesized and purified by column chromatography using silica gel (C300, in CH_2Cl_2:*n*-hexane:Et_2O 1:3:1) to afford target molecule **10** in 70% yield (14.5 mg, 13.5 μmol).

^{1}H NMR (600 MHz, $CDCl_3$); δ/ppm = 9.63 (d, J = 5.1 Hz, 1H, *β*), 8.93 (s, 1H, *β*), 8.90 (d, J = 5.1 Hz, 1H, *β*), 8.74 (m, 3H, *β*), 8.65 (d, J = 5.0 Hz, 1H, *β*), 7.96 (s, 1H, *meso*-$CH(CN)_2$), 7.79 (d, J = 1.8 Hz, 2H, *meso*-Ar), 7.78 (d, J = 1.8 Hz, 2H, *meso*-Ar), 7.74 (dd, J = 3.8, 1.8 Hz, 4H, *meso*-Ar), 7.71 (t, J = 1.8 Hz, 1H, *meso*-Ar), 1.48 (s, 36H, *t*Bu) and 1.45 (s, 18H, *t*Bu). ^{13}C NMR (151 MHz, $CDCl_3$); δ/ppm = 149.66, 149.64, 149.54, 143.91, 143.43, 143.38, 143.28, 141.93, 139.97, 138.90, 138.87, 139.71, 135.83, 134.33, 134.04, 133.72, 133.50, 130.34, 128.77, 128.71, 128.64, 123.00, 122.07, 121.96, 121.90, 121.84, 120.95, 114.22, 35.30 – 35.14 (m) and 31.85 (d). HR-APCI-TOFMS: *m*/*z* calcd for $[C_{65}H_{71}{}^{79}BrN_6{}^{58}Ni]^+$ = 1072.4277; found = 1072.4279 ($[M]^+$); UV-Vis (CH_2Cl_2): λ_{max}(nm) ($\varepsilon\times10^5$ $[M^{-1}cm^{-1}]$) = 423 (2.23), 544 (0.15), 580 (0.08).

Synthesis of 11:

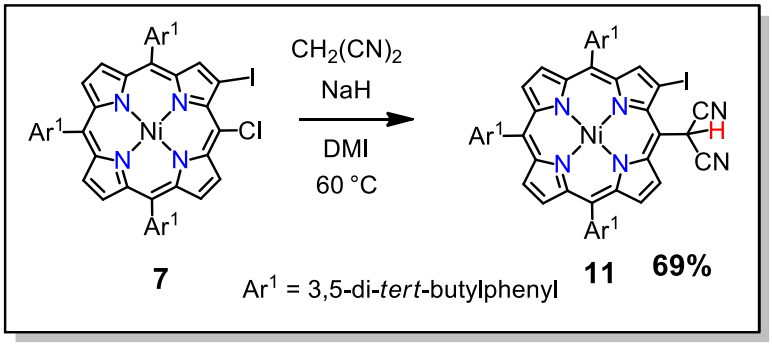

According the general procedure, starting from *meso*-chloro,*β*-iodoporphyrin **7** (20 mg, 0.018 mmol), malononitrile (12 mg, 0.18 mmol) and sodium hydride (60% in oil, 7.2 mg, 0.18 mmol) the compound **11** was synthesized and purified by column chromatography using silica gel (C300, in CH_2Cl_2:*n*-hexane:Et_2O 1:3:1) to afford target molecule **11** in 69% yield (14 mg, 12.5 µmol).

^{1}H NMR (600 MHz, $CDCl_3$); *δ*/ppm = 9.64 (d, *J* = 5.2 Hz, 1H, *β*), 9.17 (s, 1H, *β*), 8.89 (d, *J* = 5.2 Hz, 1H, *β*), 8.76 – 8.72 (m, 3H, *β*), 8.65 (d, *J* = 4.8 Hz, 1H, *β*), 7.95 (s, 1H, *meso*-$CH(CN)_2$), 7.78 (m, 4H, *meso*-Ar), 7.75 (m, 4H, *meso*-Ar), 7.71 (m, 1H, *meso*-Ar), 1.48 (m, 36H, *t*Bu) and 1.45 (s, 18H, *t*Bu). ^{13}C NMR (151 MHz, CDCl3); δ/ppm = 149.64, 149.54, 147.03, 143.88, 143.47, 143.30, 142.03, 141.93, 138.91, 138.70, 135.73, 134.31, 133.98, 133.74, 133.54, 130.52, 128.85, 128.78, 128.64, 122.91, 122.03, 121.95, 121.83, 114.28, 97.33, 35.23 and 31.86. HR-APCI-TOFMS: *m/z* calcd for $[C_{65}H_{71}IN_6{}^{58}Ni]^+$ = 1120.4138; found = 1120.4141 ($[M]^+$); UV-Vis (CH_2Cl_2): λ_{max}(nm) (ε×10^5 [$M^{-1}cm^{-1}$]) = 425 (1.97), 544 (0.14), 581 (0.07).

Synthesis of **20**:

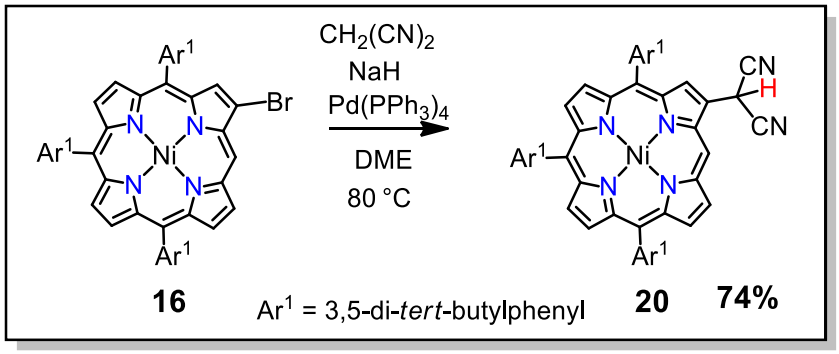

A 25 ml Schlenk tube was loaded with sodium hydride (60% in oil, 6 mg, 0.15 mmol) and 3ml Dimethoxyethane (DME) solvent and kept under N_2 atmosphere. After 10 min malononitrile (6.25 mg, 0.094 mmol) was added and the reaction mixture was stirred for 20 more min. To the reaction mixture *β*-Br porphyrin **16** **(**20 mg, 0.018 mmol) and $Pd(PPh_3)_4$ **(**4.4 mg, 3.78 µmol) was added and the resulting solution was stirred at 80 °C for 2 h. After the completion of the reaction, the mixture was quenched with 1M HCL aq. and the resulting crude mixture was extracted with CH_2Cl_2, dried over Na_2SO_4, and concentrated under reduced pressure. The compound was purified by column chromatography using silica gel (C300, in CH_2Cl_2:*n*-hexane:Et_2O 1:3:1) to afford target molecule **20** in 74% yield (14 mg, 0.014 mmol).

^{1}H NMR (600 MHz, $CDCl_3$); δ/ppm = 9.71 (s, 1H, *meso*-H), 9.16 (d, J = 4.8 Hz, 1H, β), 9.13 (s, 1H, β), 8.93 (d, J = 4.7 Hz, 1H, β), 8.85 – 8.80 (m, 4H, β), 7.89 – 7.88 (m, 2H, *meso*-Ar), 7.88 – 7.87 (m, 2H, *meso*-Ar), 7.86 – 7.85 (m, 2H, *meso*-Ar), 7.79 (m, 1H, *meso*-Ar), 7.77 – 7.75 (m, 1H, *meso*-Ar), 7.74 – 7.72 (m, 1H, *meso*-Ar), 6.52 (s, 1H, *meso*-$CH(CN)_2$), 1.51 (s, 18H, tBu), 1.49 (s, 18H, *t*Bu) and 1.47 (s, 18H, *t*Bu); ^{13}C NMR (151 MHz, $CDCl_3$); δ/ppm = 149.60, 149.43, 149.31, 144.34, 143.33, 142.97, 139.75, 139.40, 137.23, 133.69, 133.43, 133.329, 133.06, 133.00, 132.91, 129.22, 129.00, 128.89, 121.93, 121.83, 121.63, 121.61, 121.58, 120.76, 112.30, 99.96, 35.34 – 35.16 (m), 31.91 (s), 23.26 and 23.24. HR-APCI-TOFMS: *m*/*z* calcd for $[C_{65}H_{72}N_6{}^{58}Ni]^+$ = 994.5172; found = 994.5131 ($[M]^+$); UV-Vis (CH_2Cl_2): λ_{max}(nm) ($\varepsilon\times10^5$ [$M^{-1}cm^{-1}$]) = 414 (2.80), 526 (0.20), 558 (0.07).

Synthesis of 21:

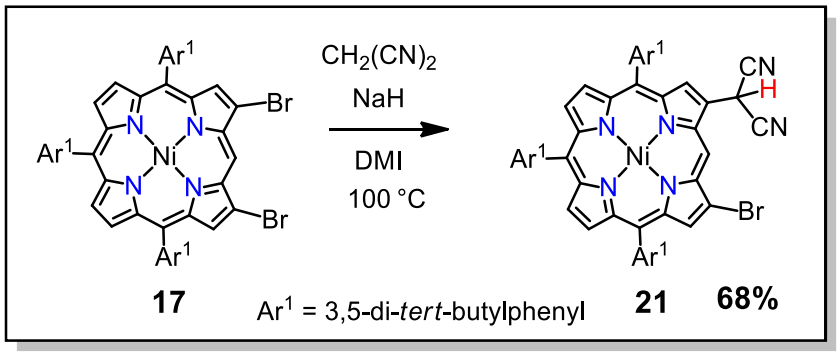

A 25 ml Schlenk tube was loaded with β-halogenated porphyrins **17 (**20 mg, 0.018 mmol), malononitrile (12 mg, 0.35 mmol) and sodium hydride (60% in oil, 7.3 mg, 0.18 mmol) was kept under N_2 atmosphere. The mixture was dissolved in dry 1,3-Dimethyl-2-imidazolidinone (DMI) 3 mL, and the resulting solution was stirred at 100 °C for 6 h. After the completion of the reaction, the mixture was quenched with 1M HCL aq. and the resulting crude mixture was filtered. The precipitate was collected and further purified by column chromatography using silica gel (C300, in CH_2Cl_2:*n*-hexane:Et_2O 1:3:1) to afford target molecule **21** in 68% yield (13.5 mg, 12.6 μmol).

^{1}H NMR (600 MHz, $CDCl_3$); δ/ppm = 9.82 (s, 1H, *meso*-H), 9.14 (d, J = 0.7 Hz, 1H, β), 8.92 (s, 1H, β), 8.87 – 8.80 (m, 4H, β), 7.89 (d, J = 1.8 Hz, 2H, *meso*-Ar), 7.86 (d, J = 1.8 Hz, 2H, *meso*-Ar), 7.84 (d, J = 1.8 Hz, 2H, *meso*-Ar), 7.80 (t, J = 1.8 Hz, 1H, *meso*-Ar), 7.78 (t, J = 1.8 Hz, 1H, *meso*-Ar), 7.75 (t, J = 1.8 Hz, 1H, *meso*-Ar), 6.55 (s, 1H, *meso*-$CH(CN)_2$), 1.53 (s, 18H, *t*Bu), 1.51 (s, 18H, *t*Bu) and 1.48 (s, 18H, *t*Bu). ^{13}C NMR (151 MHz, $CDCl_3$); δ/ppm = 149.68, 149.57, 149.38, 144.35, 144.13, 144.00, 143.68, 142.57, 140.20, 139.66, 139.11, 137.81, 134.01, 133.68, 133.62, 133.37, 133.13, 129.25, 128.85, 128.83, 126.07, 122.33, 122.23, 122.13, 121.93, 120.65, 120.42, 112.23, 98.34, 35.35 – 35.16 (m) and 31.89 (d). HR-APCI-TOFMS: *m*/*z* calcd for $[C_{65}H_{71}{}^{79}BrN_6{}^{58}Ni]^+$ = 1072.4277; found = 1072.4224 ($[M]^+$); UV-Vis (CH_2Cl_2): λ_{max}(nm) ($\varepsilon\times10^5$ [$M^{-1}cm^{-1}$]) = 416 (2.31), 528 (0.17), 558 (0.05).

Synthesis of 22:

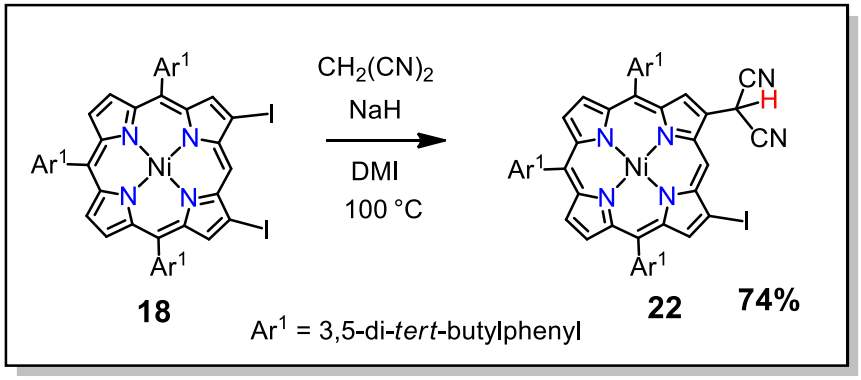

According the general procedure, starting from *β*,*β*-diiodo- porphyrin **18** (20 mg, 0.017 mmol), malononitrile (11.2 mg, 0.17 mmol) and sodium hydride (60% in oil, 6.8 mg, 0.17 mmol) the compound **22** was synthesized and purified by column chromatography using silica gel (C300, in CH_2Cl_2:*n*-hexane:Et_2O 1:3:1) to afford target molecule **22** in 74% yield (14.2 mg, 12.7 µmol).

^{1}H NMR (600 MHz, $CDCl_3$); *δ*/ppm = 9.77 (s, 1H, *meso*-H), 9.13 (s, 1H, *β*), 9.11 (s, 1H, *β*), 8.84 – 8.78 (m, 4H, *β*), 7.87 (d, *J* = 1.6 Hz, 2H, *meso*-Ar), 7.84 (d, *J* = 1.6 Hz, 2H, *meso*-Ar), 7.83 (d, *J* = 1.6 Hz, 2H, *meso*-Ar), 7.79 (t, *J* = 1.6 Hz, 1H, *meso*-Ar), 7.77 (t, *J* = 1.6 Hz, 1H, *meso*-Ar), 7.73 (t, *J* = 1.6 Hz, 1H, *meso*-Ar), 6.59 (s, 1H, *meso*-$CH(CN)_2$), 1.51 (s, 18H, tBu), 1.50 (s, 18H, *t*Bu) and 1.47 – 1.45 (m, 18H, *t*Bu). ^{13}C NMR (151 MHz, $CDCl_3$); *δ*/ppm = 149.68, 149.54, 149.37, 144.34, 144.31, 144.05, 143.64, 141.63, 141.50, 140.18, 139.23, 138.13, 133.67, 133.63, 133.57, 129.24, 128.88, 128.83, 126.12, 122.24, 122.04, 121.90, 121.69, 112.25, 100.81, 35.34 – 35.16 (m) and 31.98 – 31.80 (m). HR-APCI-TOFMS: *m*/*z* calcd for $[C_{65}H_{71}IN_6{}^{58}Ni]^+$ = 1120.4138; found = 1120.4156 ($[M]^+$); UV-Vis (CH_2Cl_2): λ_{max}(nm) ($\varepsilon\times10^5$ [$M^{-1}cm^{-1}$]) = 418 (2.39), 530 (0.18), 561 (0.04).

Synthesis of 23:

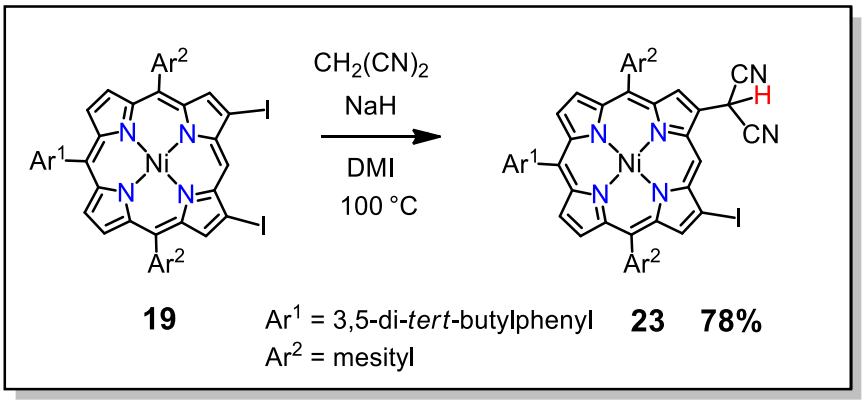

According the general procedure, starting from *β*,*β*-diiodo-porphyrin **19** (20 mg, 0.019 mmol), malononitrile (12.5 mg, 0.19 mmol) and sodium hydride (60% in oil, 7.6 mg, 0.19 mmol) the compound **23** was synthesized and purified by column chromatography using silica gel (C300, in CH_2Cl_2:*n*-hexane:Et_2O 1:3:1) to afford target molecule **23** in 78% yield (14.6 mg, 0.015 mmol).

^{1}H NMR (600 MHz, $CDCl_3$); δ/ppm = 9.79 (s, 1H, *meso*-H), 8.93 (s, 1H, β), 8.88 (d, J = 0.6 Hz, 1H, β), 8.75 (m, 2H, β), 8.60 (dd, J = 4.9, 1.4 Hz, 2H, β), 7.87 (d, J = 1.8 Hz, 2H, *meso*-Ar), 7.74 (t, J = 1.8 Hz, 1H, *meso*-Ar), 7.24 (d, J = 1.4 Hz, 4H, *meso*-Ar), 6.59 (s, 1H, *meso*-$CH(CN)_2$), 2.59 (d, J = 3.0 Hz, 6H, Me), 1.80 (d, J = 1.6 Hz, 12H, Me) and 1.47 (s, 18H, *t*Bu). ^{13}C NMR (151 MHz, $CDCl_3$); δ/ppm = 149.34, 144.70, 144.37, 143.98, 143.77, 143.37, 141.84, 140.13, 139.85, 139.64, 139.15, 139.01, 138.62, 138.45, 136.48, 136.27, 134.25, 133.87, 132.35, 132.30, 131.48, 129.07, 128.34, 128.21, 126.74, 122.07, 121.64, 119.30, 117.20, 112.29, 100.83, 92.69, 35.25, 31.87, 23.21 and 21.62 (d). HR-APCI-TOFMS: *m*/*z* calcd for $[C_{55}H_{51}IN_6{}^{58}Ni]^+$ = 980.2573; found = 980.2529 ($[M]^+$); UV-Vis (CH_2Cl_2): λ_{max}(nm) ($\varepsilon\times10^5$ $[M^{-1}cm^{-1}]$) = 416 (2.46), 528 (0.19), 561 (0.07).

Synthesis of 12:

The CH_2Cl_2 solution of a precursor **8** (20 mg, 0.02 mmol), **9**(20 mg, 18.8 µmol), **10** (20 mg, 18.8 µmol) or **11** (20 mg, 17.8 µmol) was kept under nitrogen atmosphere and added excess amount of PbO_2 (200 eq). The resulting solution was allowed to stir at room temperature for 2 h. After completion, the reaction mixture was filtered through celite and concentrated by a rotary evaporator. The compound was purified by column chromatography using silica gel (C300, in CH_2Cl_2:*n*-hexane (**2:5**) afforded the respective stable radical **12** (14 mg 0.014 mmol, 70% Yield), **13** (14 mg 0.013 mmol, 70% Yield), **14** (13 mg 0.012 mmol, 65% Yield) or **15** (12.5 mg 0.011 mmol, 63% Yield).

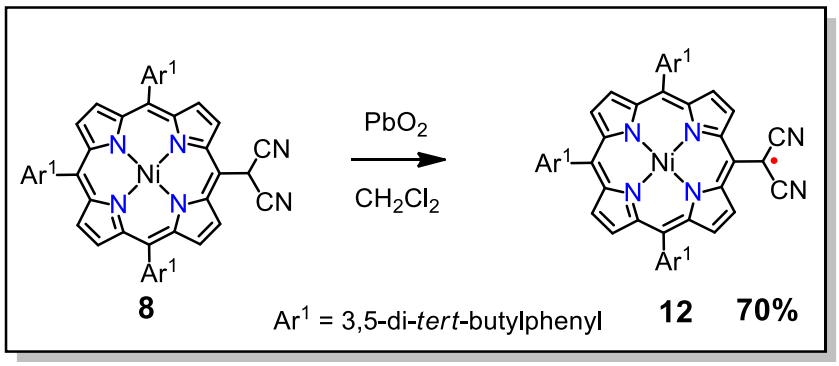

This compound was synthesized and purified according to the general procedure.

HR-APCI-TOFMS: *m*/*z* calcd for $[C_{65}H_{71}N_6{}^{58}Ni]^+$ = 993.5094; found = 993.5037 ($[M]^+$); UV-Vis (CH_2Cl_2): λ_{max}(nm) ($\varepsilon\times10^5$ $[M^{-1}cm^{-1}]$) = 466 (0.90), 537 (0.22), 638 (0.26), 804 (0.06).

Synthesis of 13

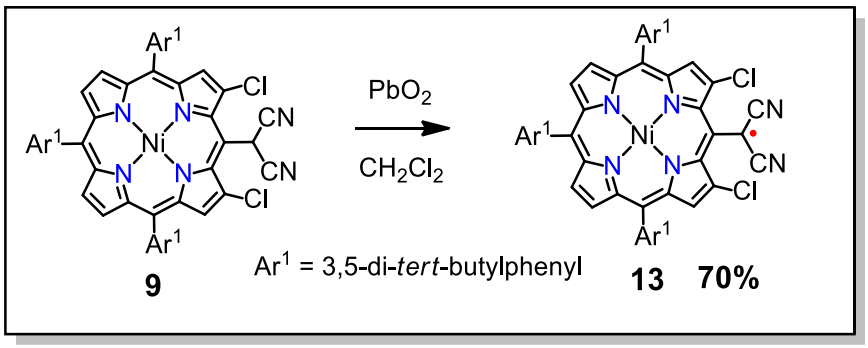

This compound was synthesized and purified according to the general procedure.

HR-APCI-TOFMS: *m/z* calcd for $[C_{65}H_{69}Cl_2N_6{}^{58}Ni]^+$ = 1061.4314; found = 1061.4273 ($[M]^+$); UV-Vis (CH_2Cl_2): λ_{max}(nm) ($\varepsilon\times10^5$ [$M^{-1}cm^{-1}$]) = 451 (0.53), 472 (0.54), 537 (0.22), 636 (0.16), 855 (0.08), and 1600 (0.012).

Synthesis of 14:

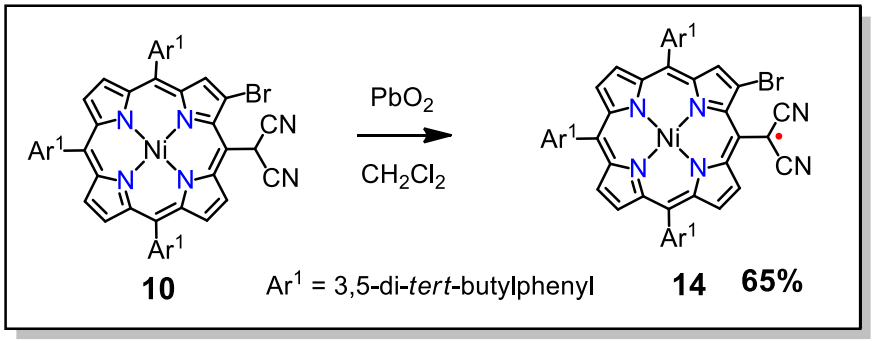

This compound was synthesized and purified according to the general procedure.

HR-APCI-TOFMS: *m/z* calcd for $[C_{65}H_{70}{}^{79}BrN_6{}^{58}Ni]^+$ = 1071.4199; found = 1071.4147 ($[M]^+$); UV-Vis (CH_2Cl_2): λ_{max}(nm) ($\varepsilon\times10^5$ [$M^{-1}cm^{-1}$]) = 468 (0.67), 539 (0.21), 638 (0.19), 850 (0.06).

Synthesis of 15:

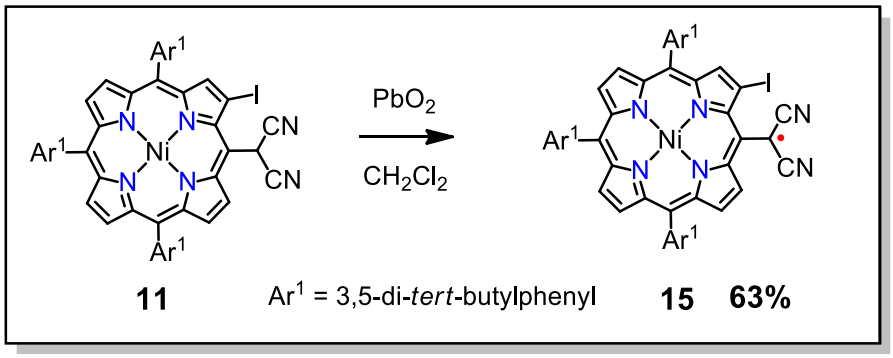

This compound was synthesized and purified according to the general procedure.

HR-APCI-TOFMS: *m/z* calcd for $[C_{65}H_{70}IN_6{}^{58}Ni]^+$ = 1119.4060; found = 1119.4007 ($[M]^+$); UV-Vis (CH_2Cl_2): λ_{max}(nm) ($\varepsilon\times10^5$ [$M^{-1}cm^{-1}$]) = 469 (0.66), 536 (0.21), 640 (0.18), 848 (0.06).

Synthesis of 24-27:

The CH_2Cl_2 solution of a precursor **20** (20 mg, 0.02 mmol), **21** (20 mg, 18.6 µmol), **22** (20 mg, 17.8 µmol) or **23** (20 mg, 0.02 mmol), was kept under nitrogen atmosphere and added excess amount of PbO_2 (200 eq). The resulting solution was allowed to stir at room temperature for 2 h. After completion, the reaction mixture was filtered through celite and concentrated by a rotary evaporator. The compound was purified by column chromatography using silica gel (C300, in CH_2Cl_2:*n*-hexane (**2:7**) afforded the respective stable radical **24** (10 mg 0.01 mmol, 50% Yield), **25** (12 mg 0.011 mmol, 60% Yield), **26** (12 mg 0.011 mmol, 60% Yield) or **27** (14 mg 0.014 mmol, 71% Yield).

Synthesis of $(24)_2$:

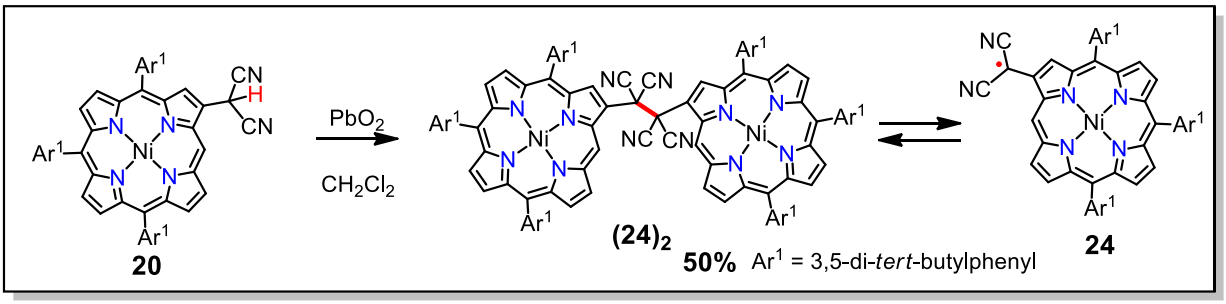

^{1}H NMR (600 MHz, 213 K, $CDCl_3$); δ/ppm = 9.22 (s, 1H, *meso*-H), 9.02 (s, 1H, *meso*-H), 8.91 – 8.74 (m, 5H, β), 8.59 (d, J = 4.3 Hz, 1H, β), 8.47 (m, 2H, β), 8.41 (d, J = 4.3 Hz, 1H, β), 8.37 – 8.27 (m, 4H, β), 8.22 – 8.09 (m, 3H, *meso*-Ar), 7.97 (m, 2H, β, *meso*-Ar), 7.82 – 7.57 (m, 7H, *meso*-Ar), 7.46 – 7.30 (m, 4H, *meso*-Ar), 7.15 (d, J = 24.8 Hz, 2H, *meso*-Ar), 1.88 (s, 6H, *t*Bu), 1.73 (s, 3H, *t*Bu), 1.68 (s, 6H, *t*Bu), 1.61 (s, 6H, *t*Bu), 1.58 – 1.48 (m, 30H, *t*Bu), 1.37 – 1.23 (m, 42H, *t*Bu), 1.23 – 1.19 (m, 6H, *t*Bu), 1.14 (s, 6H, *t*Bu) and 0.65 (s, 3H, *t*Bu); HR-APCI-TOFMS: *m/z* calcd for $[C_{65}H_{71}N_6{}^{58}Ni]^+$ = 993.5094; found = 993.5096 ($[M]^+$); UV-Vis (CH_2Cl_2): λ_{max}(nm) ($\varepsilon\times10^5$ [$M^{-1}cm^{-1}$]) = 415 (1.20), 490 (0.22), 683 (0.11), 1000-1450 (broad).

Synthesis of $(25)_2$:

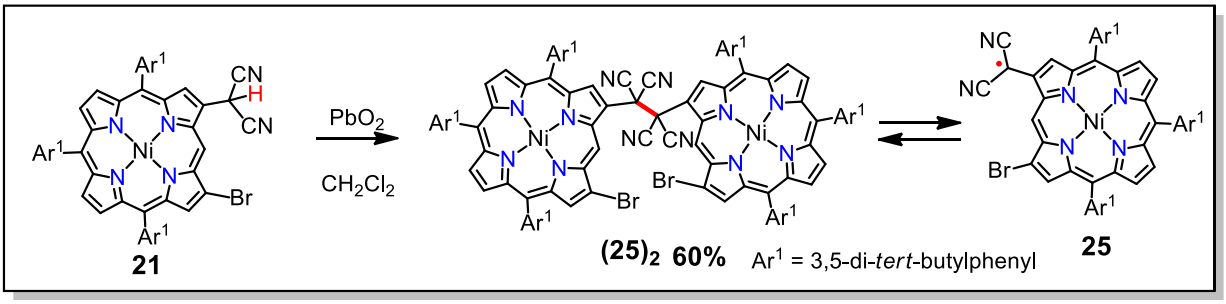

This compound was synthesized and purified according to the general procedure.

^{1}H NMR (600 MHz, 213 K, CD_2Cl_2); δ/ppm = 10.82 (s, 1H, *meso*-H), 8.96 (s, 1H, β), 8.77 (d, J = 4.8 Hz, 1H, β), 8.59 – 8.54 (m, 2H, β, *meso*-Ar), 8.45 (d, J = 5.0 Hz, 1H, β), 8.39 (d, J = 11.4 Hz, 2H, *meso*-Ar), 8.21 (s, 1H,), 8.15 (d, J = 4.7 Hz, 1H, β), 8.07 (d, J = 4.7 Hz, 1H, β), 7.93 (d, J = 4.9 Hz, 2H, β), 7.79 – 7.71 (m, 3H, *meso*-Ar, β), 7.64 (d, J = 24.3 Hz, 4H), 7.53 (s, 1H), 7.40 (s, 2H), 7.27 (s, 1H, *meso*-Ar), 7.15 (s, 1H), 7.00 (d, J = 23.1 Hz, 2H), 6.58 (s, 1H, , β), 6.21 (s, 1H, *meso*-H), 6.14 (s, 1H), 5.81 (s, 1H), 5.62 (s, 1H), 1.69 (s, 9H, *t*Bu), 1.62 (s, 9H, *t*Bu), 1.59 (s, 9H, *t*Bu), 1.55 (s, 9H, *t*Bu), 1.46 (s, 9H, *t*Bu), 1.34 (s, 9H, *t*Bu), 1.26 (s, 9H, *t*Bu), 1.17 (s, 9H, *t*Bu), 1.15 (s, 9H, *t*Bu), 1.03 (s, 9H, *t*Bu), 0.91 (s, 9H, *t*Bu) and -0.15 (s, 9H, *t*Bu); HR-APCI-TOFMS: *m/z* calcd for $[C_{65}H_{70}{}^{79}BrN_6{}^{58}Ni]^+$ = 1071.4199; found = 1071.4191 ($[M]^+$); UV-Vis (CH_2Cl_2): λ_{max}(nm) ($\varepsilon\times10^5$ [$M^{-1}cm^{-1}$]) = 416 (1.03), 488 (0.17), 518 (0.14), 691 (0.08), 1000-1450 (broad).

Synthesis of $(26)_2$:

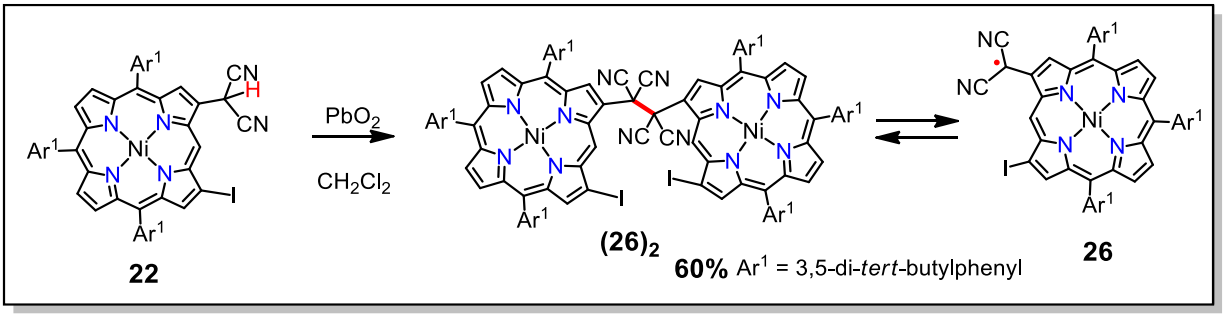

This compound was synthesized and purified according to the general procedure.

^{1}H NMR (600 MHz, 233 K, CD_2Cl_2); δ/ppm = 10.70 (s, 1H, *meso*-H), 9.13 (s, 1H, β), 8.73 (d, J = 4.8 Hz, 1H, β), 8.57 (s, 1H, β), 8.52 (d, J = 4.9 Hz, 1H, β), 8.45 (d, J = 4.9 Hz, 1H, β), 8.42 (s, 2H, β), 8.21 (s, 1H, *meso*-Ar), 8.14 (d, J = 4.7 Hz, 1H, β), 8.08 (d, J = 4.7 Hz, 1H, β), 7.94 (m, 2H, β, *meso*-Ar), 7.79 (s, 1H, *meso*-Ar), 7.77 (s, 1H, *meso*-Ar), 7.73 (s, 1H, *meso*-Ar), 7.66 (m, 2H, *meso*-Ar), 7.63 (s, 1H, *meso*-Ar), 7.60 (d, J = 4.9 Hz, 1H, β), 7.49 (s, 1H, *meso*-Ar), 7.45 (m, 2H, β, *meso*-Ar), 7.29 (s, 1H, *meso*-Ar), 7.09 (s, 1H, *meso*-Ar), 7.02 (s, 1H, *meso*-Ar), 7.00(s, 1H, *meso*-Ar), 6.63 (s, 1H, *meso*-Ar), 6.23 (s, 1H, *meso*-H), 6.14 (s, 1H, *meso*-Ar), 5.99 (s, 1H, *meso*-Ar), 5.85 (s, 1H, *meso*-Ar), 1.71 (s, 9H, *t*Bu), 1.62 (s, 18H, *t*Bu), 1.56 (s, 9H, *t*Bu), 1.45 (s, 9H, *t*Bu), 1.35 (s, 9H, *t*Bu), 1.25 (s, 9H, *t*Bu), 1.19 (s, 9H, *t*Bu), 1.16 (s, 9H, *t*Bu), 1.06 (s, 9H, *t*Bu), 0.90 (s, 9H, *t*Bu) and -0.14 (s, 9H, *t*Bu); HR-APCI-TOFMS: *m*/*z* calcd for $[C_{65}H_{70}IN_6{}^{58}Ni]^+$ = 1119.4060; found = 1119.4040 ($[M]^+$); UV-Vis (CH_2Cl_2): λ_{max}(nm) ($\varepsilon\times10^5$ [$M^{-1}cm^{-1}$]) = 417 (1.23), 488 (0.21), 516 (0.18), 691 (0.09), 1000-1450 (broad).

Synthesis of $(27)_2$:

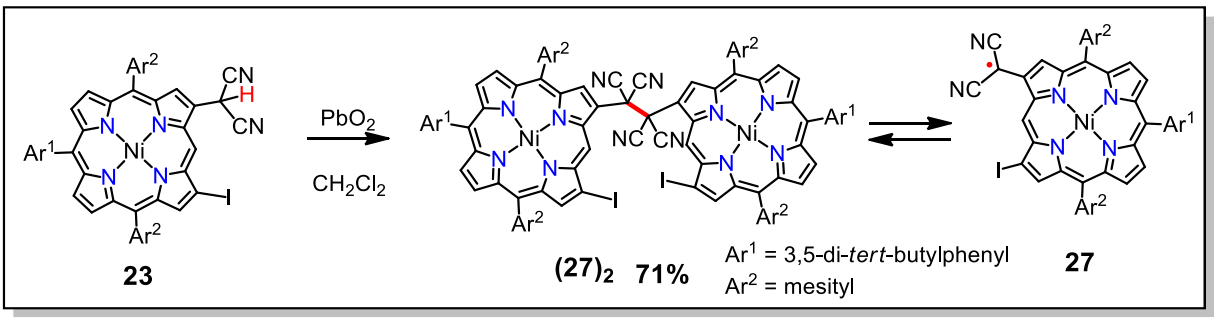

This compound was synthesized and purified according to the general procedure.

^{1}H NMR (600 MHz, 193 K, CD_2Cl_2); δ/ppm = 11.03 (s, 1H, *meso*-H), 9.23 (s, 1H, β), 8.98 (s, 1H, β), 8.76 (d, J = 4.5 Hz, 1H, β), 8.61 (m, 2H, β, *meso*-Ar), 8.52 (m, 2H, β), 8.27 – 8.17 (m, 3H, *meso*-Ar, β), 7.96 (s, 1H, *meso*-Ar), 7.88 (s, 1H, *meso*-Ar), 7.71 (d, J = 17.6 Hz, 2H, *meso*-Ar), 7.62 (d, J = 4.6 Hz, 1H, β), 7.53 (s, 1H, *meso*-Ar), 7.48 (s, 1H, *meso*-Ar), 7.42 (s, 1H, *meso*-Ar), 7.33 (s, 1H, *meso*-Ar), 7.12 (d, J = 19.3 Hz, 3H, *meso*-Ar), 6.88 (s, 1H, *meso*-Ar), 6.73 (s, 2H, *meso*-Ar), 6.38 (s, 1H, *meso*-H), 3.12 (s, 1H, *meso*-Ar), 2.60 (s, 3H, Mesityl), 2.52 (s, 3H, Mesityl), 2.22 (s, 6H, Mesityl), 1.99 (s, 3H, Mesityl), 1.69 (s, 3H, Mesityl), 1.44 (s, 9H, *t*Bu), 1.41 (s, 6H, Mesityl), 1.31 (s, 18H, *t*Bu), 1.12 (s, 9H, *t*Bu), 0.84 (s, 3H, Mesityl) and -2.79 (s, 3H, Mesityl); HR-APCI-TOFMS: *m*/*z* calcd for $[C_{55}H_{50}IN_6{}^{58}Ni]^+$ = 979.2495; found = 979.2468 ($[M]^+$); UV-Vis (CH_2Cl_2): λ_{max}(nm) ($\varepsilon\times10^5$ [$M^{-1}cm^{-1}$]) = 414 (1.29), 535 (0.16), 571 (0.08), 687 (0.06), 1000-1450 (broad).

Mass spectral analysis:

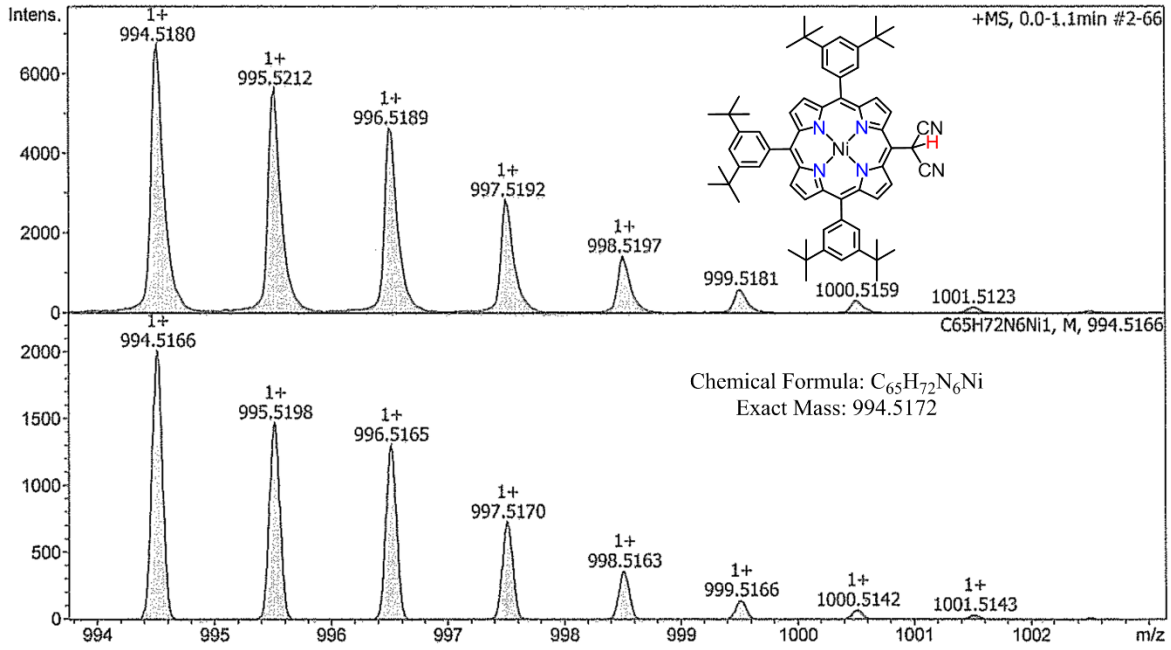

***Figure S1*:** HR-APCI-TOF mass spectra of **8** (top: observed, bottom: simulated).

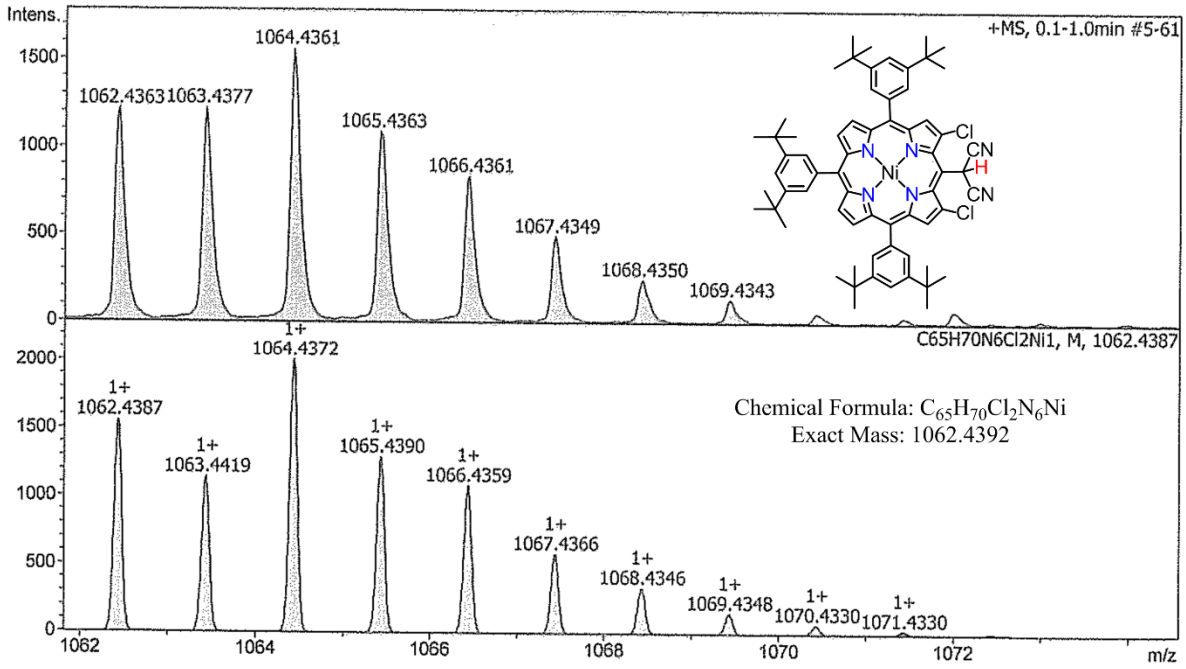

***Figure S2*:** HR-APCI-TOF mass spectra of **9** (top: observed, bottom: simulated).

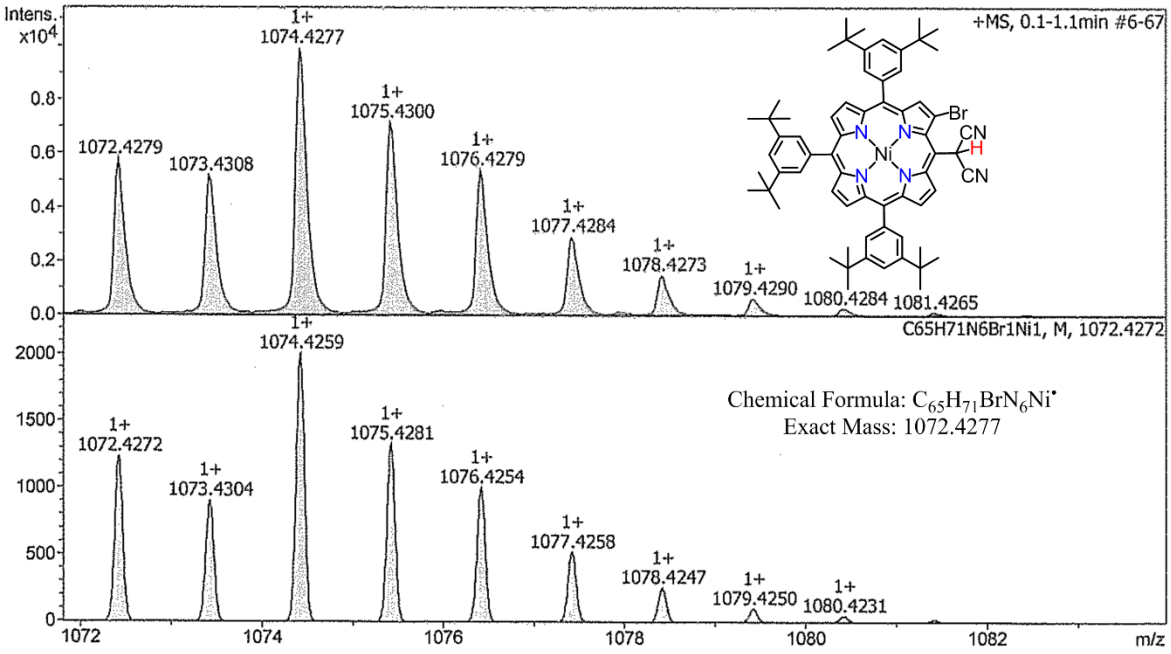

***Figure S3*:** HR-APCI-TOF mass spectra of **10** (top: observed, bottom: simulated).

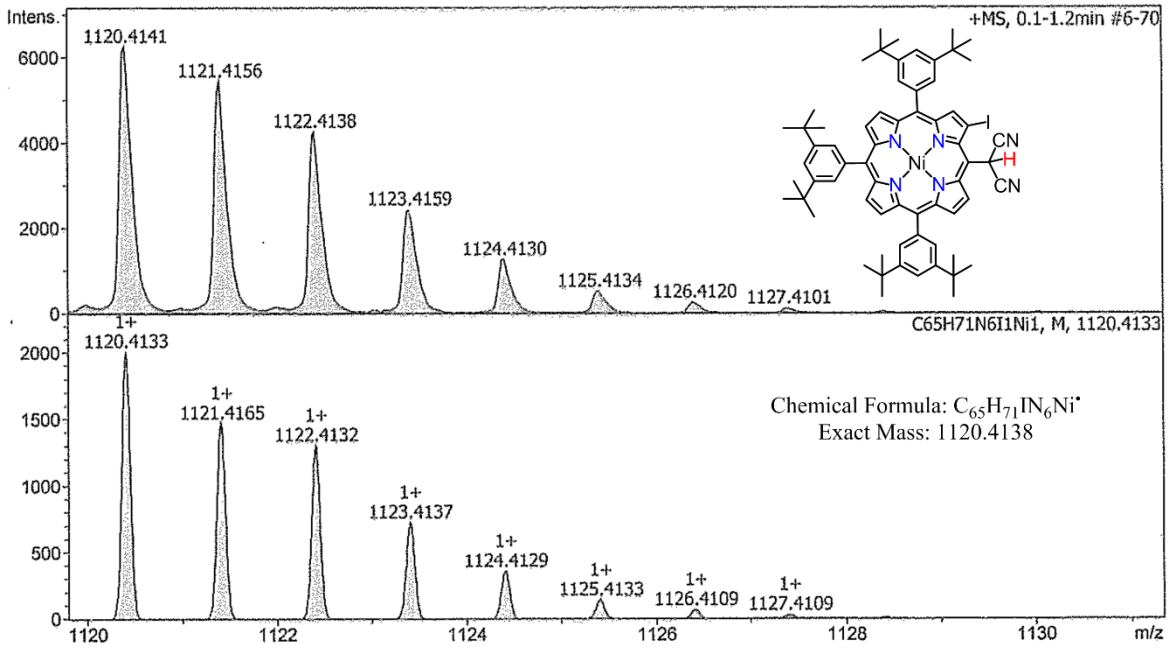

***Figure S4*:** HR-APCI-TOF mass spectra of **11** (top: observed, bottom: simulated).

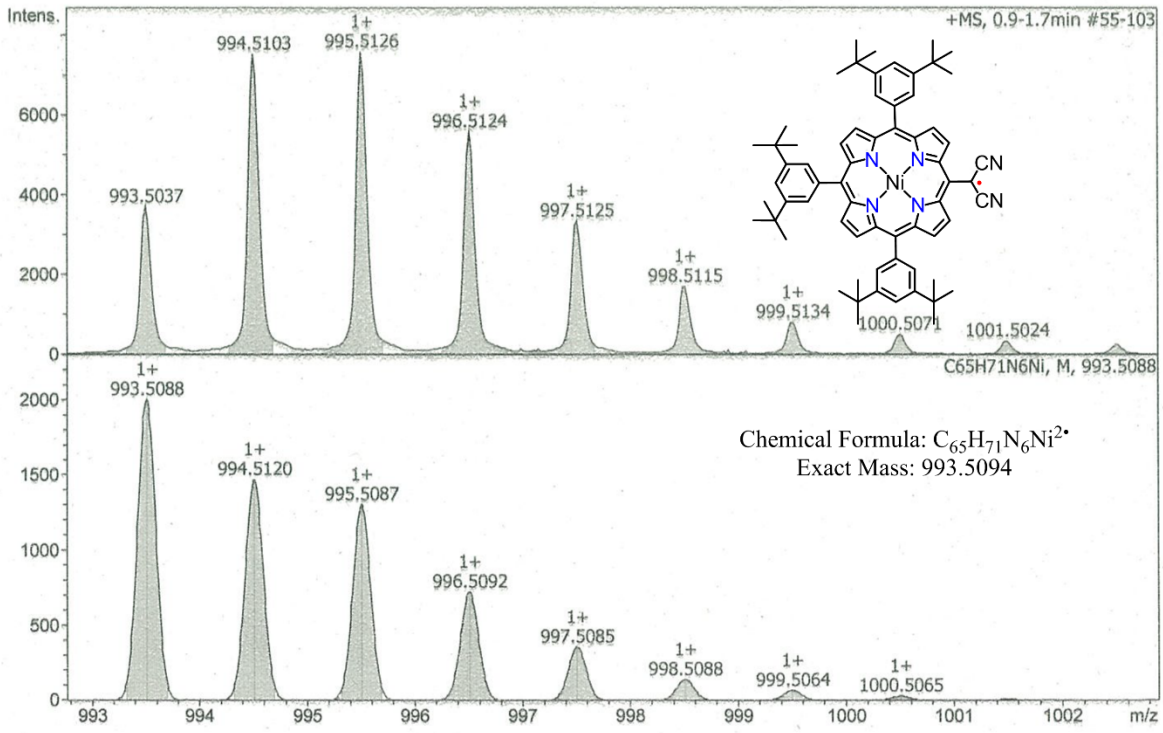

***Figure S5*:** HR-APCI-TOF-MS of **12** (top: observed, bottom: simulated).

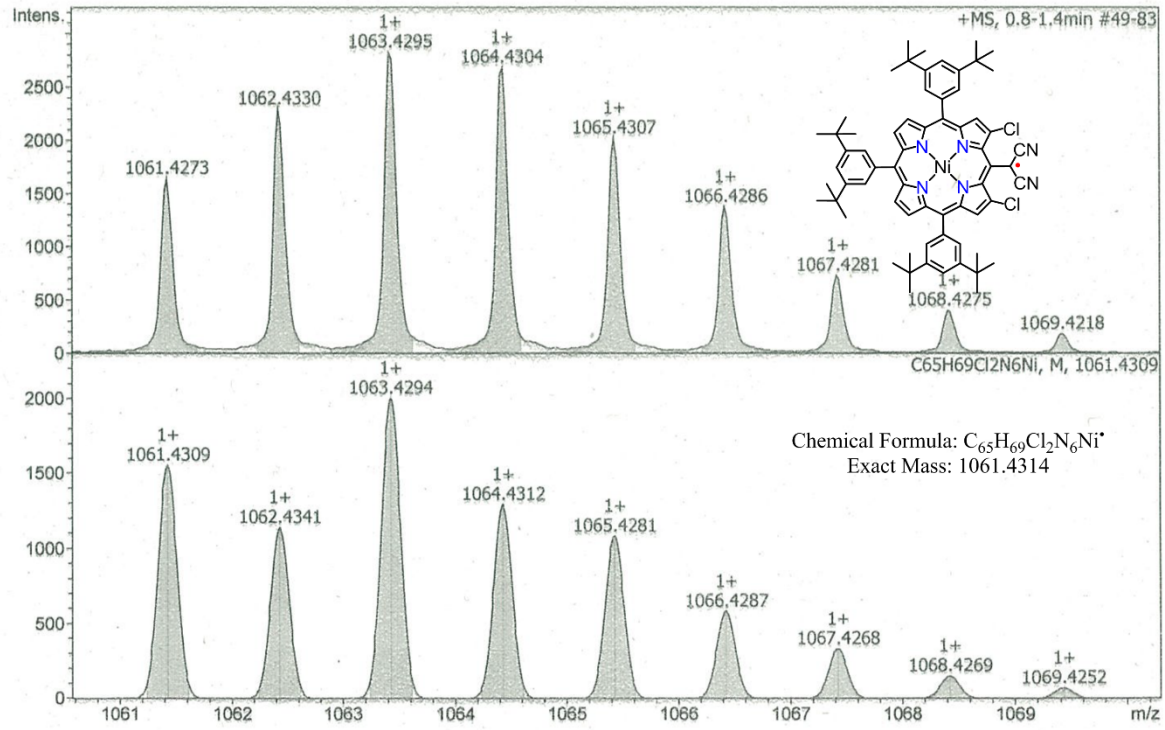

***Figure S6*:** HR-APCI-TOF mass spectra of **13** (top: observed, bottom: simulated).

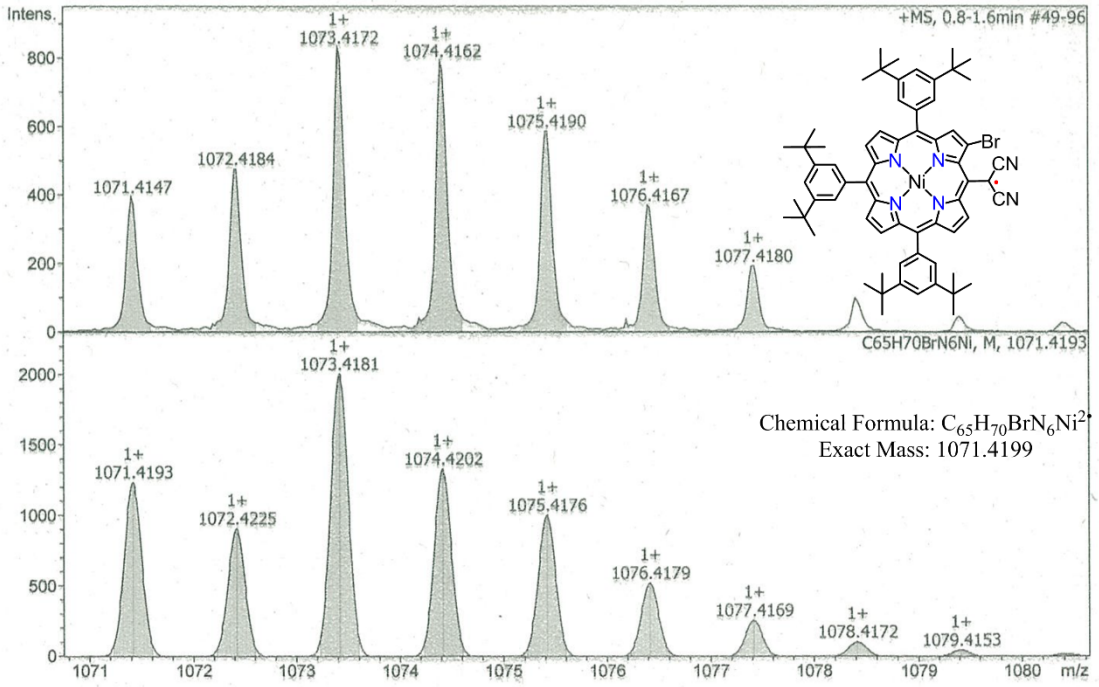

***Figure S7*:** HR-APCI-TOF mass spectra of **14** (top: observed, bottom: simulated).

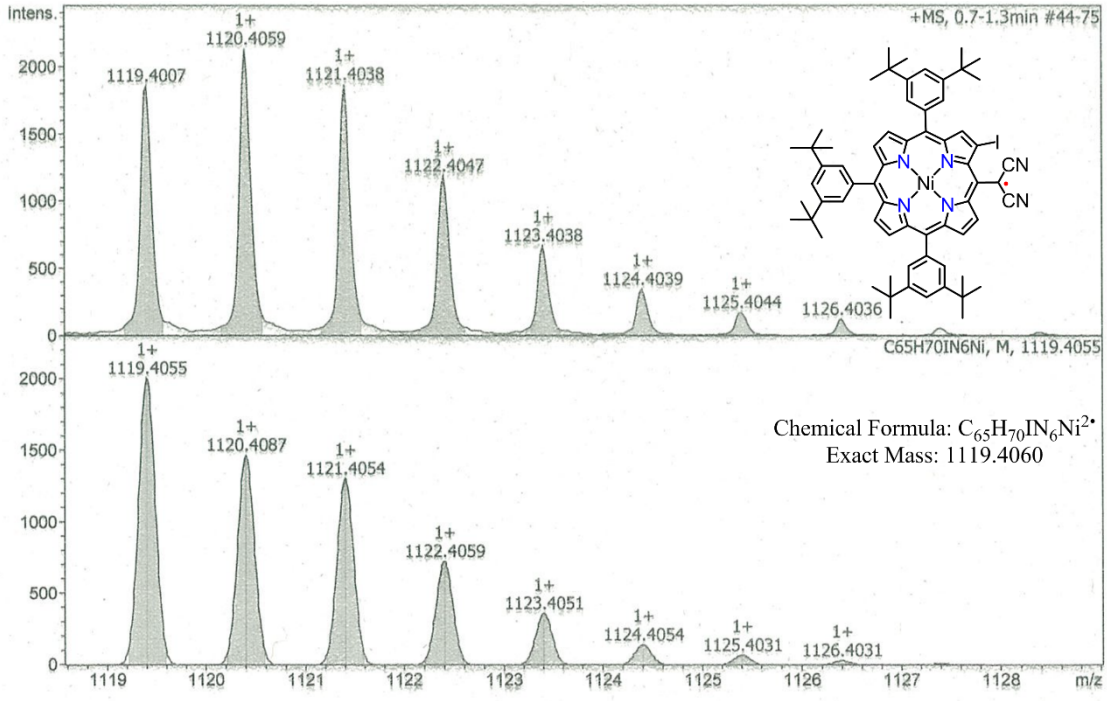

***Figure S8*:** HR-APCI-TOF mass spectra of **15** (top: observed, bottom: simulated).

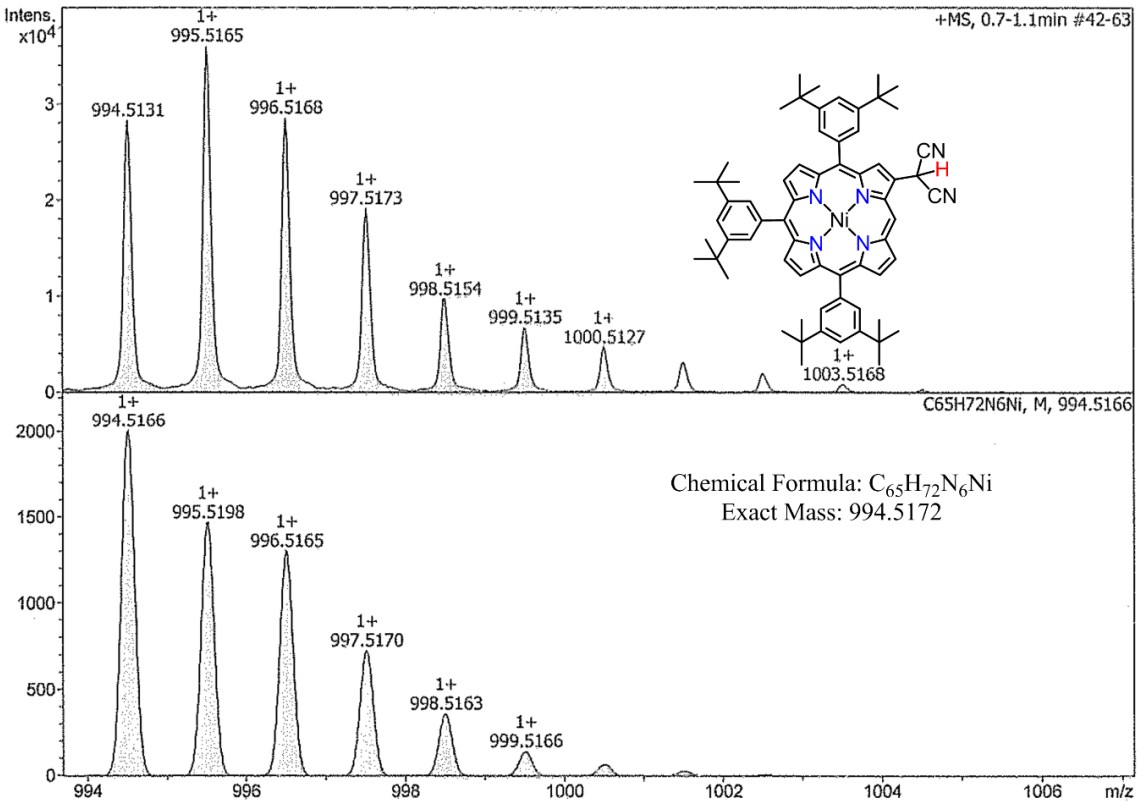

***Figure S9*:** HR-APCI-TOF mass spectra of **20** (top: observed, bottom: simulated).

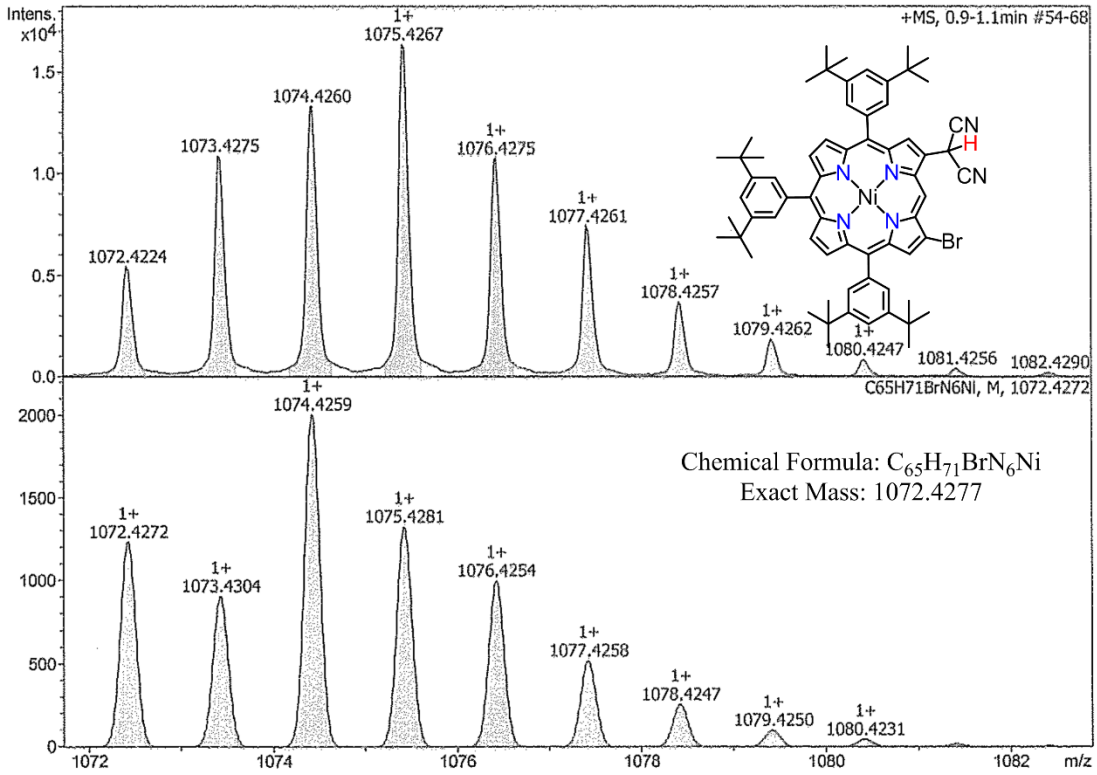

***Figure S10*:** HR-APCI-TOF mass spectra of **21** (top: observed, bottom: simulated).

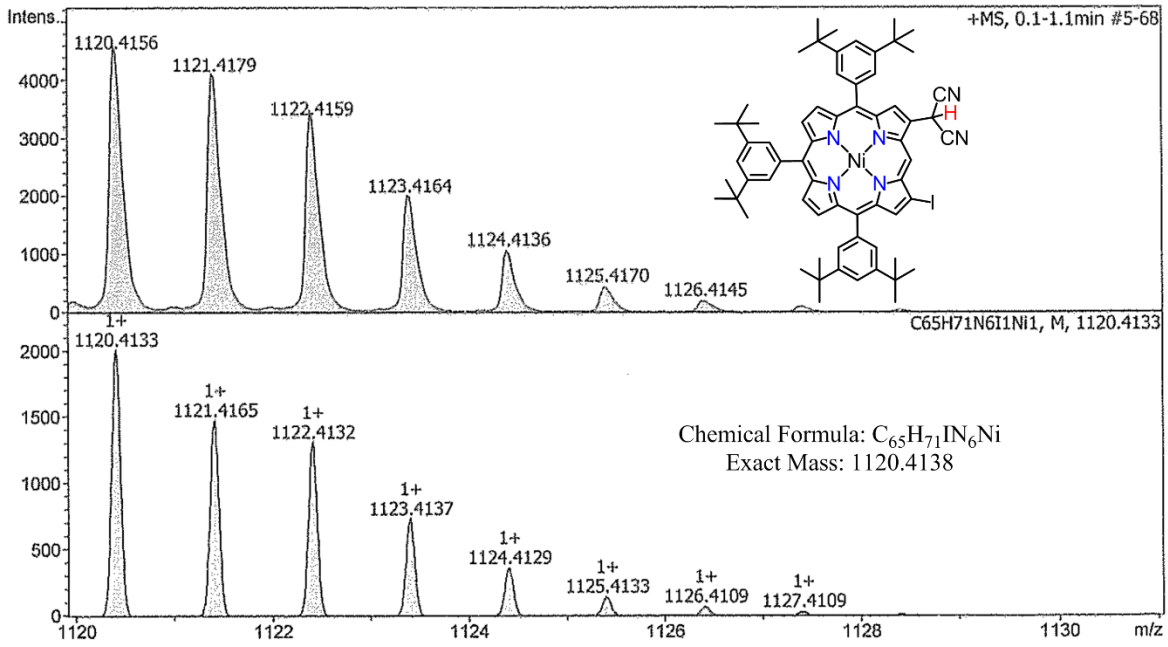

***Figure S11*:** HR-APCI-TOF-MS of **22** (top: observed, bottom: simulated).

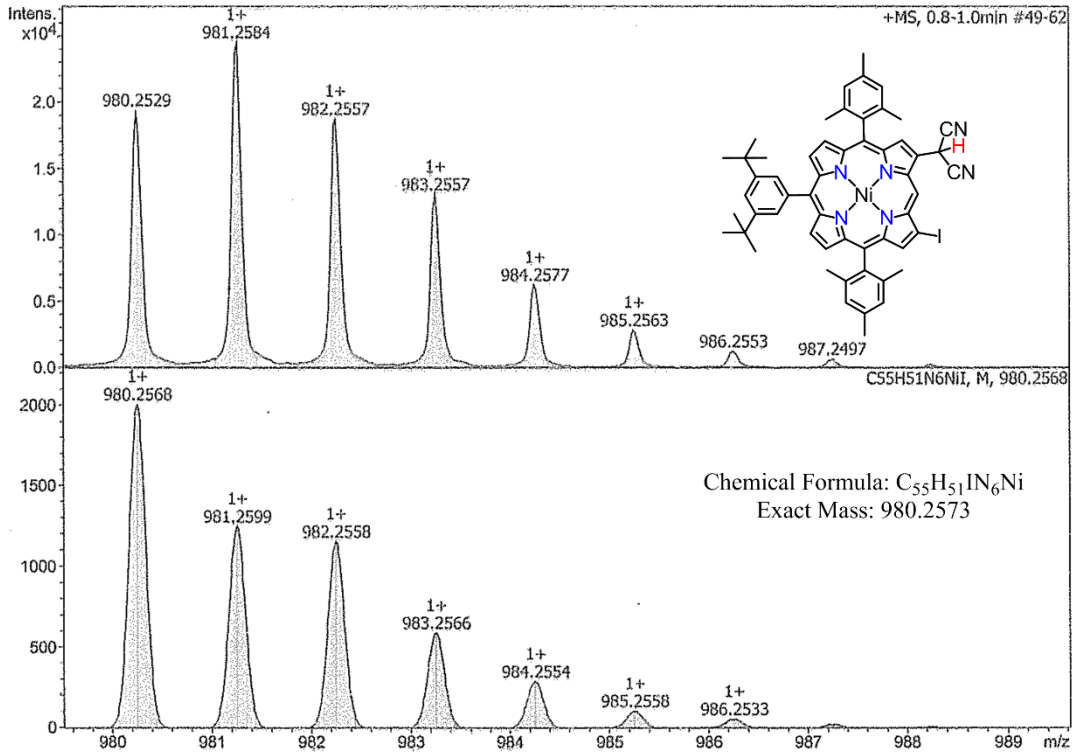

***Figure S12*:** HR-APCI-TOF mass spectra of **23** (top: observed, bottom: simulated).

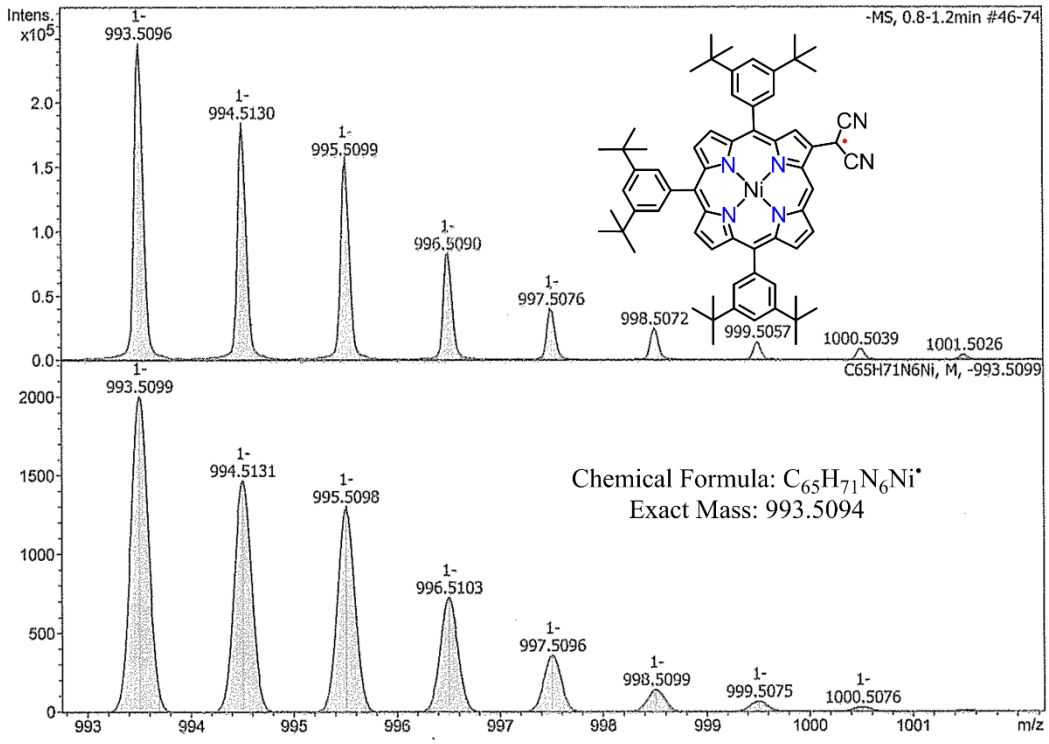

***Figure S13*:** HR-APCI-TOF mass spectra of **24** (top: observed, bottom: simulated).

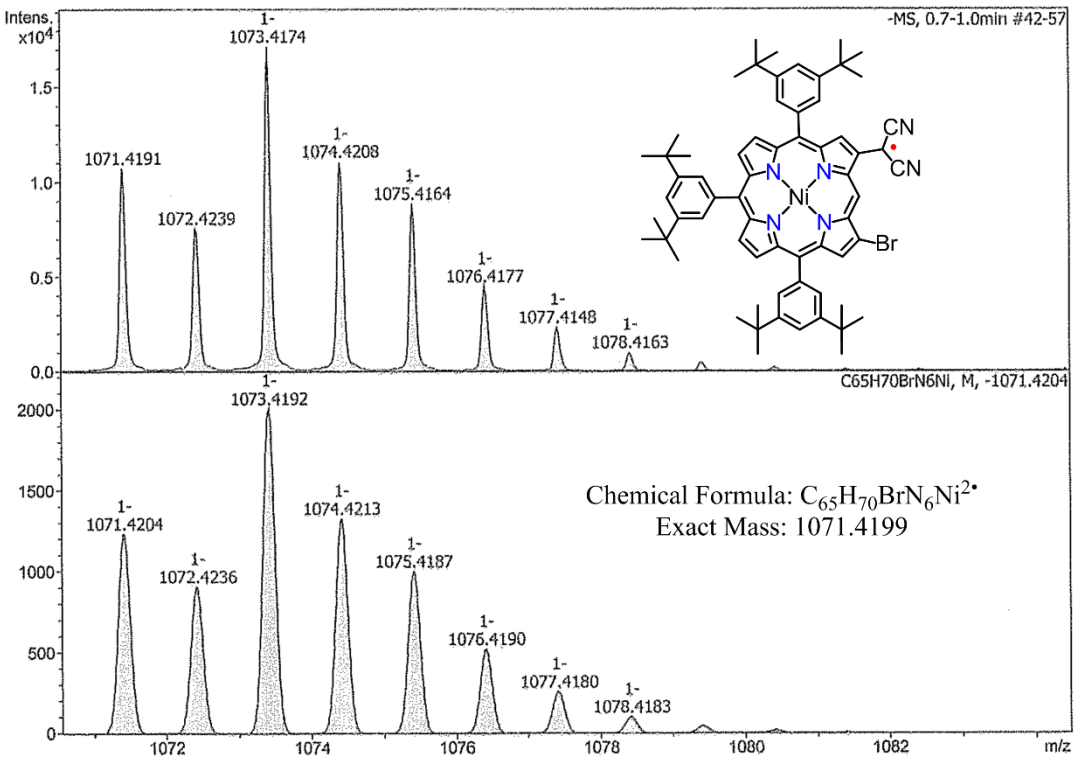

***Figure S14*:** HR-APCI-TOF mass spectra of **25** (top: observed, bottom: simulated).

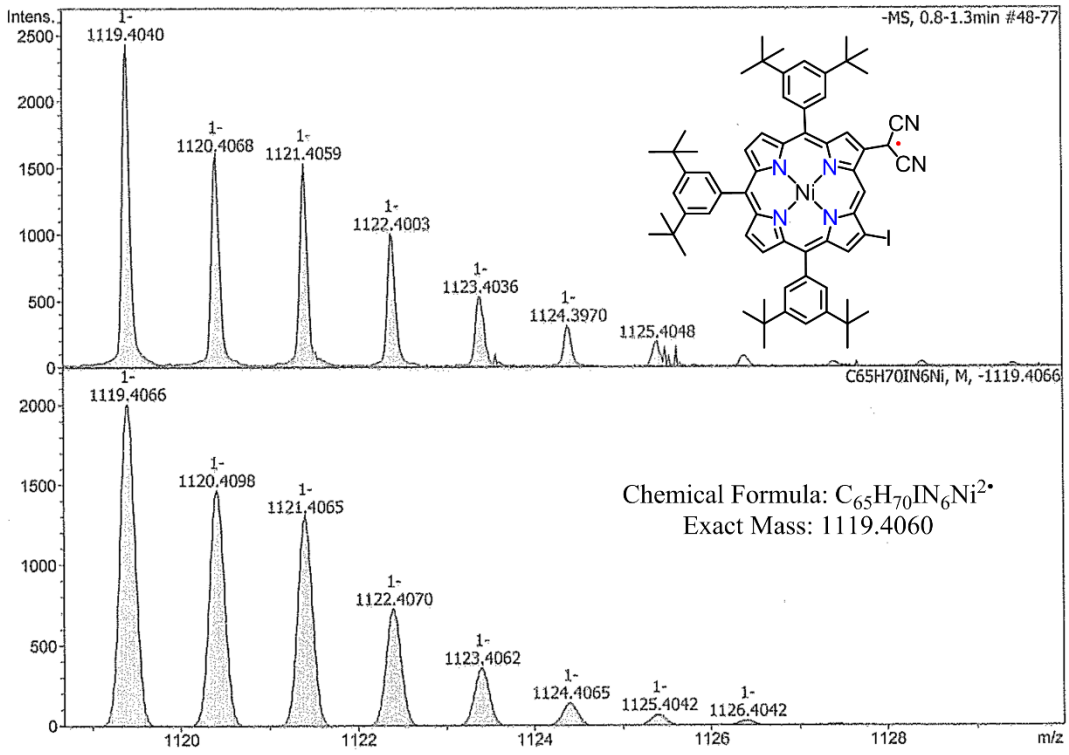

***Figure S15*:** HR-APCI-TOF mass spectra of **26** (top: observed, bottom: simulated).

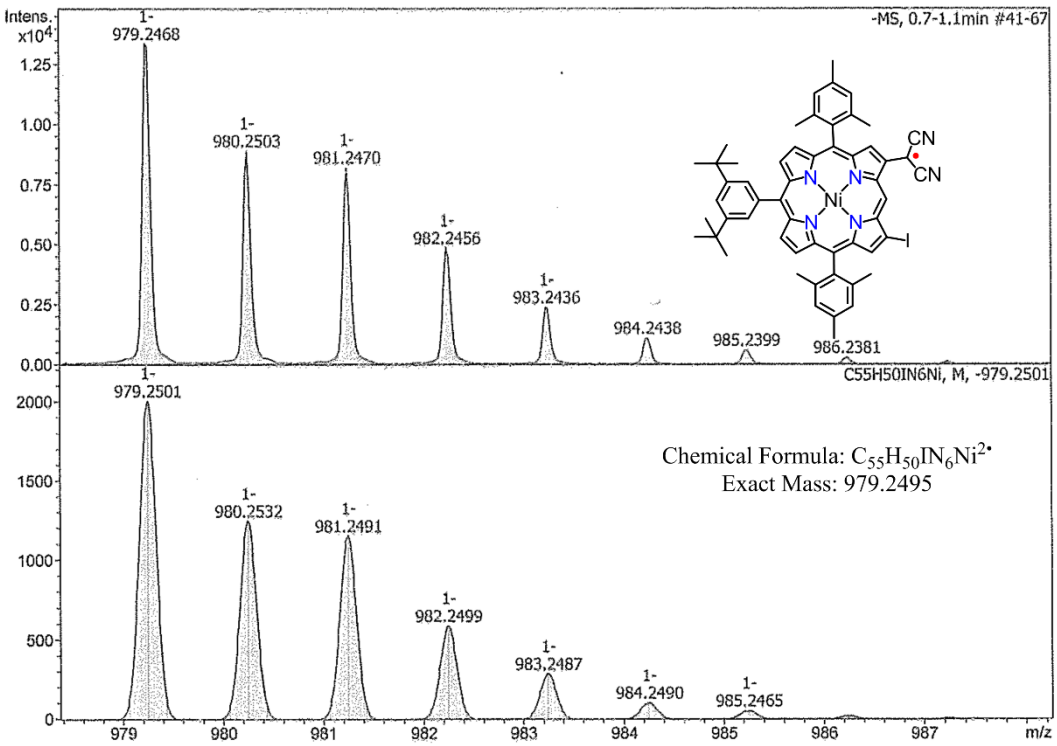

***Figure S16*:** HR-APCI-TOF mass spectra of **27** (top: observed, bottom: simulated).

4. NMR spectral analysis:

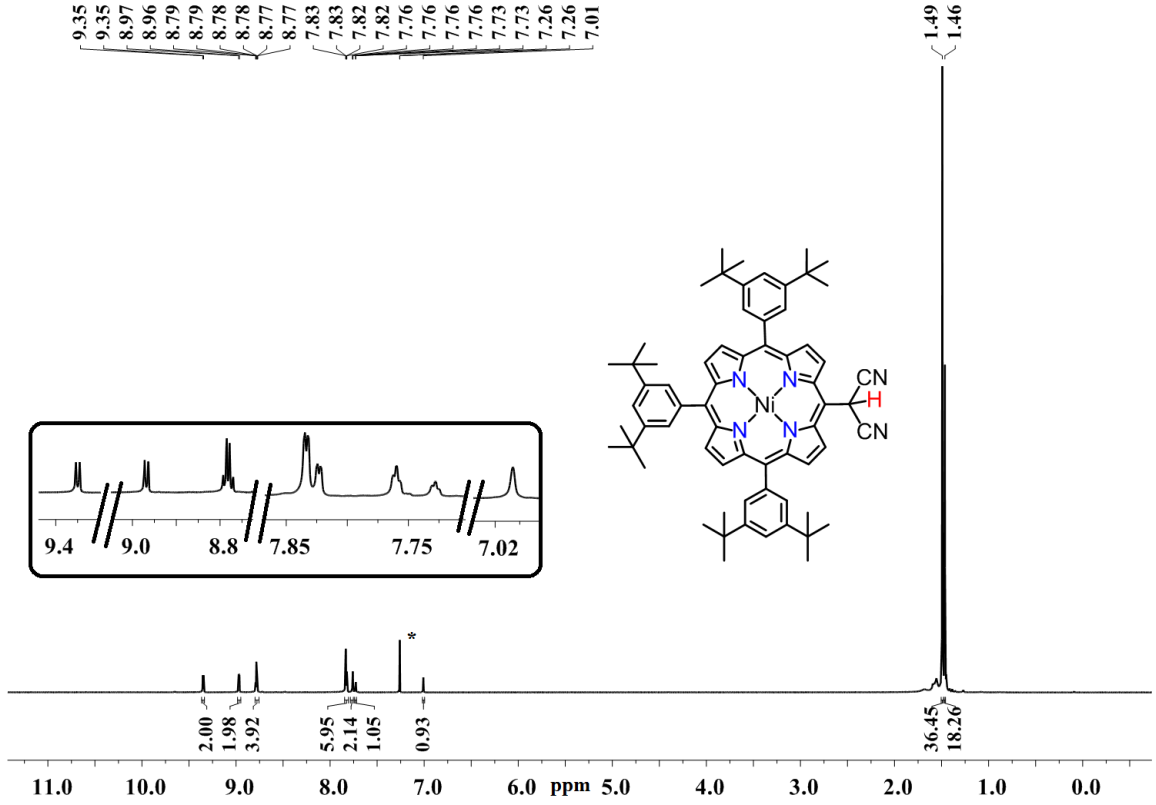

Figure S17: ^{1}H-NMR spectrum of **8** in $CDCl_3$. (* represents residual solvents and impurity grease).

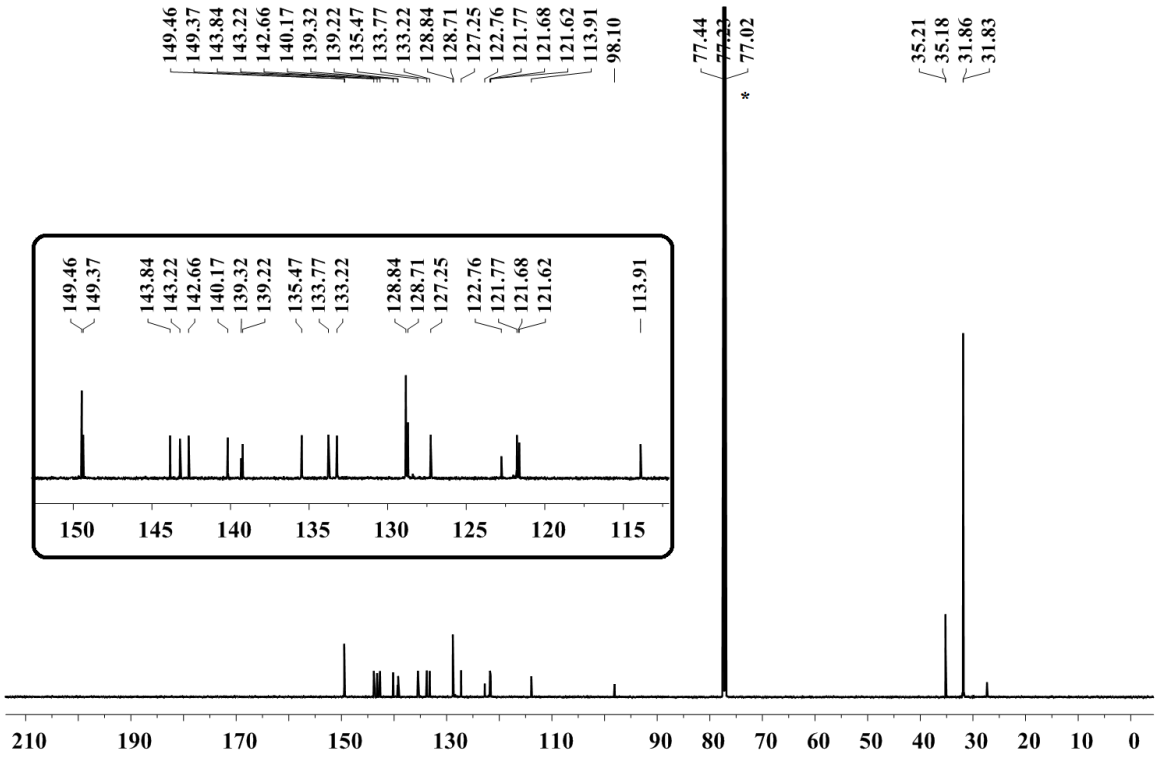

***Figure S18*:** ^{13}C-NMR spectrum of **8** in $CDCl_3$. (* represents residual solvents and impurity grease).

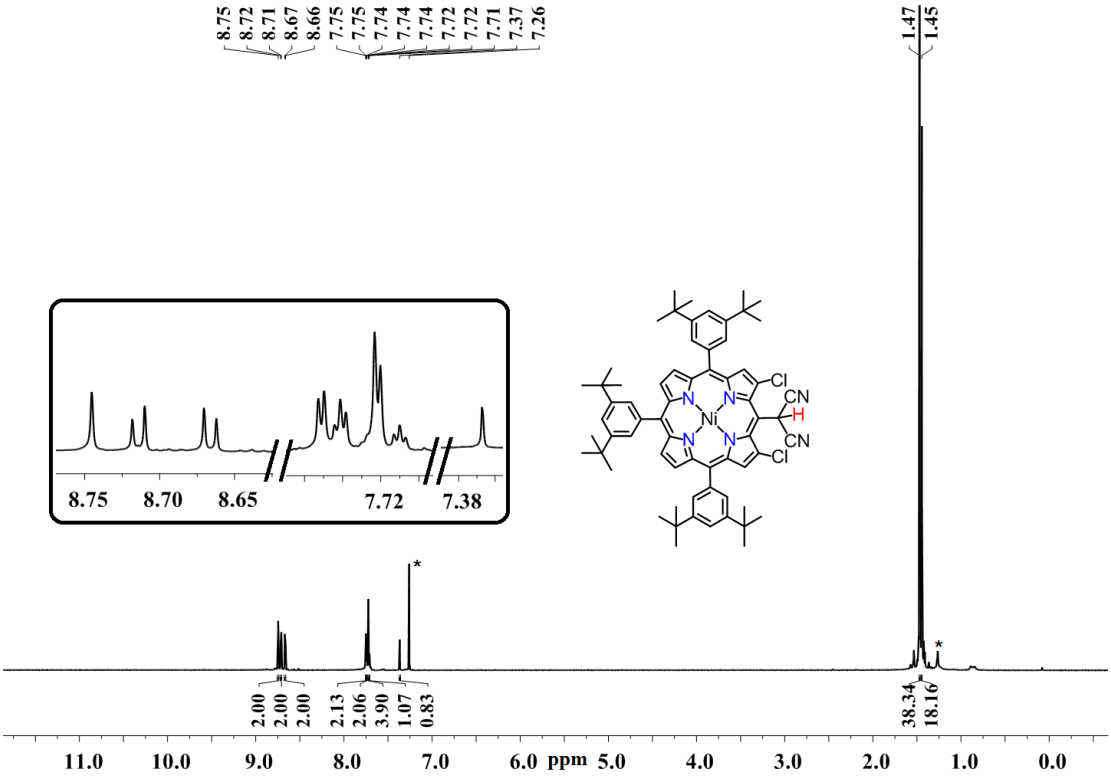

***Figure S19*:** ^{1}H-NMR spectrum of **9** in $CDCl_3$. (* represents residual solvents and impurity grease).

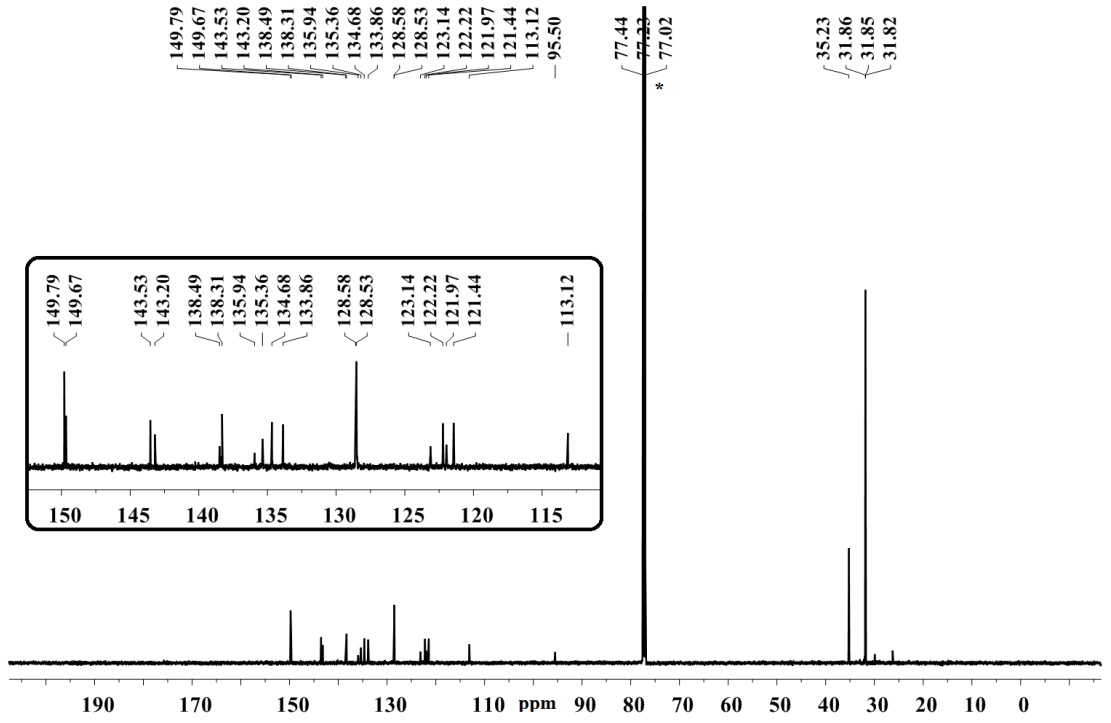

***Figure S20*:** ^{13}C-NMR spectrum of **9** in $CDCl_3$. (* represents residual solvents and impurity grease).

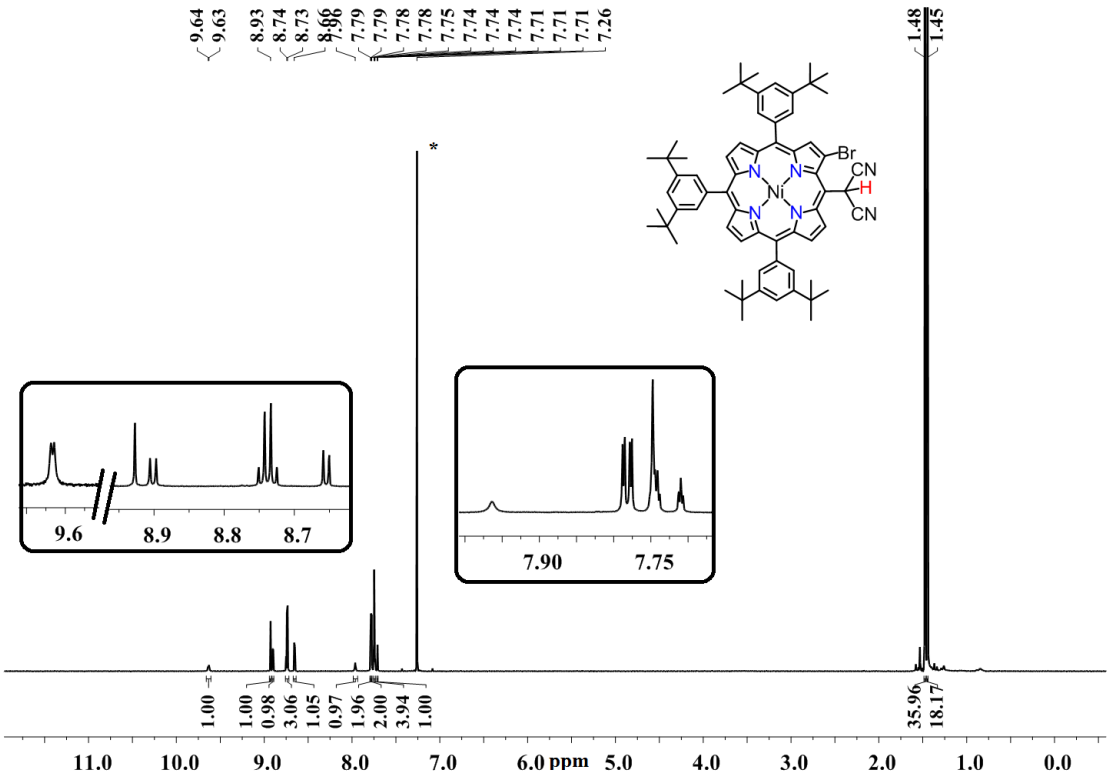

***Figure S21*:** ^{1}H-NMR spectrum of **10** in $CDCl_3$. (* represents residual solvents and impurity grease).

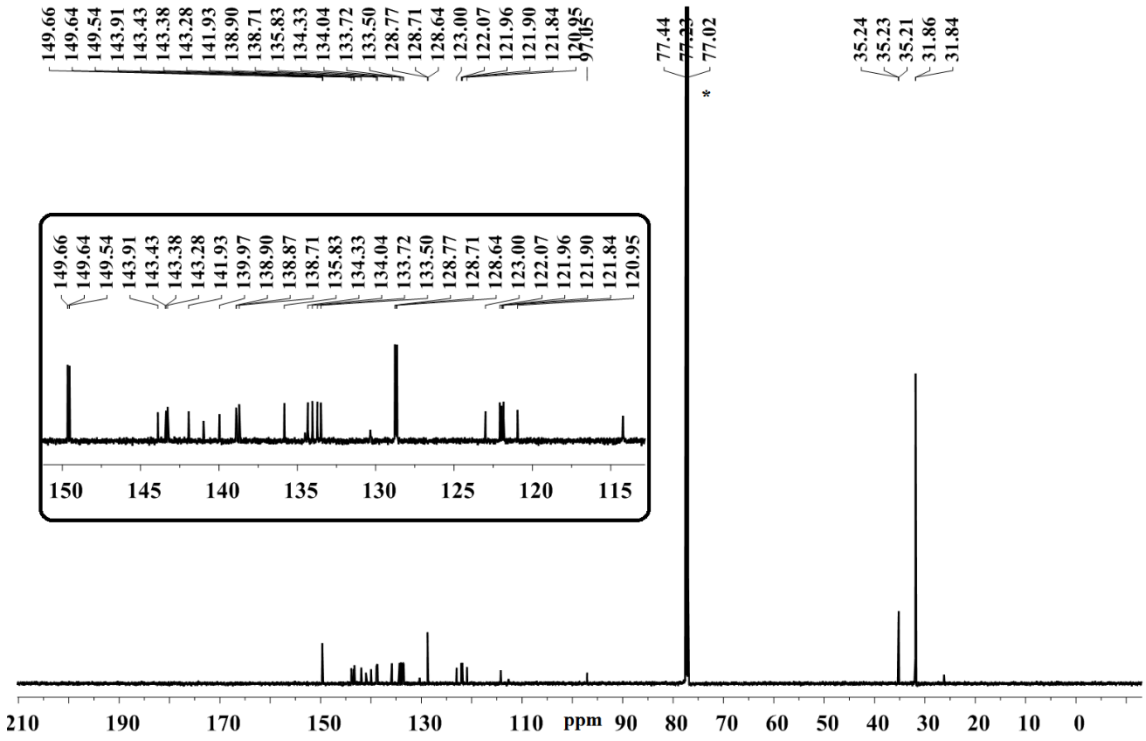

***Figure S22*:** ^{13}C-NMR spectrum of **10** in $CDCl_3$. (* represents residual solvents and impurity grease).

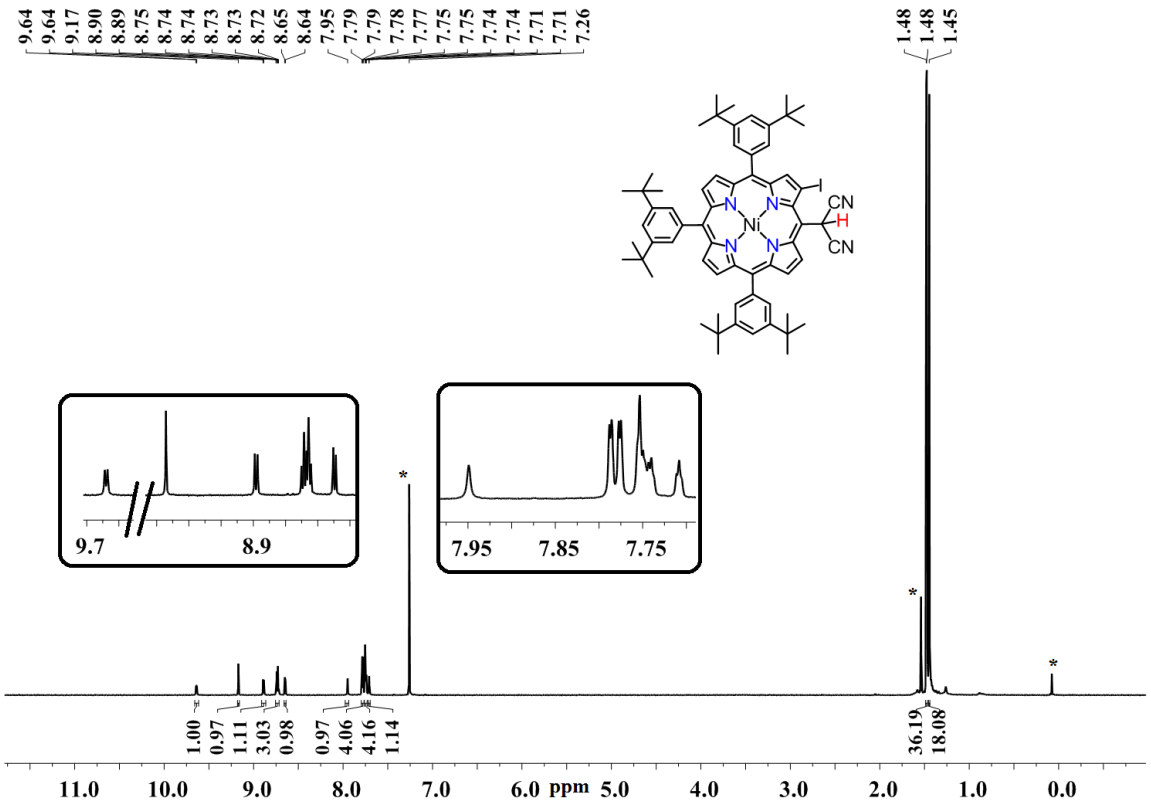

Figure S23: ^{1}H-NMR spectrum of **11** in $CDCl_3$. (* represents residual solvents and impurity grease).

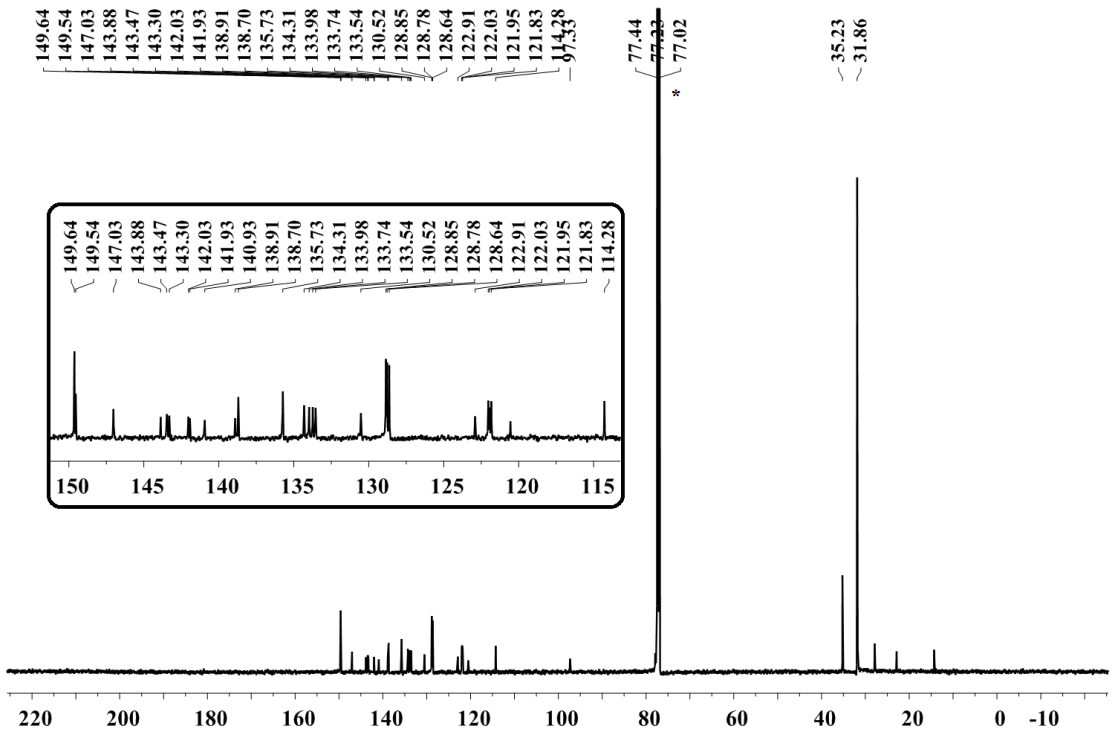

***Figure S24*:** ^{13}C-NMR spectrum of **11** in $CDCl_3$. (* represents residual solvents and impurity grease).

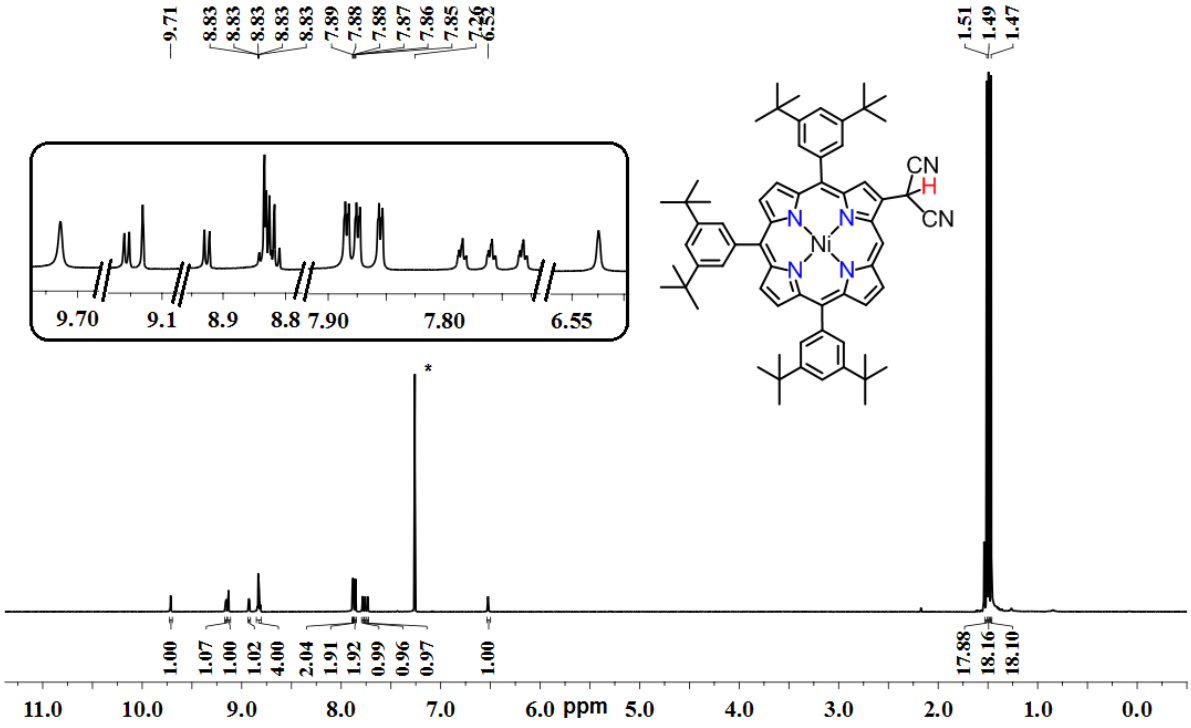

***Figure S25*:** ^{1}H-NMR spectrum of **20** in $CDCl_3$. (* represents residual solvents and impurity grease).

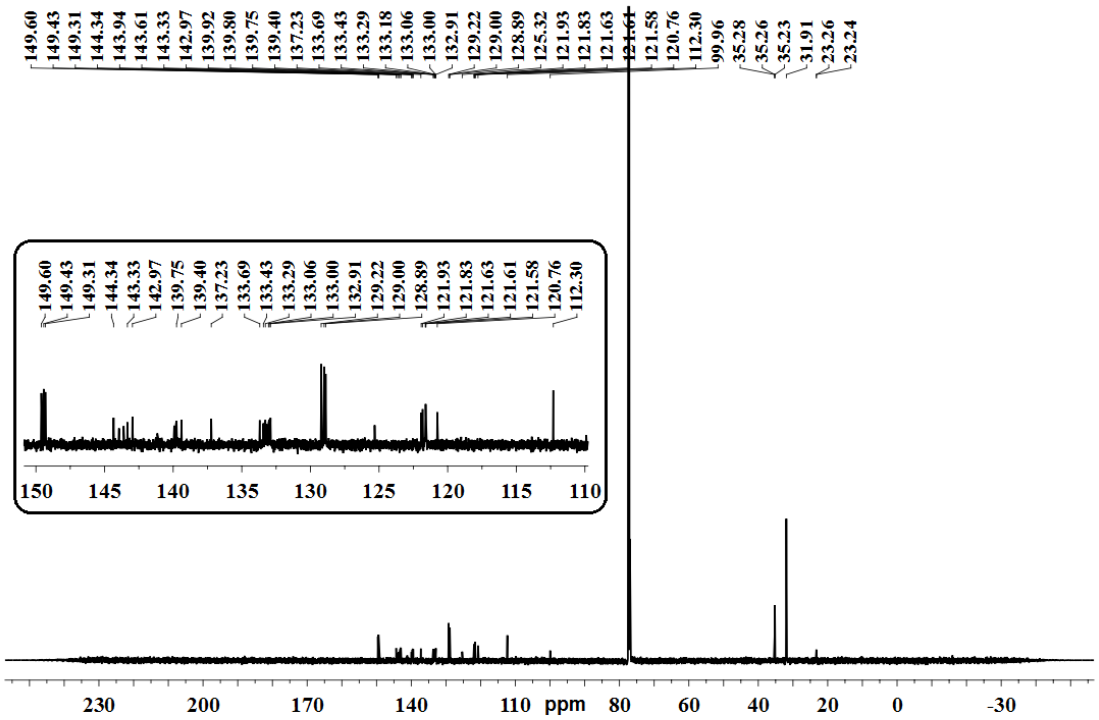

***Figure S26*:** ^{13}C-NMR spectrum of **20** in $CDCl_3$. (* represents residual solvents and impurity grease).

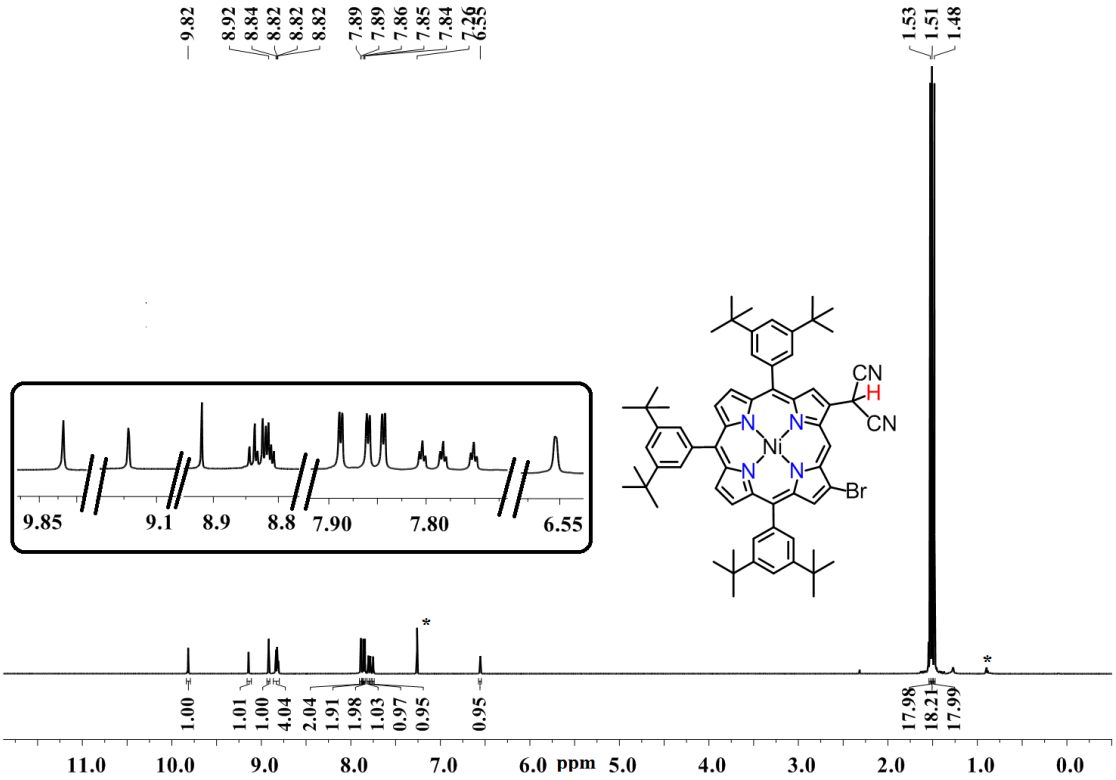

***Figure S27*:** ^{1}H-NMR spectrum of **21** in $CDCl_3$. (* represents residual solvents and impurity grease).

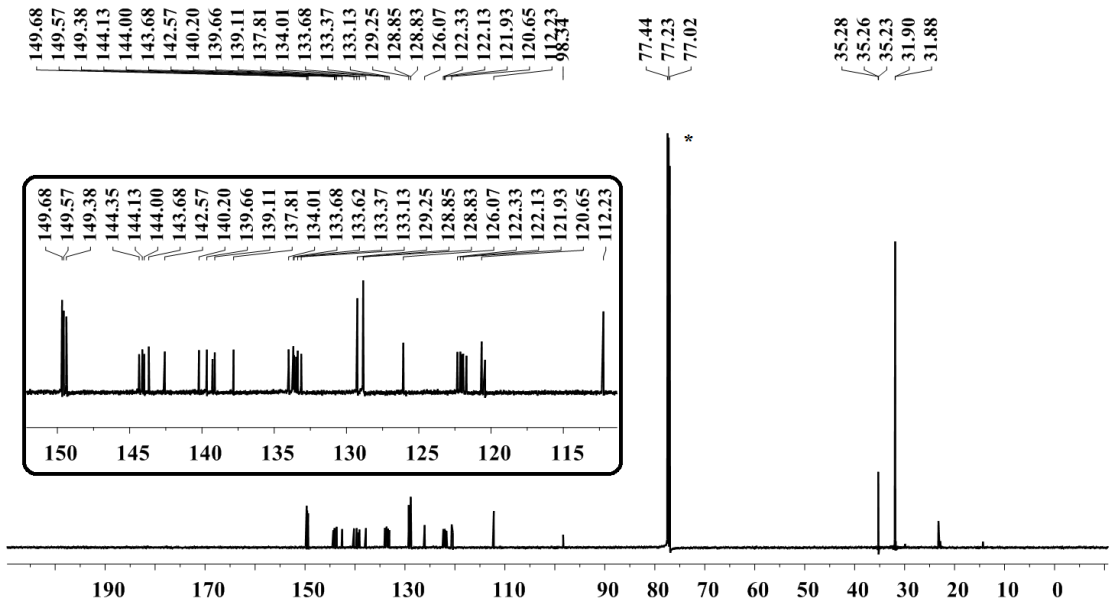

***Figure S28*:** ^{13}C-NMR spectrum of **21** in $CDCl_3$. (* represents residual solvents and impurity grease).

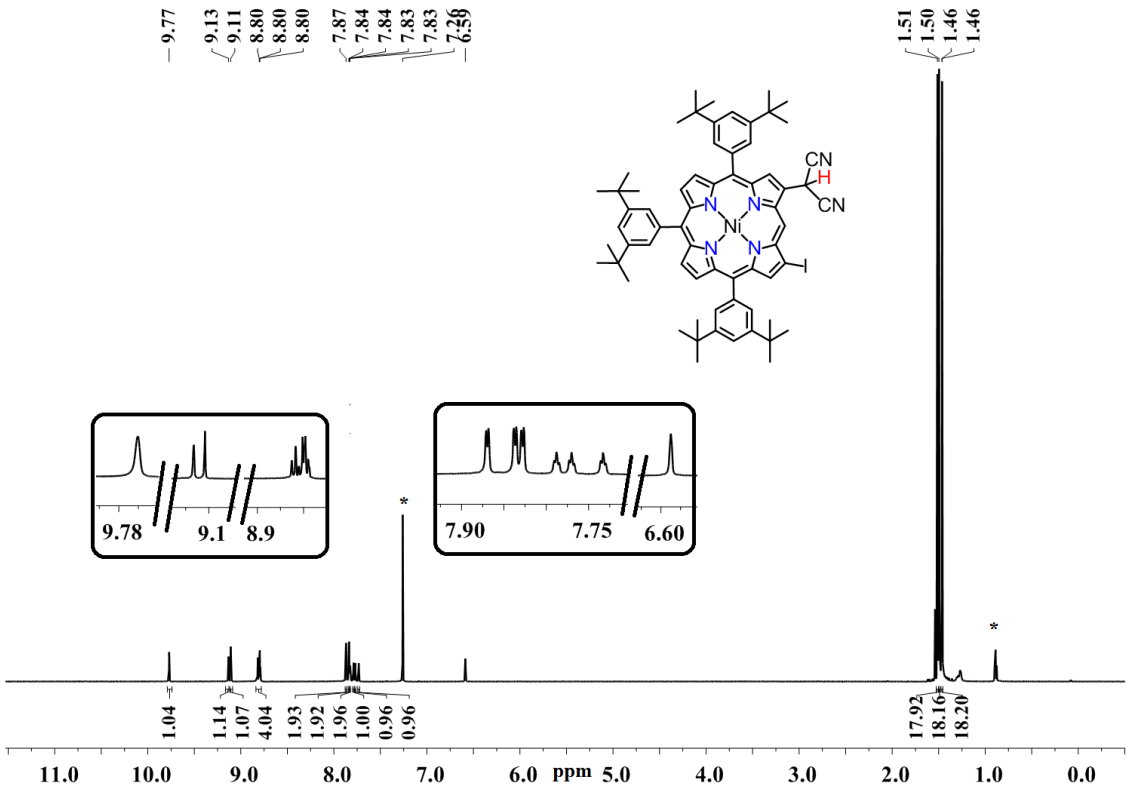

***Figure S29*:** ^{1}H-NMR spectrum of **22** in $CDCl_3$. (* represents residual solvents and impurity grease).

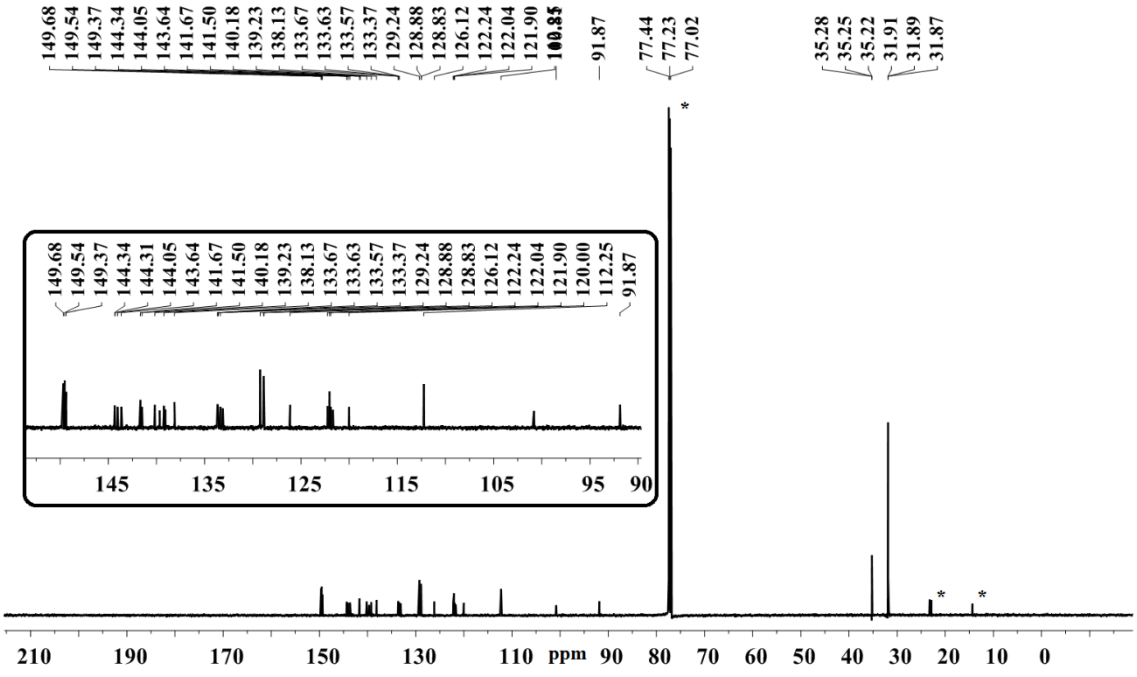

***Figure S30*:** ^{13}C-NMR spectrum of **22** in $CDCl_3$. (* represents residual solvents and impurity grease).

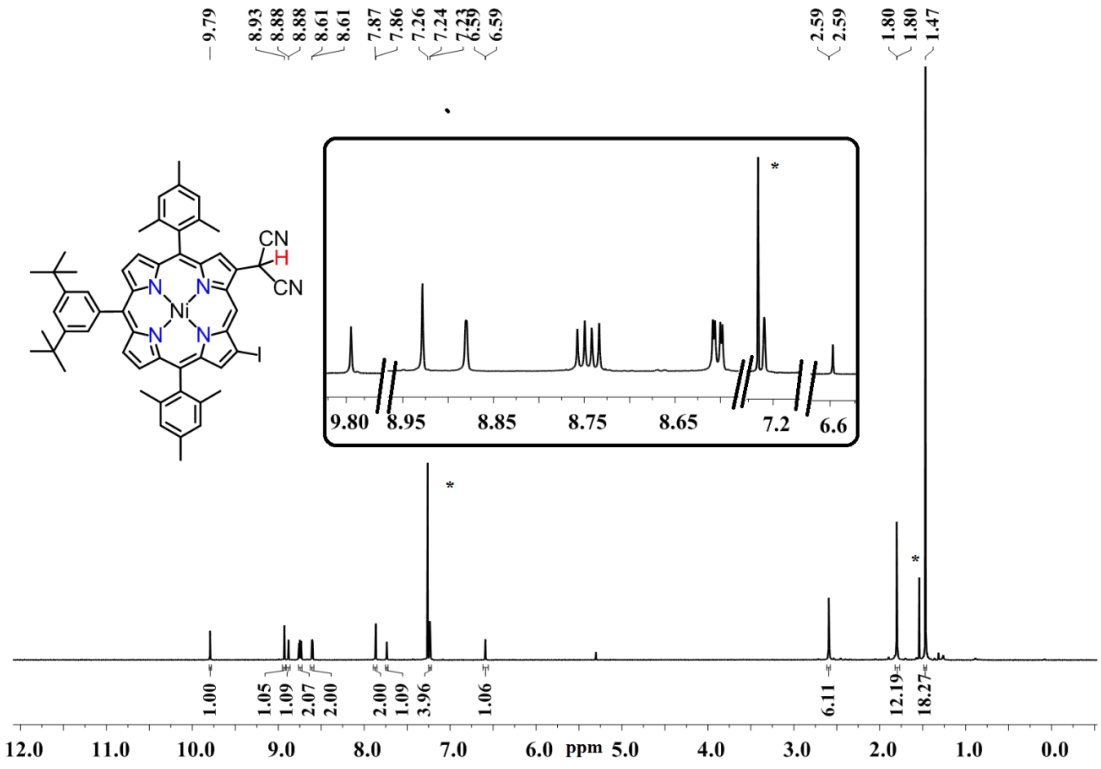

***Figure S31*:** ^{1}H-NMR spectrum of **23** in $CDCl_3$. (* represents residual solvents and impurity grease).

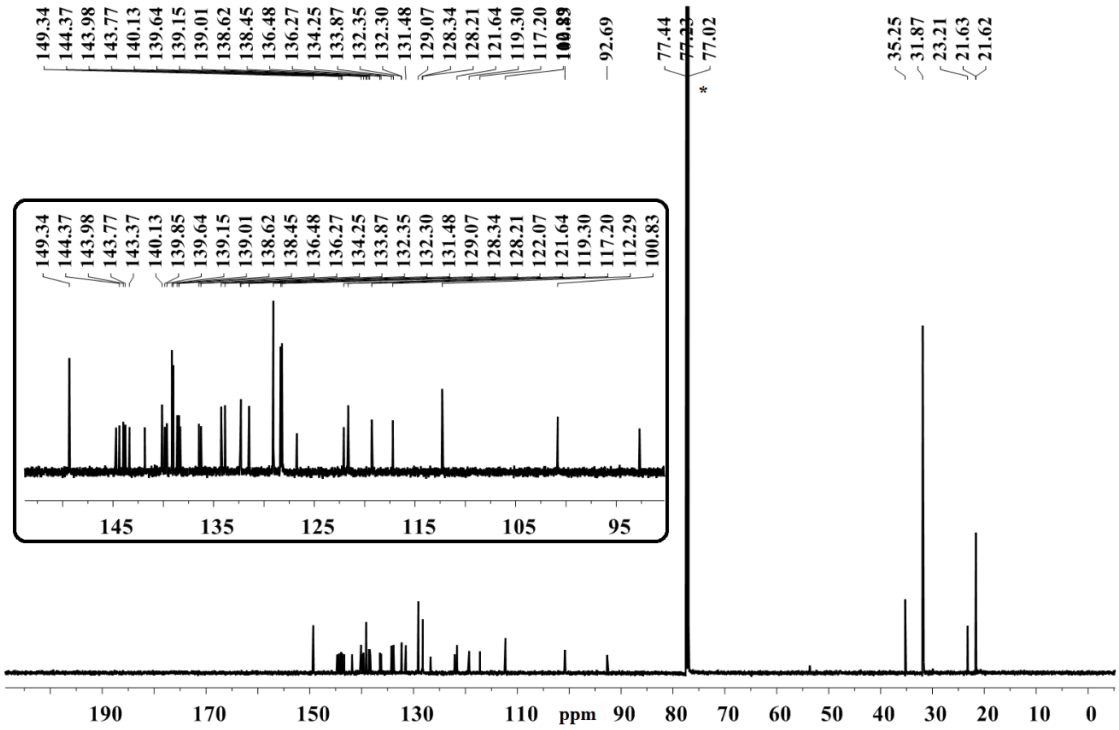

***Figure S32*:** ^{13}C-NMR spectrum of **23** in $CDCl_3$. (* represents residual solvents and impurity grease).

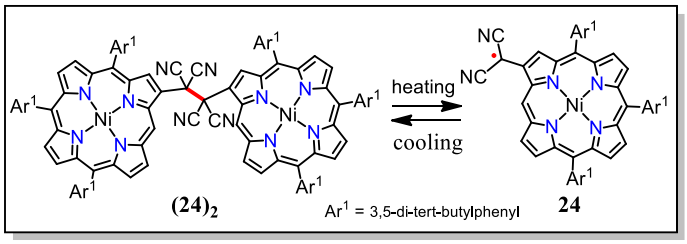

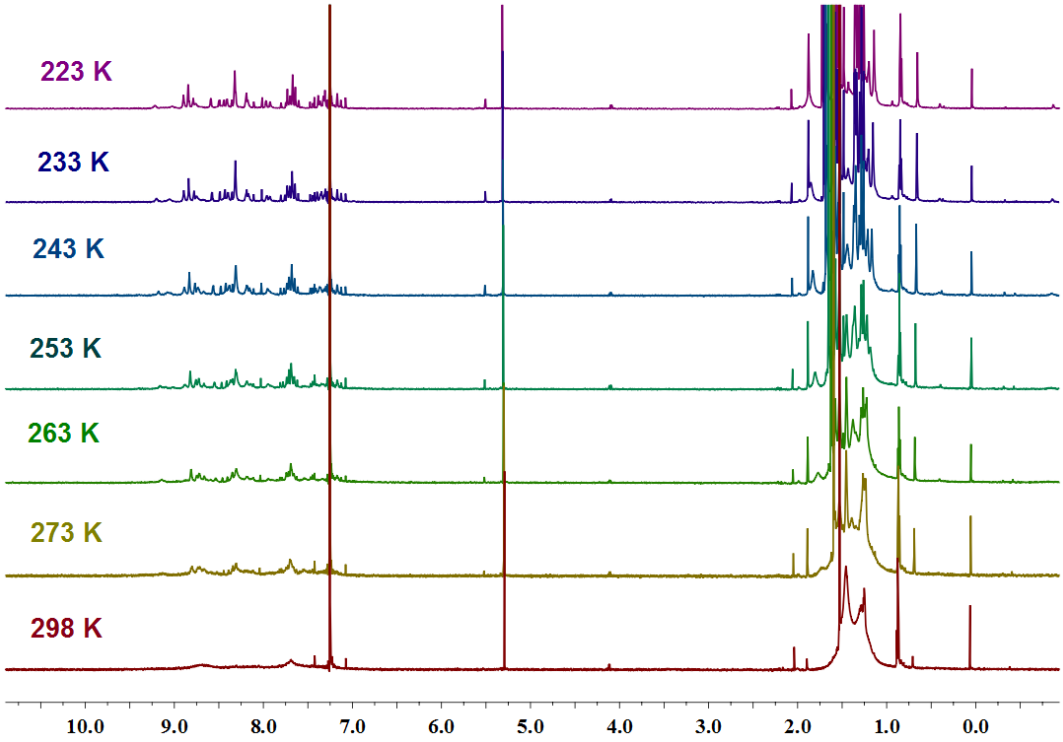

***Figure S33*:** LT-^{1}H-NMR spectrum of **(24)$_2$** in $CDCl_3$.

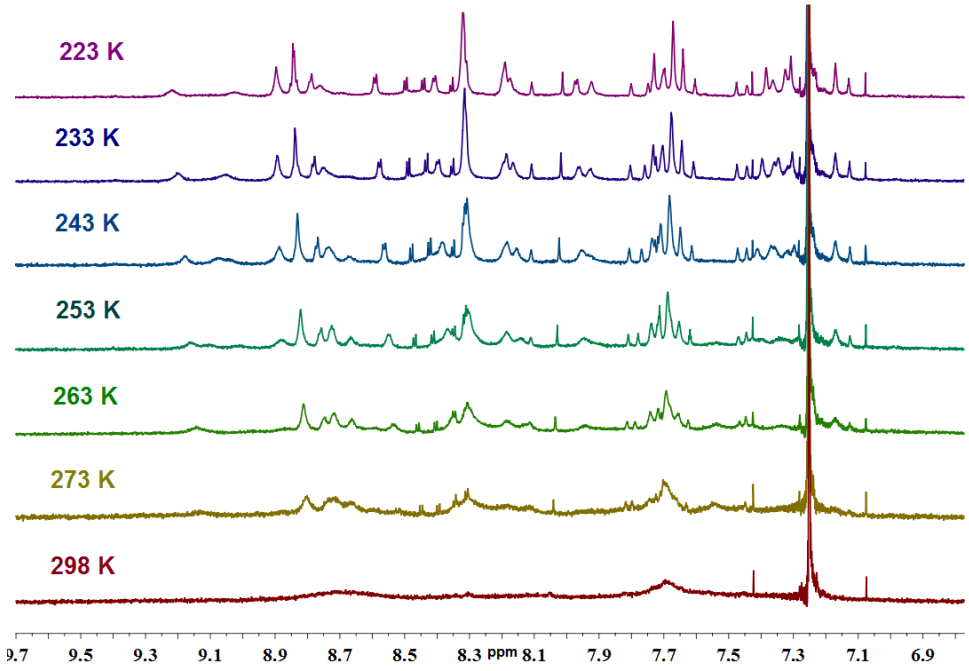

***Figure S34*:** LT-^{1}H-NMR expanded spectrum of **(24)$_2$** in $CDCl_3$.

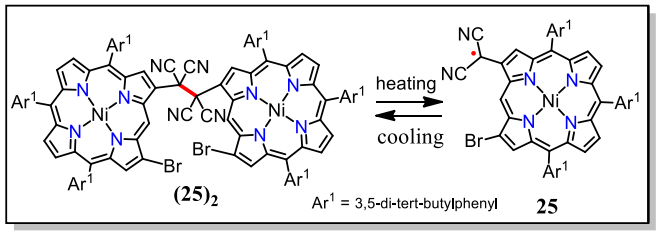

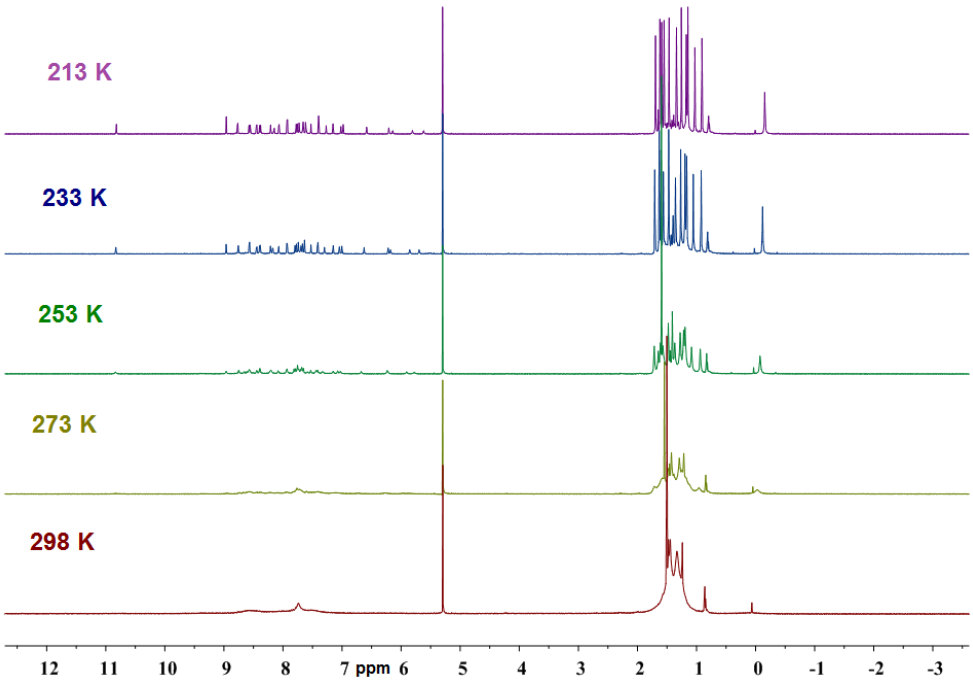

***Figure S35*:** LT-^{1}H-NMR spectrum of **$(25)_2$** in CD_2Cl_2.

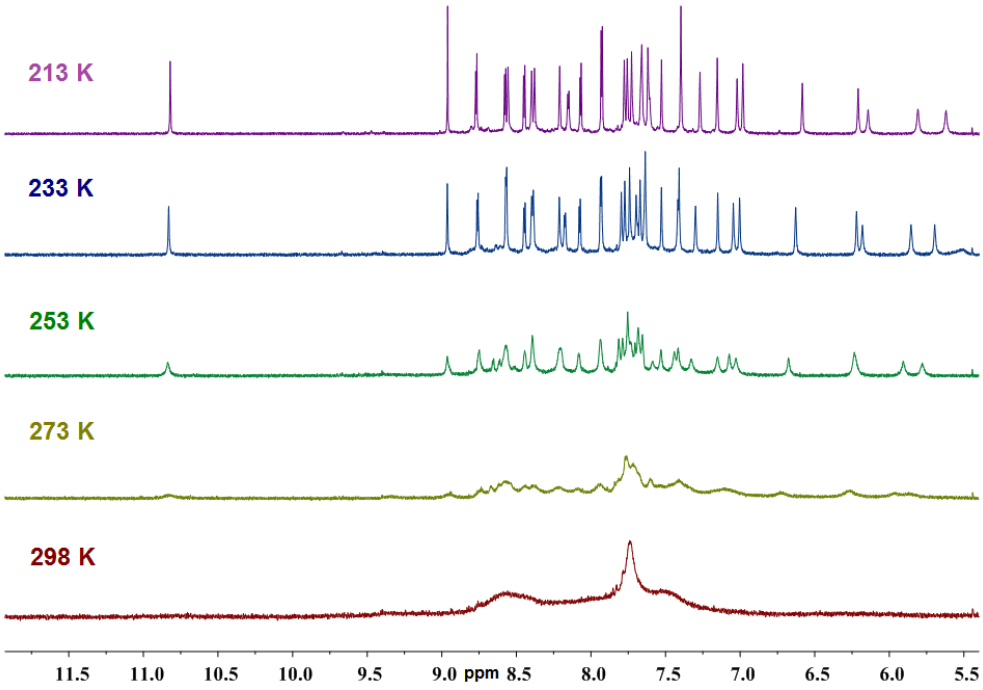

***Figure S36*:** LT-^{1}H-NMR expanded spectrum of **$(25)_2$** in CD_2Cl_2.

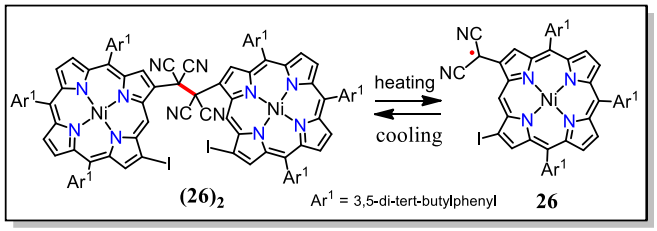

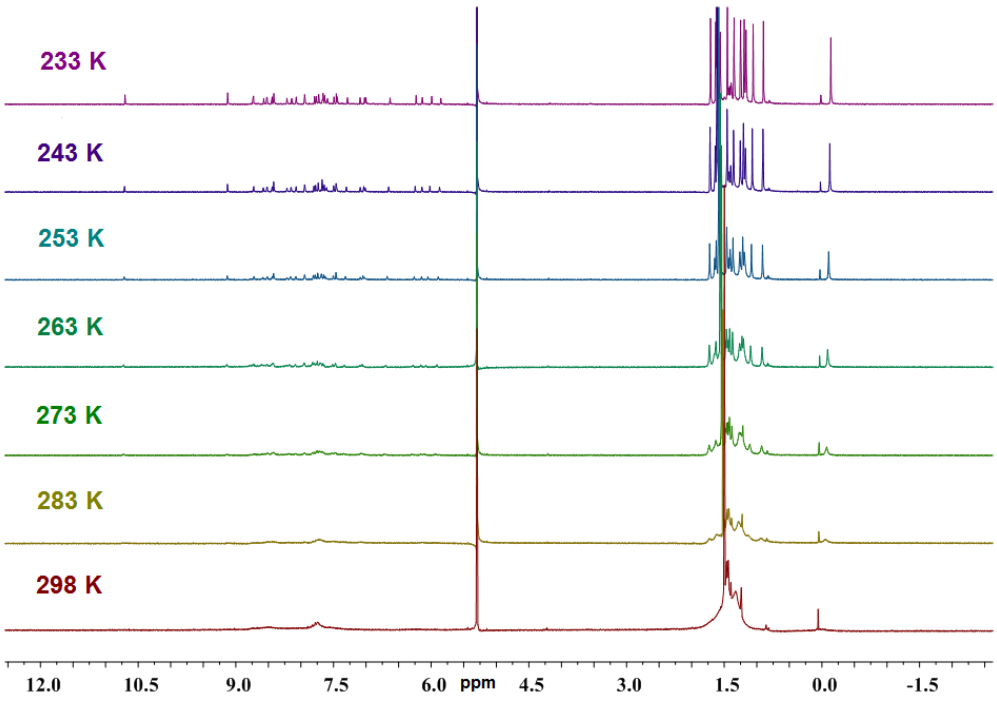

***Figure S37*:** LT-^{1}H-NMR spectrum of **(26)$_2$** in CD_2Cl_2.

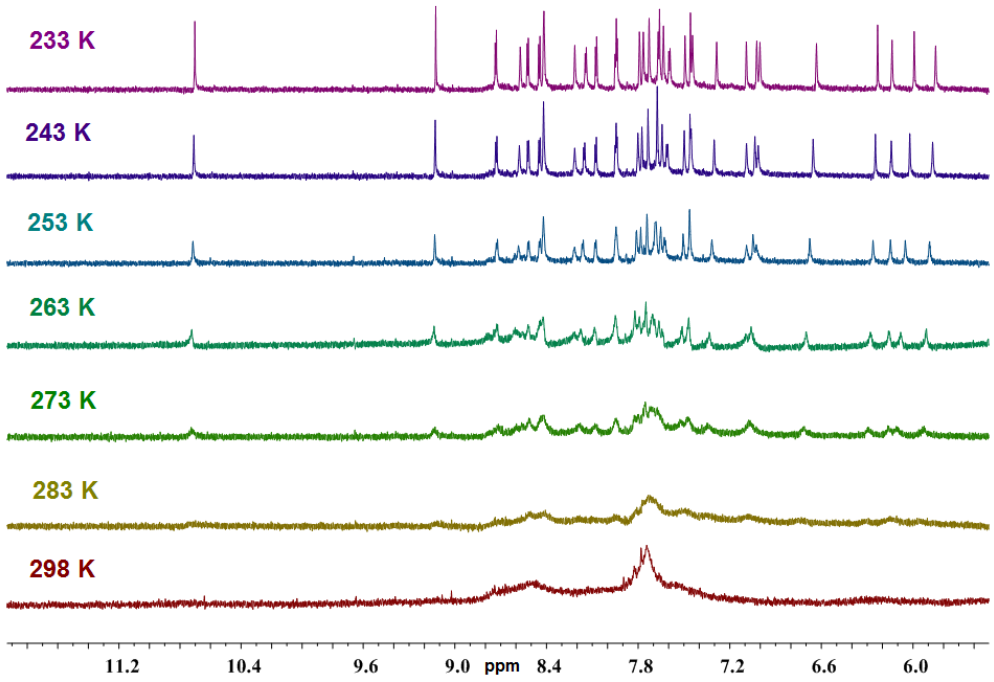

***Figure S38*:** LT-^{1}H-NMR expanded spectrum of **(26)$_2$** in CD_2Cl_2.

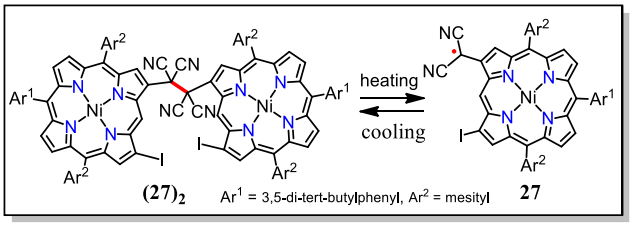

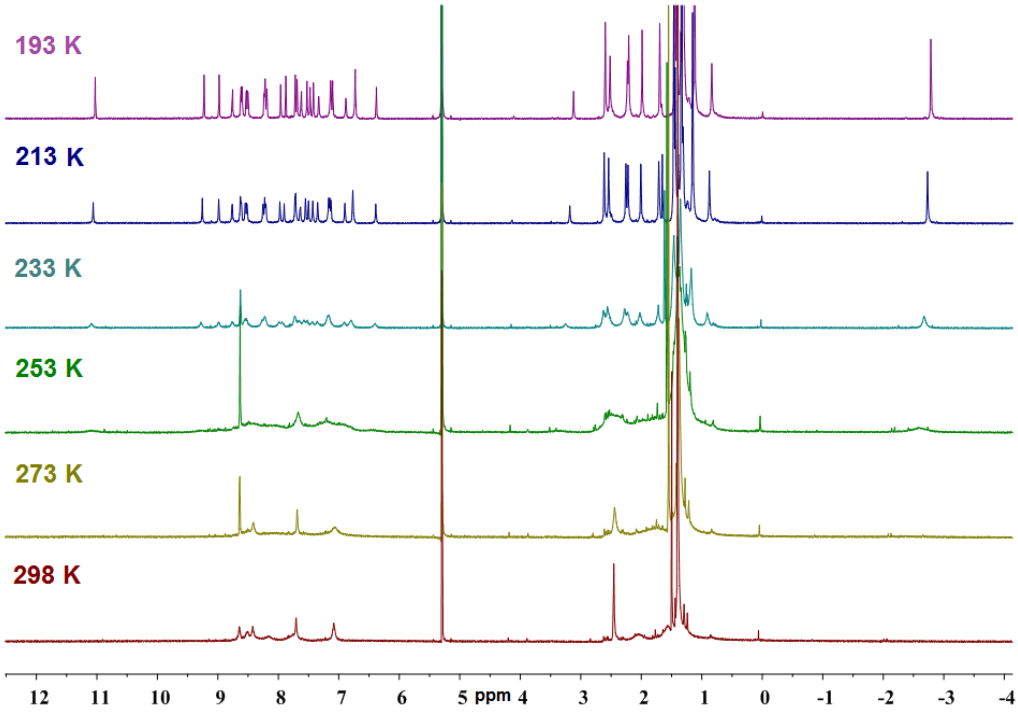

***Figure S39*:** LT-^{1}H-NMR spectrum of **(27)$_2$** in CD_2Cl_2.

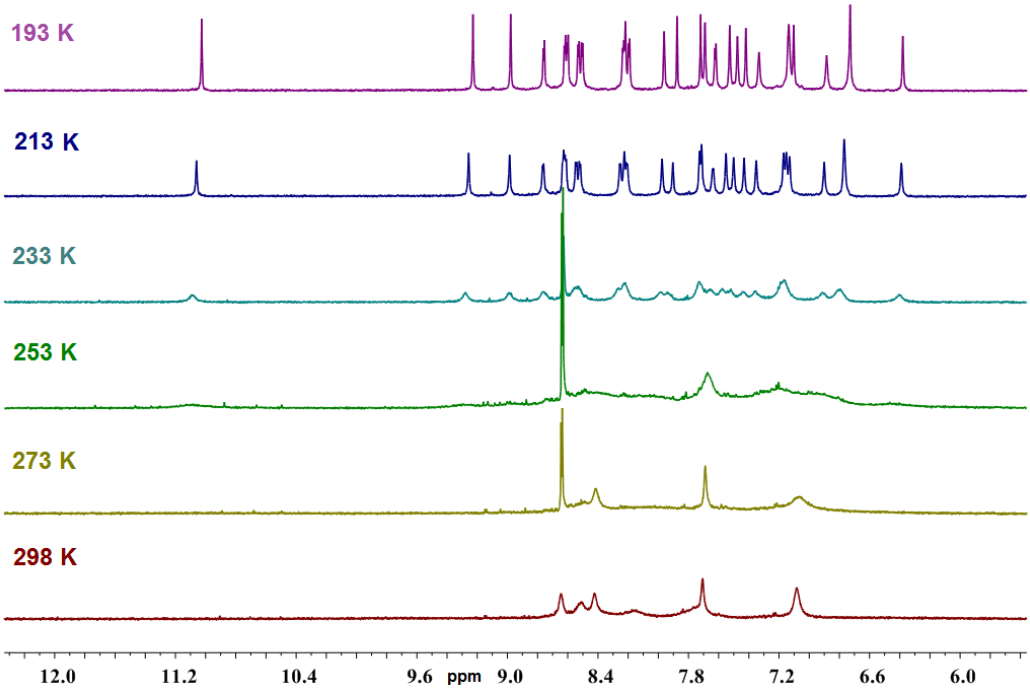

***Figure S40*:** LT-^{1}H-NMR expanded spectrum of **(27)$_2$** in CD_2Cl_2.

5. Single crystal X-ray structure and analysis:

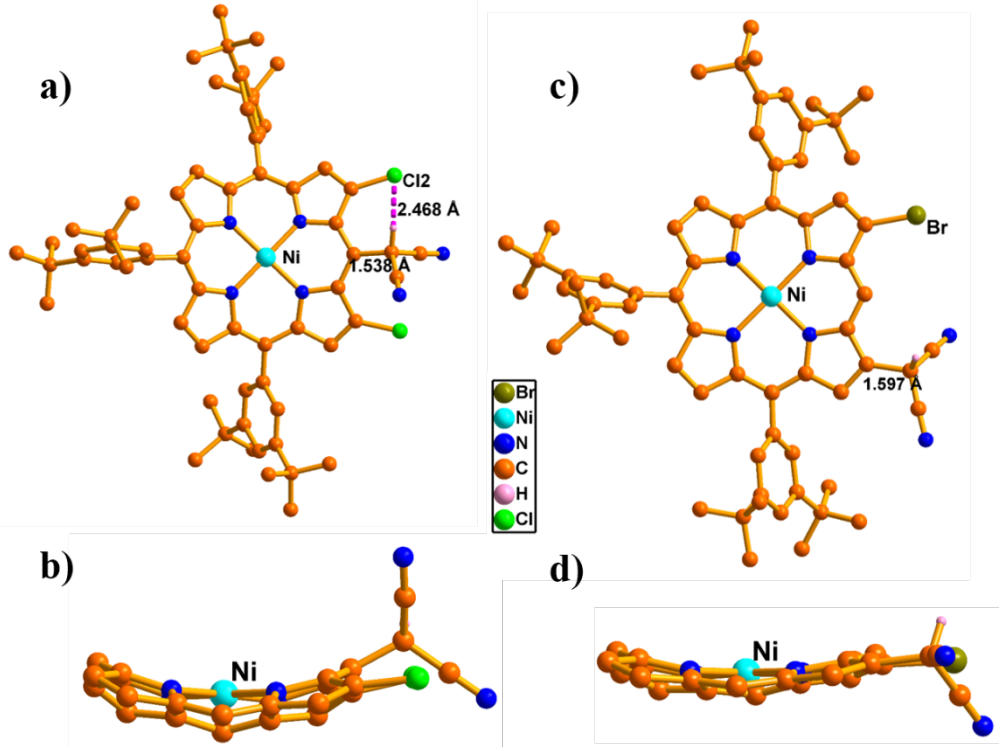

***Figure S41*:** Single crystal X-ray structure of **9** and **21**. a), c) Top view and b), d) side view and the peripheral hydrogen atoms, the *meso*-aryl groups in side view are omitted for clarity.

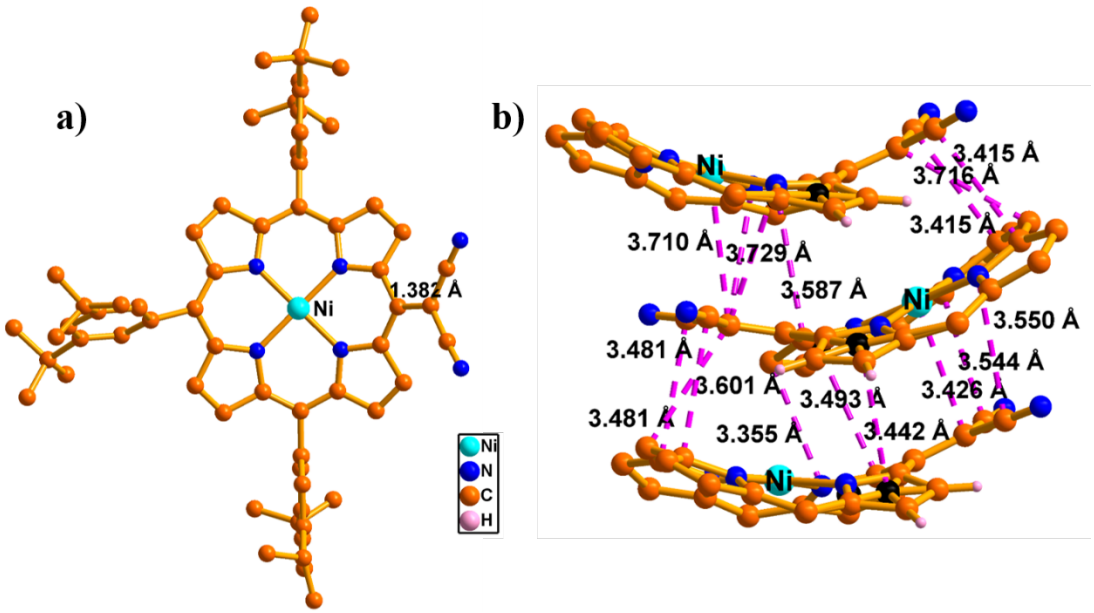

***Figure S42*:** Single crystal X-ray structure of **12**. a) Top view, b) close interaction between radical pairs. The *meso*-aryl groups in b) and the peripheral hydrogen atoms in a) and b) are omitted for clarity.

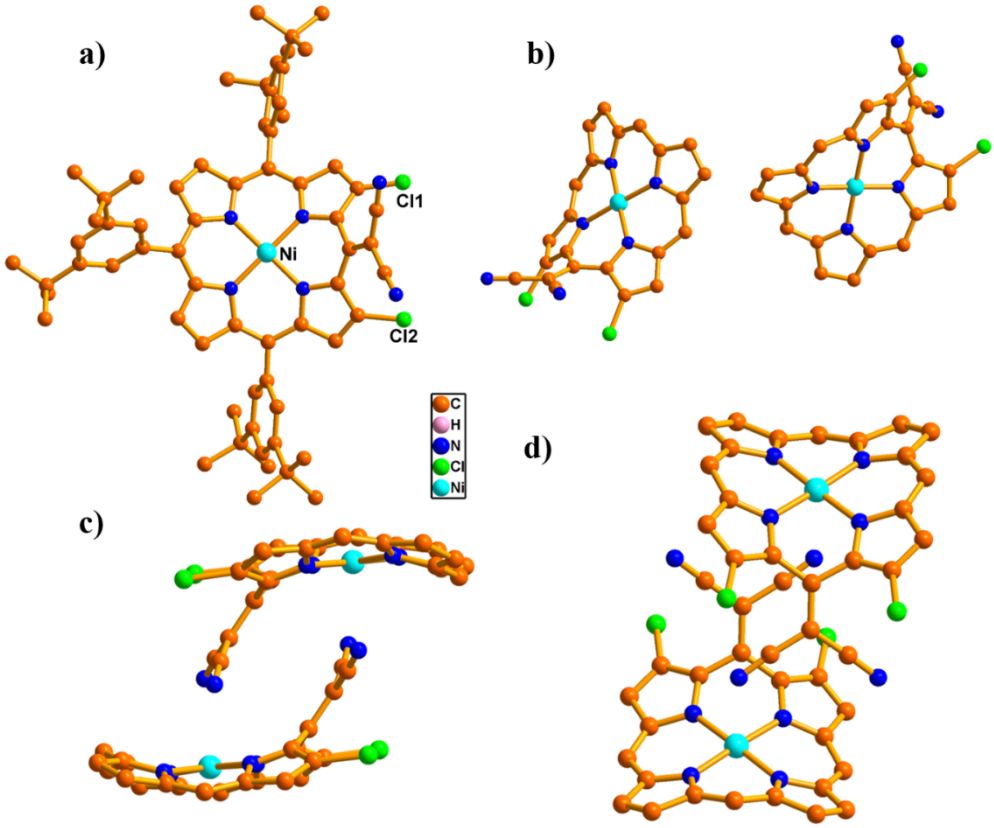

***Figure S43*:** Single crystal X-ray structure of **13**. a) Top view, b) molecule present in the unit cell, c) and d) close interaction between radical pairs. The *meso*-aryl groups in b), c) & d) and the peripheral hydrogen atoms in a)-d) are omitted for clarity.

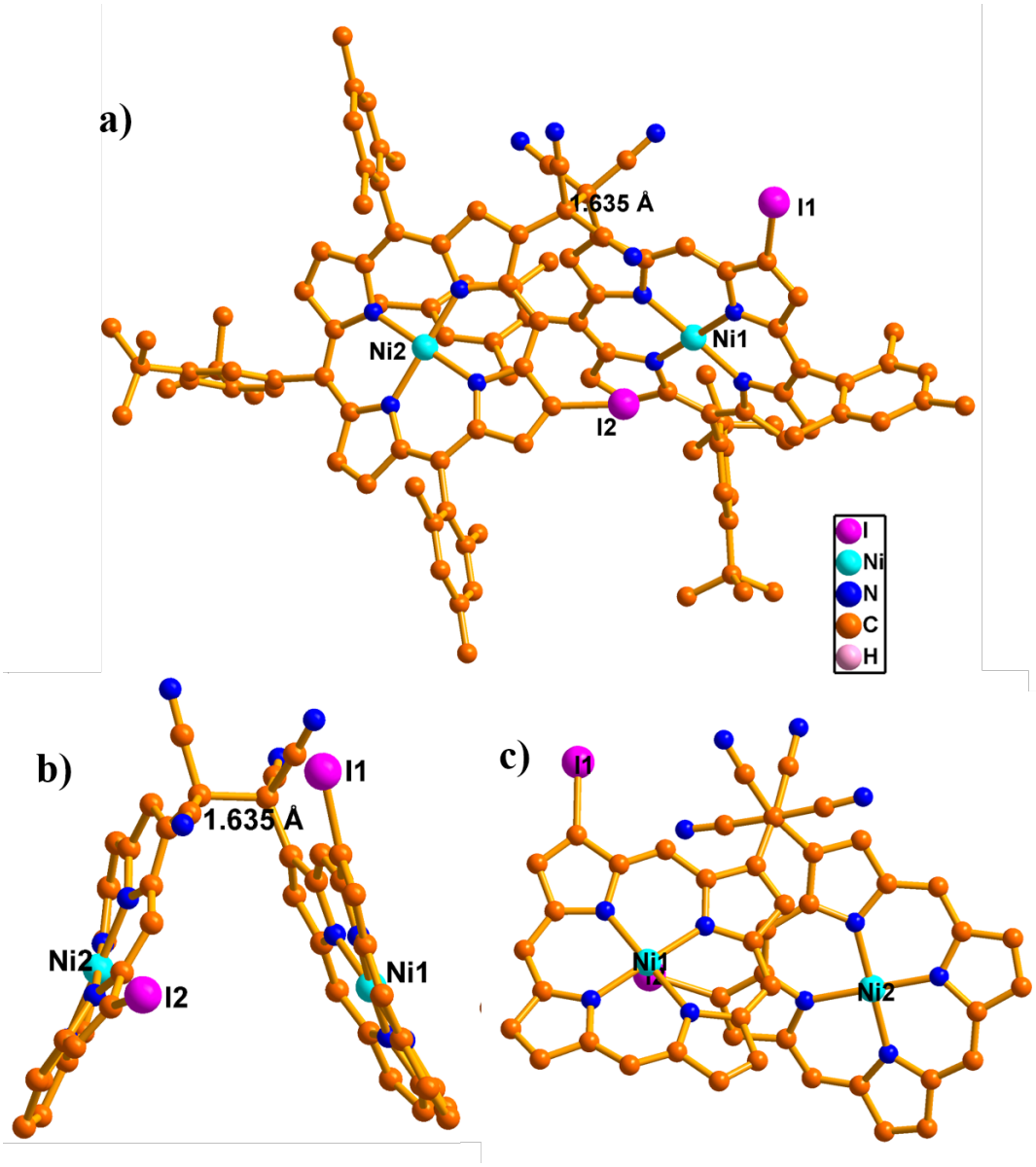

***Figure S44*:** Single crystal X-ray structure of **(27)$_2$**. a), c) Top view and b) side view and the peripheral hydrogen atoms in a), b) and c), the *meso*-aryl groups in b) and d) are omitted for clarity.

Table S1: Crystal data for **9** and **21**:

Crystal parameters	**9**	**21**
Formula	$C_{65.2}H_{70.2}Cl_{2.6}N_6NiO_{0.4}$	$C_{66}H_{73}BrCl_2N_6Ni$
M/g mol^{-1}	1095.14	1159.82
T/K	93	93
Crystal dimensions/mm^3	0.34 × 0.24 × 0.05	0.52 × 0.35 × 0.10
Crystal system	monoclinic	monoclinic
Space group	*C*2/*c*	$P2_1/n$
a/Å	40.0152(8)	11.3078(7)
b/Å	12.8645(3)	21.1896(11)
c/Å	23.9666(6)	25.4949(17)
α/°	90	90
β/°	102.621(2)	100.698(3)
γ/°	90	90
V/Å^3	12039.3(5)	6002.6(6)
Z	8	4
ρ_{calcd}/mg m^{-3}	1.208	1.283
μ/mm^{-1}	1.864	2.403
F(000)	4630.0	2432.0
Reflns. collected	41466	41753
Indep.reflns. [*R*(int)]	11807 [R_{int} = 0.0424, R_{sigma} = 0.0437]	11695 [R_{int} = 0.0246, R_{sigma} = 0.0192]
Max/min transmission	1.000/0.653	1.000/0.817
Data/restraints /parameters	11807/189/811	11695/324/771
GOF on F^2	1.025	1.034
Final R indices[$I > 2\sigma(I)$]	R_1 = 0.0719, wR_2 = 0.2039	R_1 = 0.0819, wR_2 = 0.2541
R indices (all data)	R_1 = 0.0851, wR_2 = 0.2171	R_1 = 0.0863, wR_2 = 0.2591
Largest diff peak and hole [e Å^{-3}]	1.31/-0.71	1.75 and -2.46
CCDC	1900738	1900741

Table S2: Crystal data for **12**, **13** and **(27)$_2$**:

Crystal parameters	**12**	**13**	**(27)$_2$**
Formula	$C_{201}H_{227}N_{18}Ni_3$	$C_{133}H_{144}Cl_{10}N_{12}Ni_2$	$C_{110}H_{100}I_2N_{12}Ni_2$
M/g mol^{-1}	3071.08	2382.51	1961.2
T/K	93	93	93
Crystal dimensions/mm^3	0.20 × 0.11 × 0.01	0.15 × 0.12 × 0.02	0.15 × 0.08 × 0.02
Crystal system	monoclinic	triclinic	triclinic
Space group	*Cm*	*P*-1	*P*-1
a/Å	24.352(5)	14.2135(4)	16.4887(2)
b/Å	26.043(4)	17.6443(8)	17.6517(2)
c/Å	16.592(3)	26.4127(11)	18.6605(2)
α/°	90	76.353(4)	82.3860(10)
β/°	122.777(3)	82.030(3)	73.3520(10)
γ/°	90	78.350(3)	69.5290(10)
V/Å^3	8847(3)	6275.5(4)	4871.78(10)
Z	2	2	2
ρ_{calcd}/mg m^{-3}	1.153	1.261	1.337
μ/mm^{-1}	0.805	2.742	5.869
F(000)	3286.0	2504.0	2012.0
Reflns. collected	29723	85166	58669
Indep.reflns. [R(int)]	13484 [R_{int} = 0.0416, R_{sigma} = 0.0455]	23864 [R_{int} = 0.0900, R_{sigma} = 0.0861]	15394 [R_{int} = 0.0581, R_{sigma} = 0.0445]
Max/min transmission	1.000/0.796	1.000/0.226	1.000/0.579
Data/restraints /parameters	13484/170/1154	23864/160/1506	15394/185/1238
GOF on F^2	1.038	1.420	1.047
Final R indices[$I > 2\sigma(I)$]	R_1 = 0.0586, wR_2 = 0.1502	R_1 = 0.1495, wR_2 = 0.3772	R_1 = 0.0686, wR_2 = 0.1871
R indices (all data)	R_1 = 0.0667, wR_2 = 0.1558	R_1 = 0.1945, wR_2 = 0.4111	R_1 = 0.0870, wR_2 = 0.2004
Largest diff peak and hole [e Å^{-3}]	0.63/-0.38	4.20/-1.14	2.54/-1.45
CCDC	1900739	1905150	1900740

6. EPR spectral analysis:

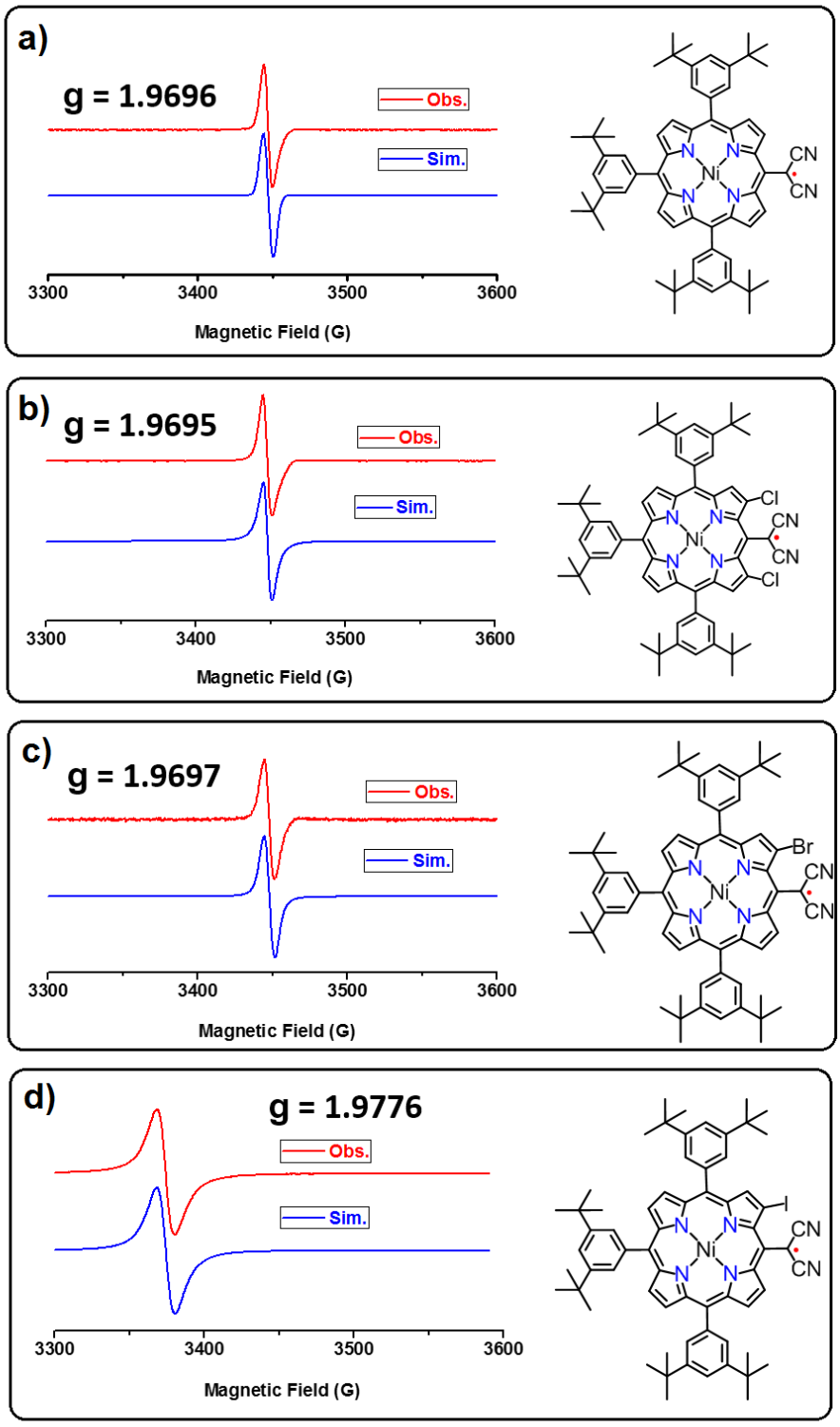

Figure S45: EPR spectral analysis of a) **12**, b) **13**, c) **14** and d) **15** in toluene at room temperature. (Red lines: observed and blue lines: simulated).

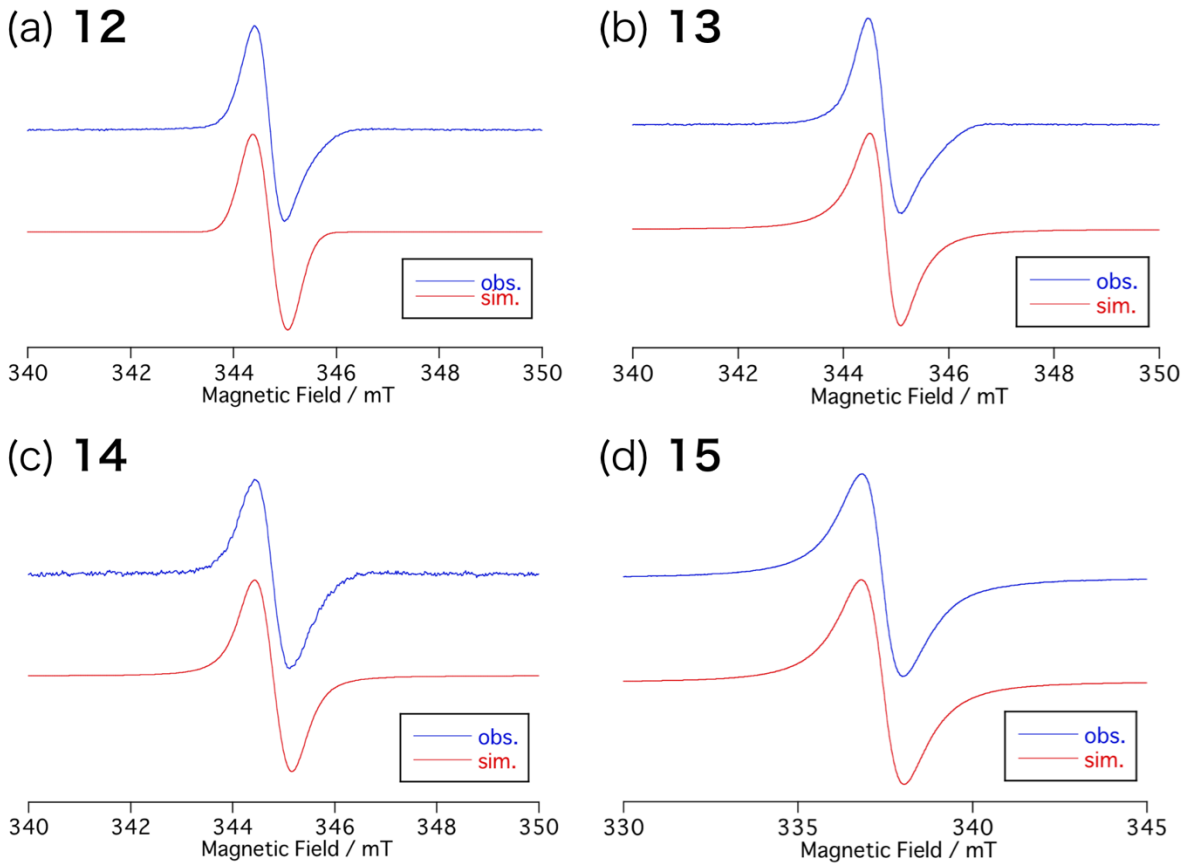

Figure S46 EPR spectral analysis of a) **12**, b) **13**, c) **14** and d) **15** in toluene at 15 K. (Red lines: observed and blue lines: simulated).

7. SQUID measurements:

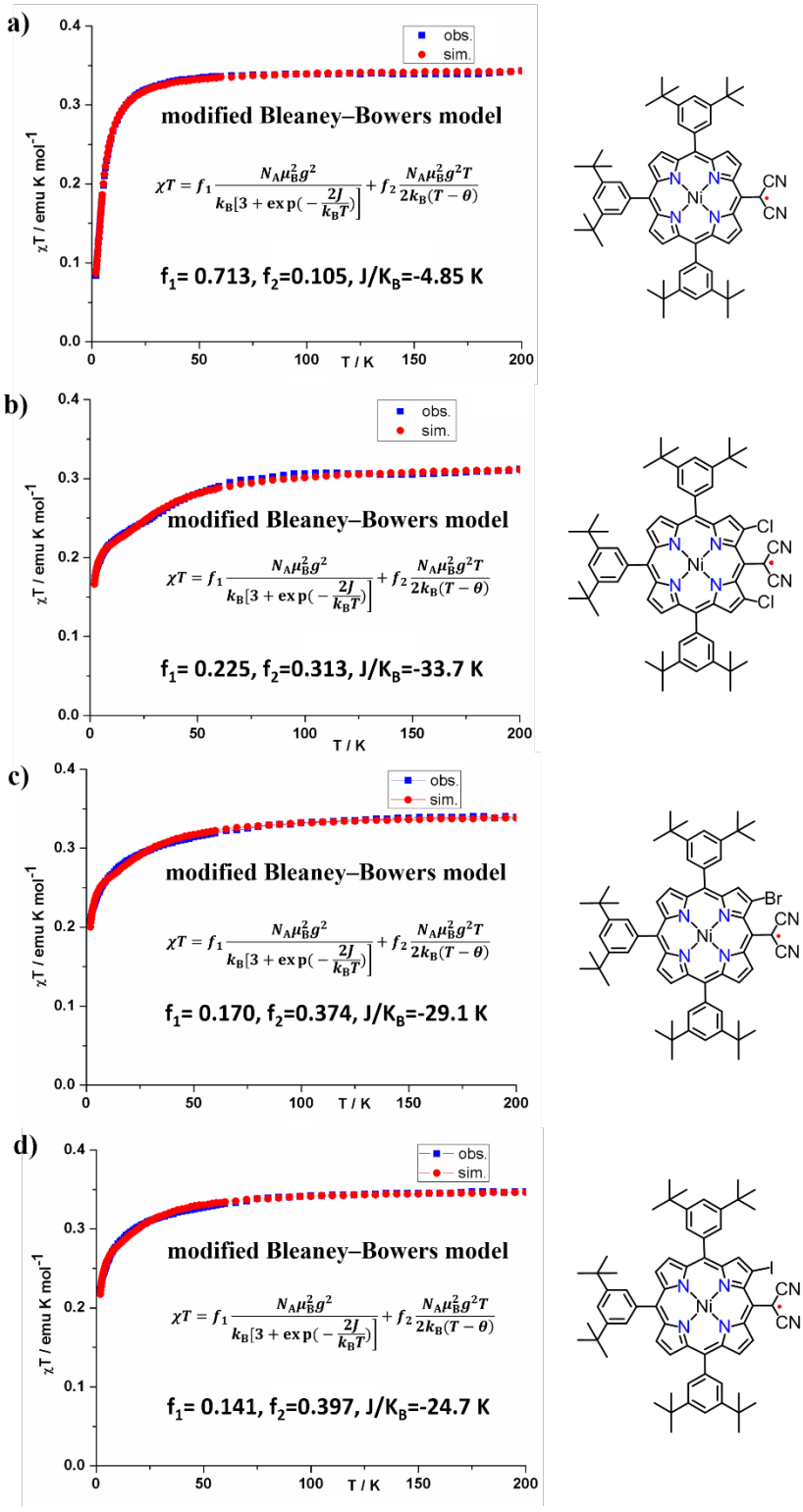

Figure S47: Temperature-dependent magnetic susceptibility of a) **12**, b) **13**, c) **14** and d) **15**. (Blue circles: observed and red lines: simulated).

8. Electronic absorption spectral analysis:

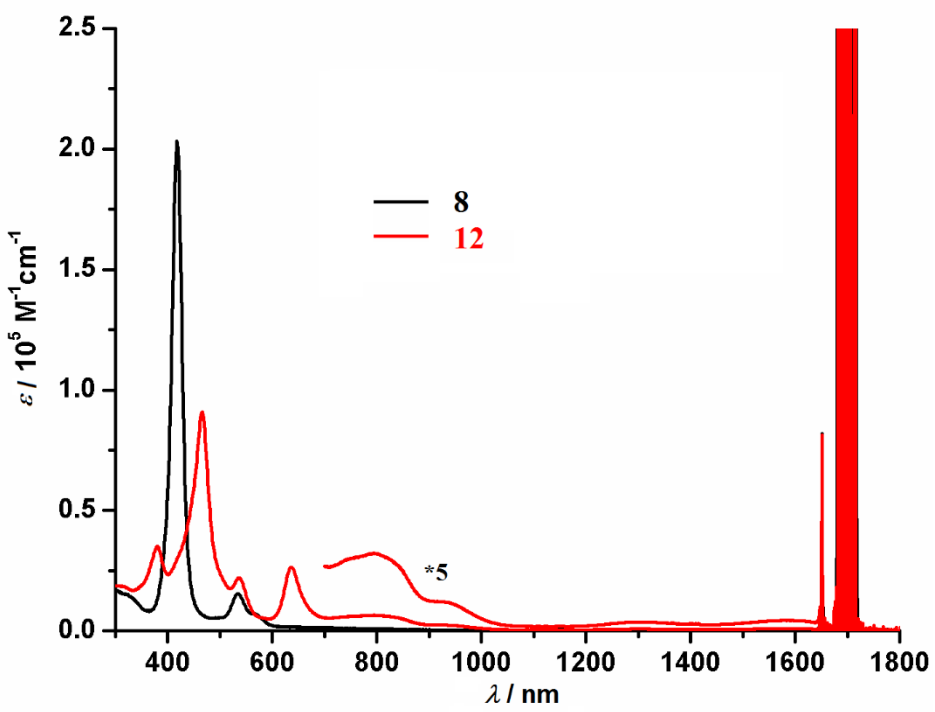

Figure S48: Electronic absorption spectra of **8** and **12** in CH_2Cl_2.

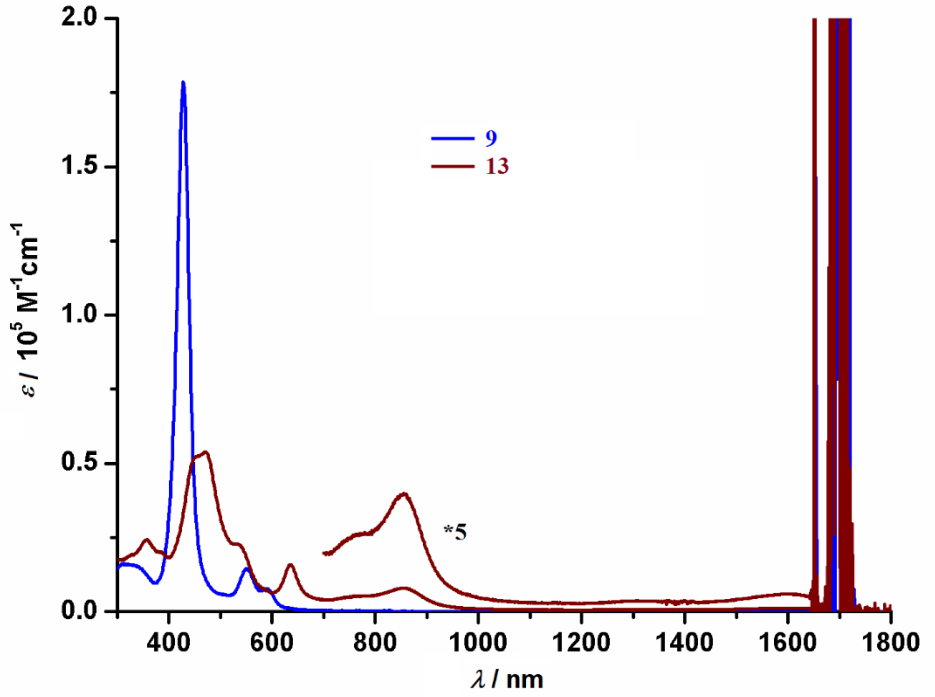

Figure S49: Electronic absorption spectra of **9** and **13** in CH_2Cl_2.

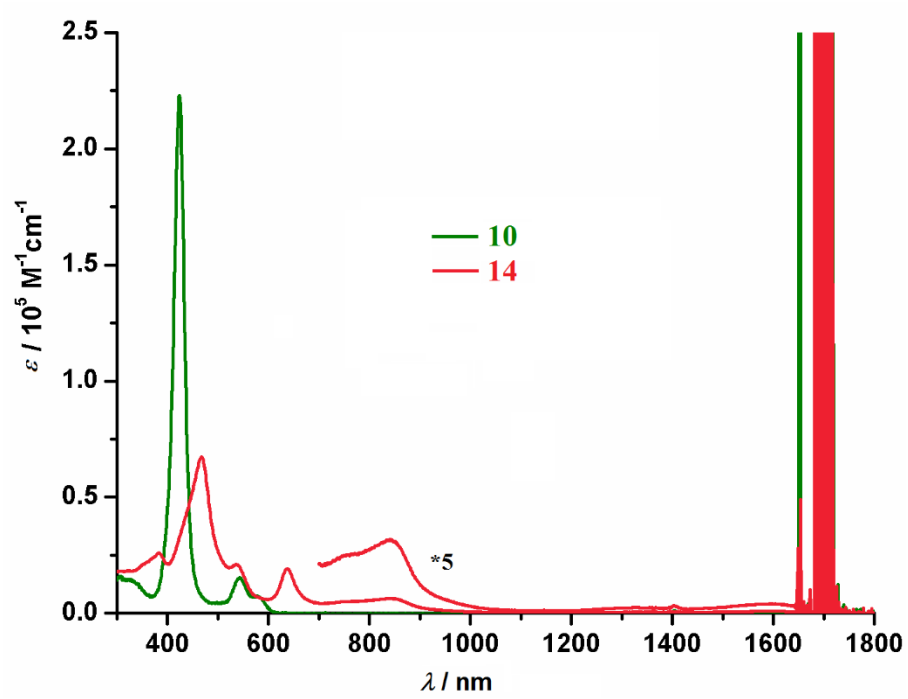

Figure S50: Electronic absorption spectra of **10** and **14** in CH_2Cl_2.

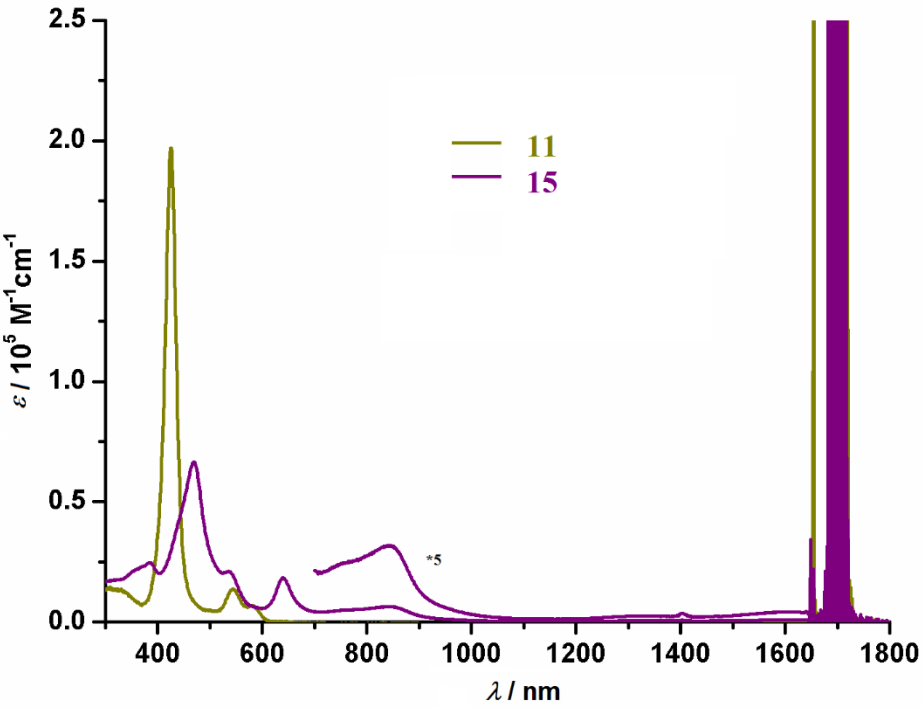

Figure S51: Electronic absorption spectra of **11** and **15** in CH_2Cl_2.

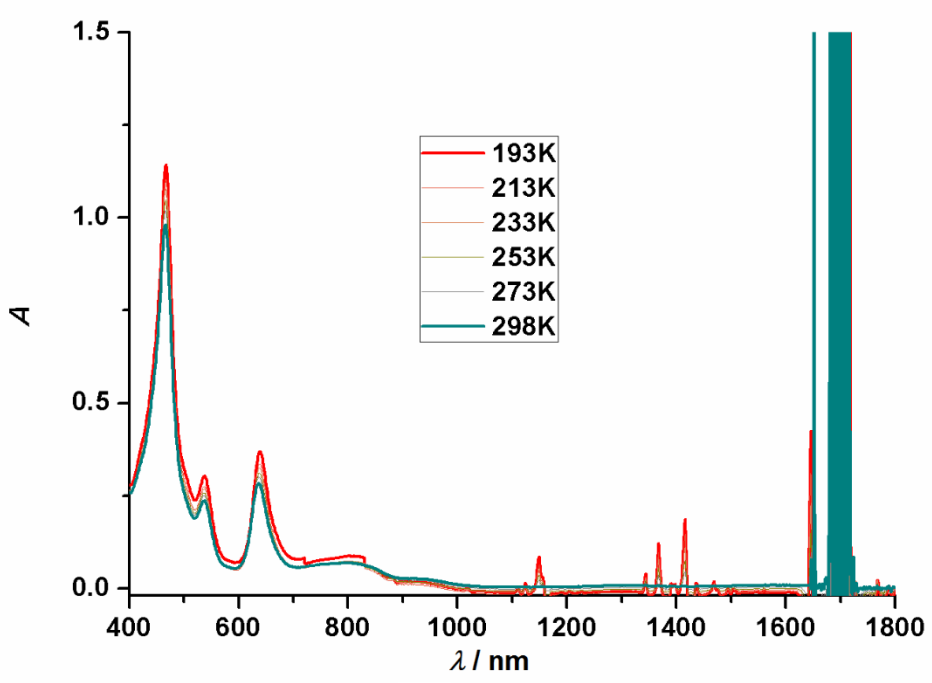

Figure S52: LT Electronic absorption spectra of **12** in CH_2Cl_2.

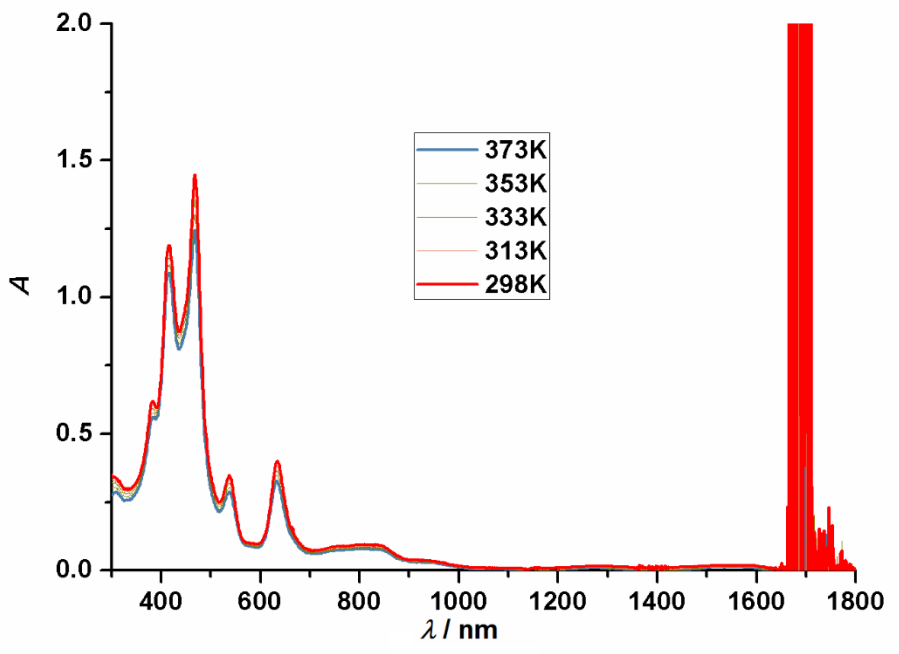

Figure S53: HT Electronic absorption spectra of **12** in toluene.

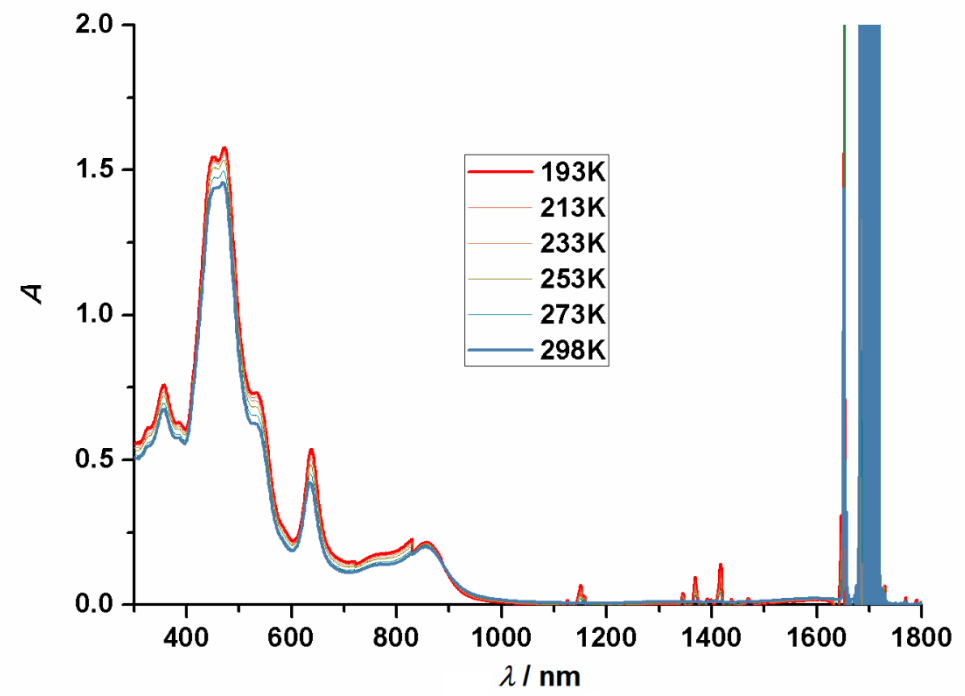

Figure S54: LT Electronic absorption spectra of **13** in CH_2Cl_2.

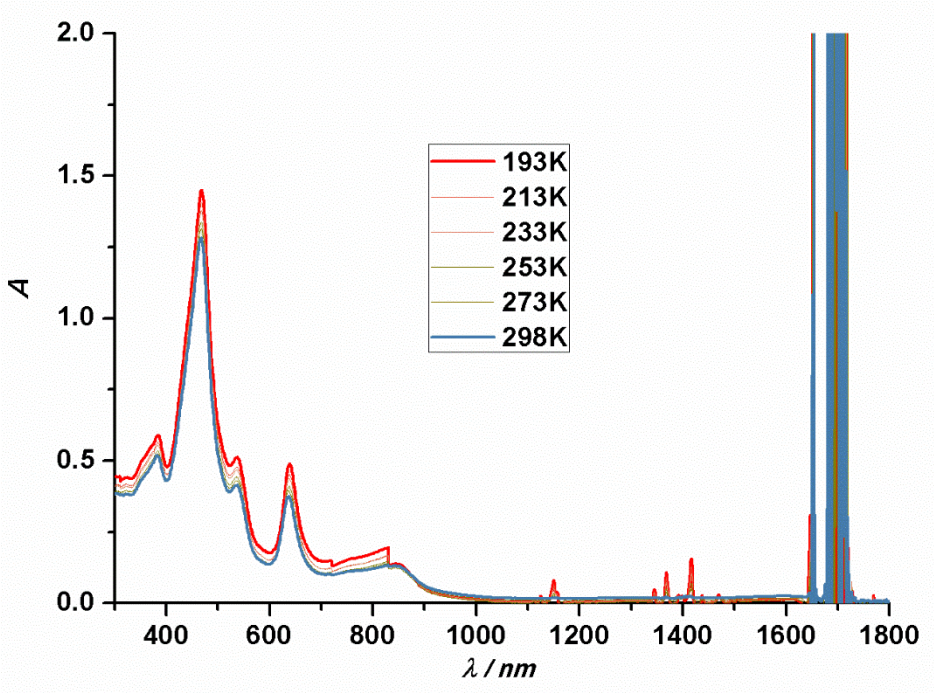

Figure S55: LT Electronic absorption spectra of **14** in CH_2Cl_2.

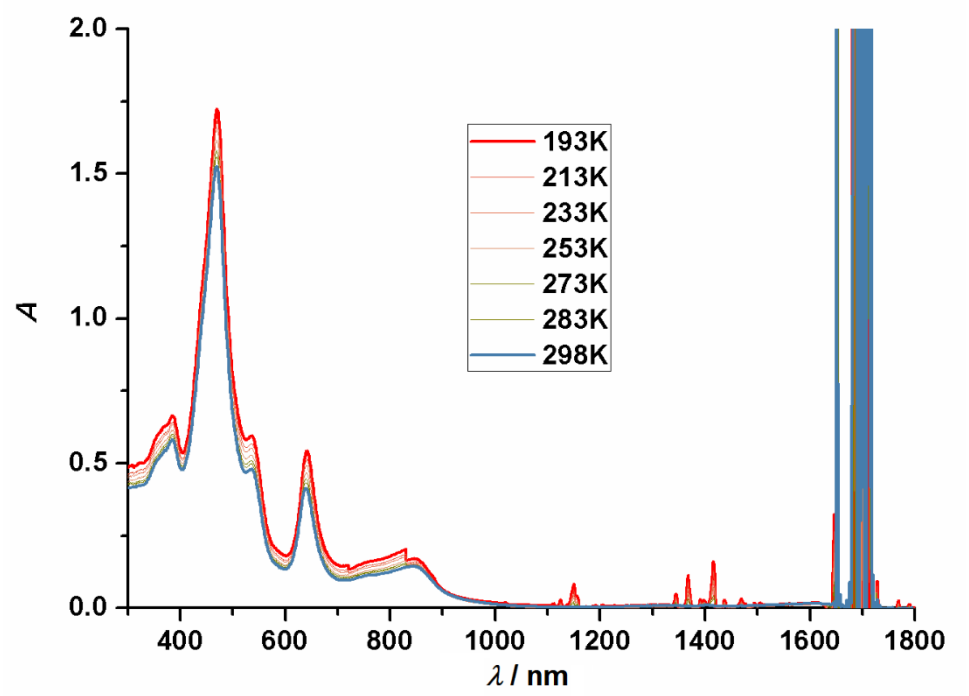

Figure S56: LT Electronic absorption spectra of **15** in CH_2Cl_2.

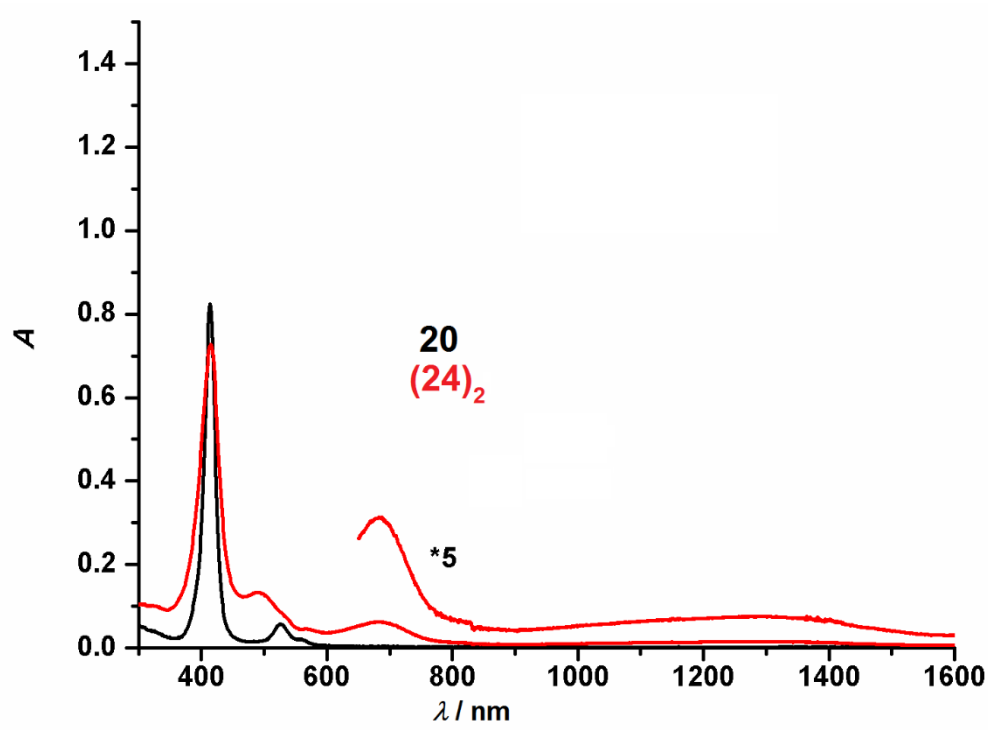

Figure S57: Electronic absorption spectra of **20** and **(24)$_2$** in CH_2Cl_2.

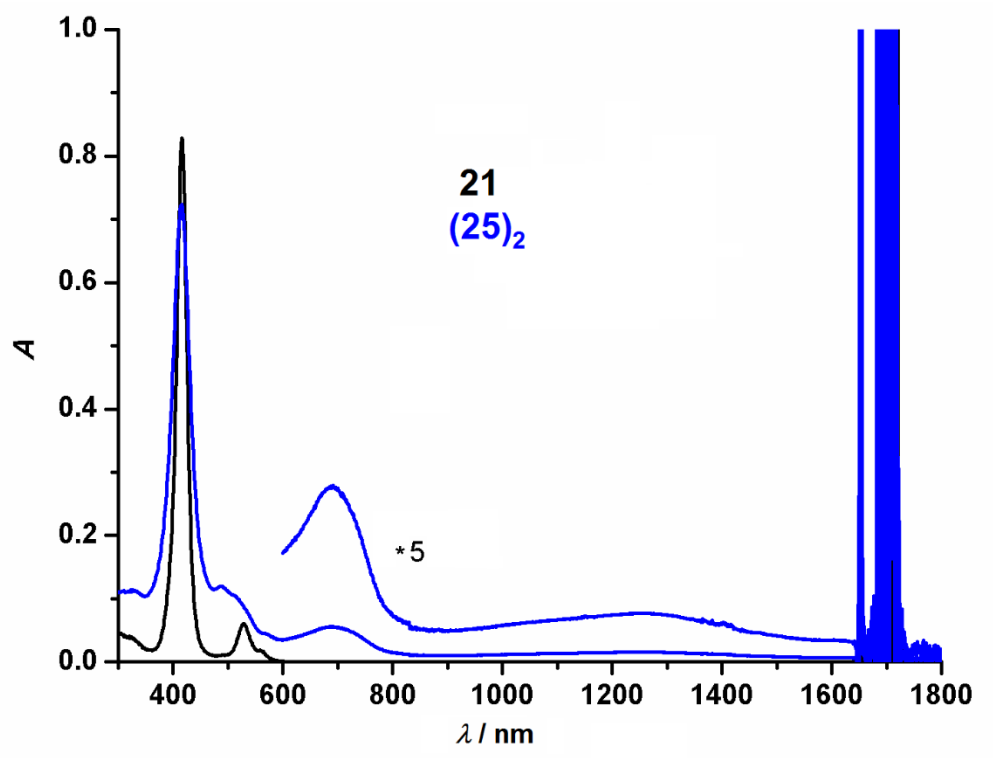

Figure S58: Electronic absorption spectra of **21** and **(25)$_2$** in CH_2Cl_2.

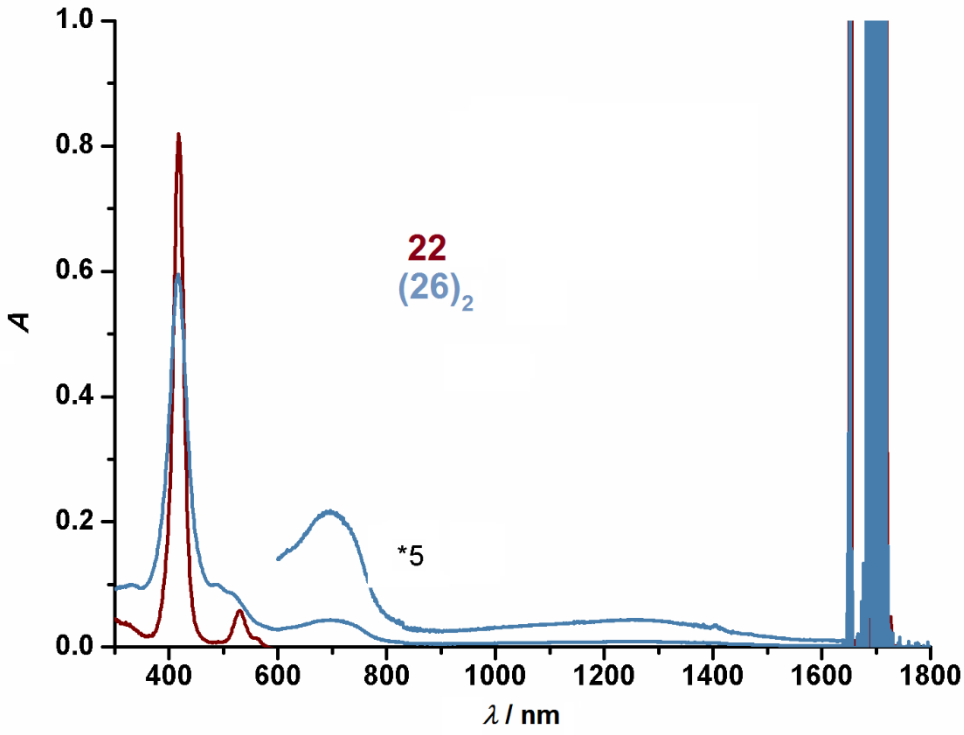

Figure S59: Electronic absorption spectra of **22** and **(26)$_2$** in CH_2Cl_2.

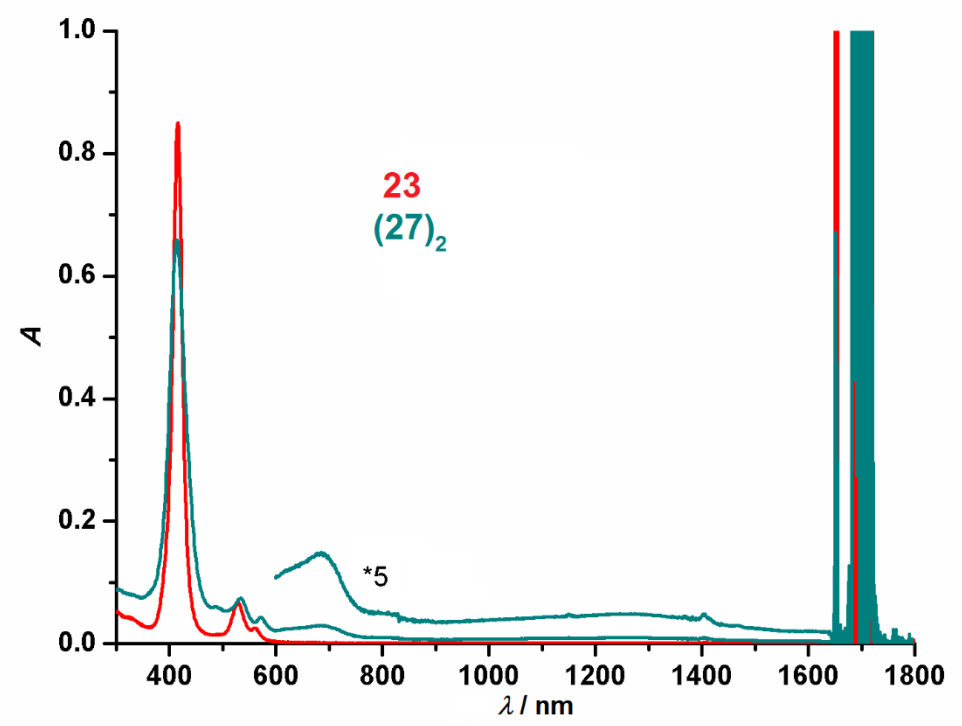

Figure S60: Electronic absorption spectra of **23** and **(27)$_2$** in CH_2Cl_2.

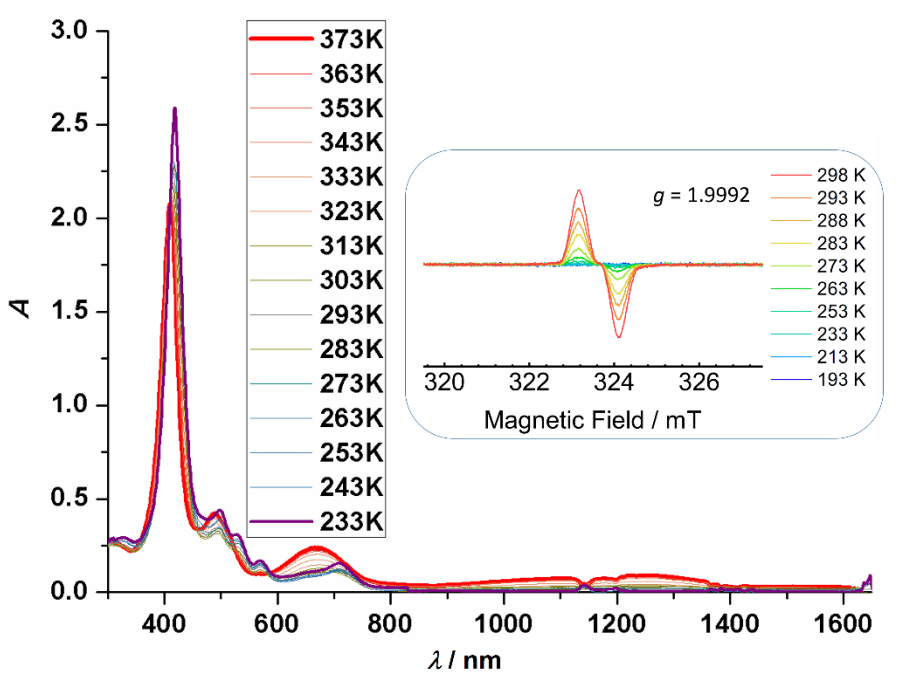

Figure S61: VT Electronic absorption spectra of **(24)$_2$** in toluene. Inset VT EPR spectrum of **(24)$_2$** in toluene.

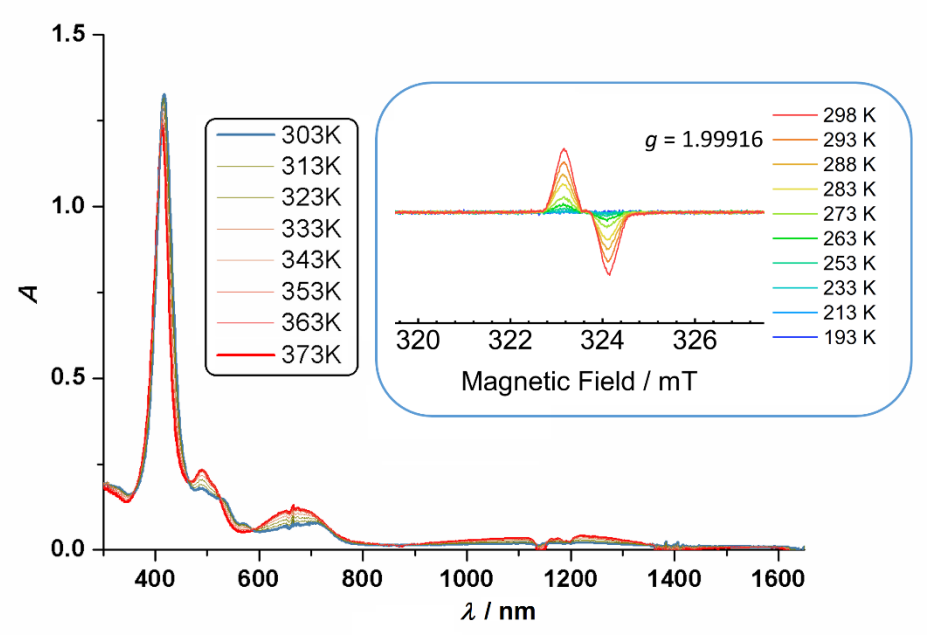

Figure S62: HT Electronic absorption spectra of **(25)$_2$** in toluene. Inset VT EPR spectrum of **(25)$_2$** in toluene.

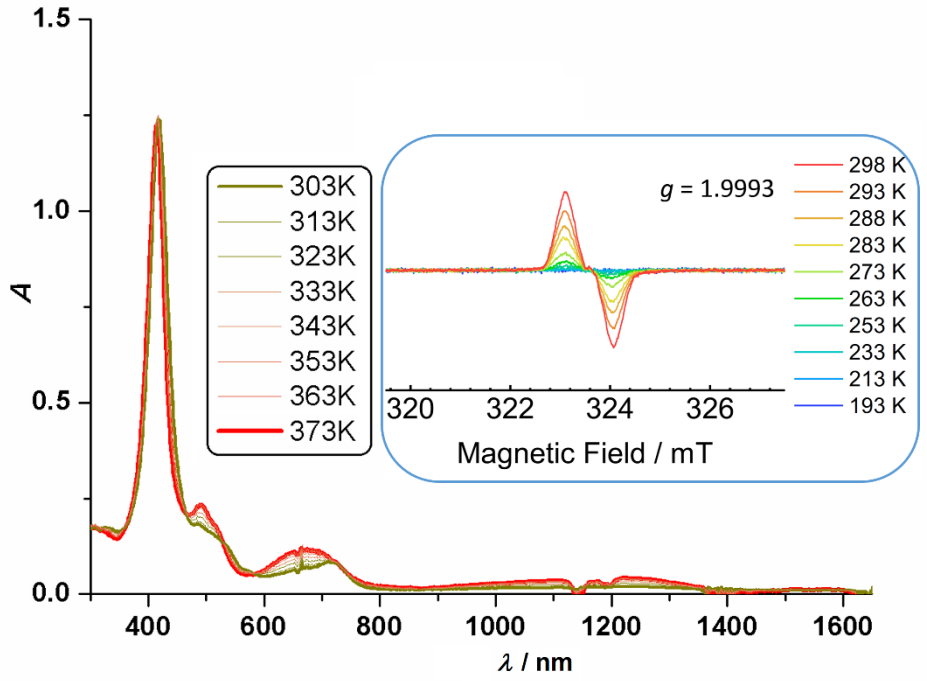

Figure S63: HT Electronic absorption spectra of **(26)$_2$** in toluene. Inset VT EPR spectrum of **(26)$_2$** in toluene.

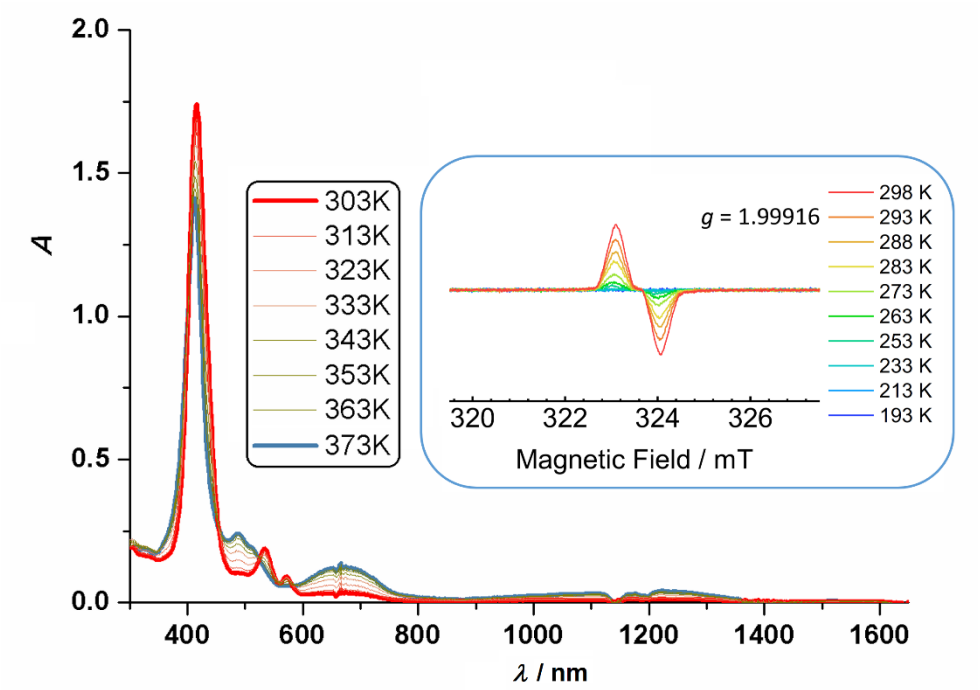

Figure S64: HT Electronic absorption spectra of **(27)$_2$** in toluene. Inset VT EPR spectrum of **(27)$_2$** in toluene.

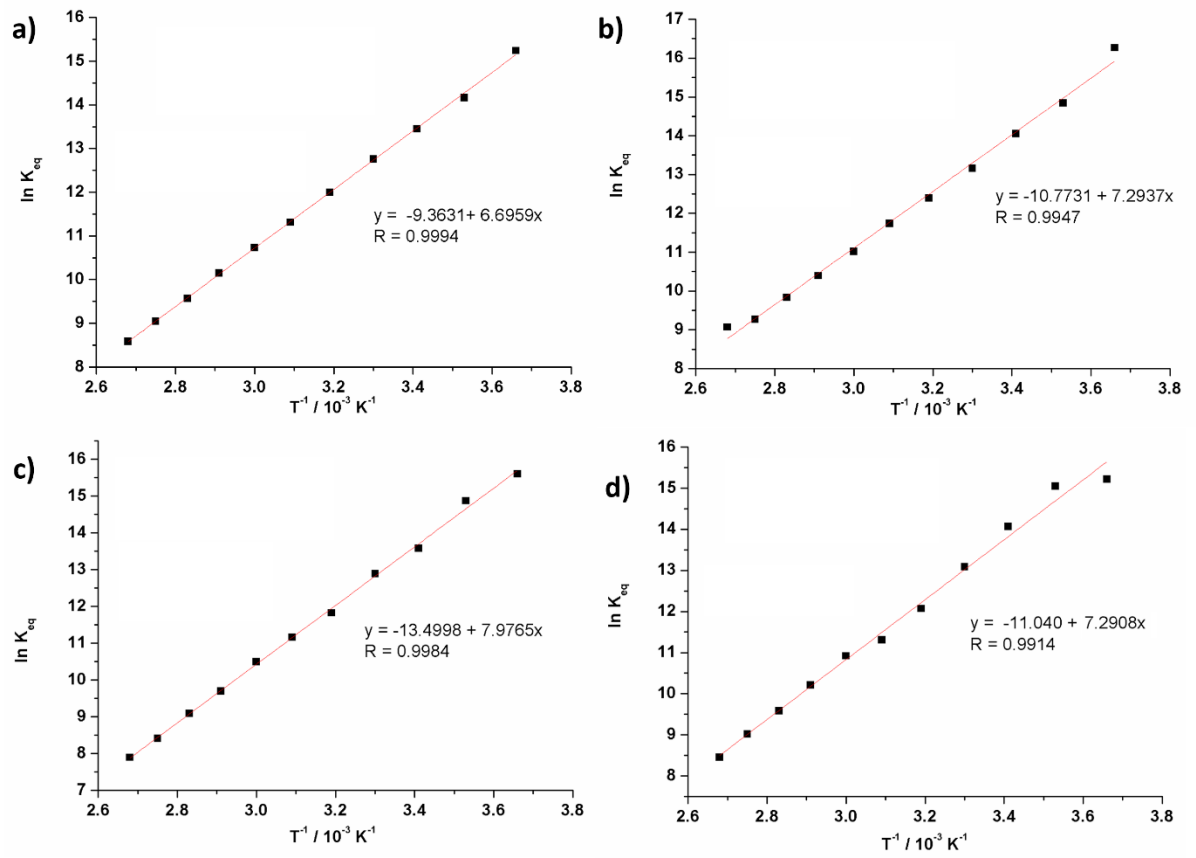

Figure S65: van't Hoff plots (ln K_{eq} vs T^{-1}) for a) **24**, b) **25**, c) **26** and d) **27** in toluene.

9. Cyclic voltammograms:

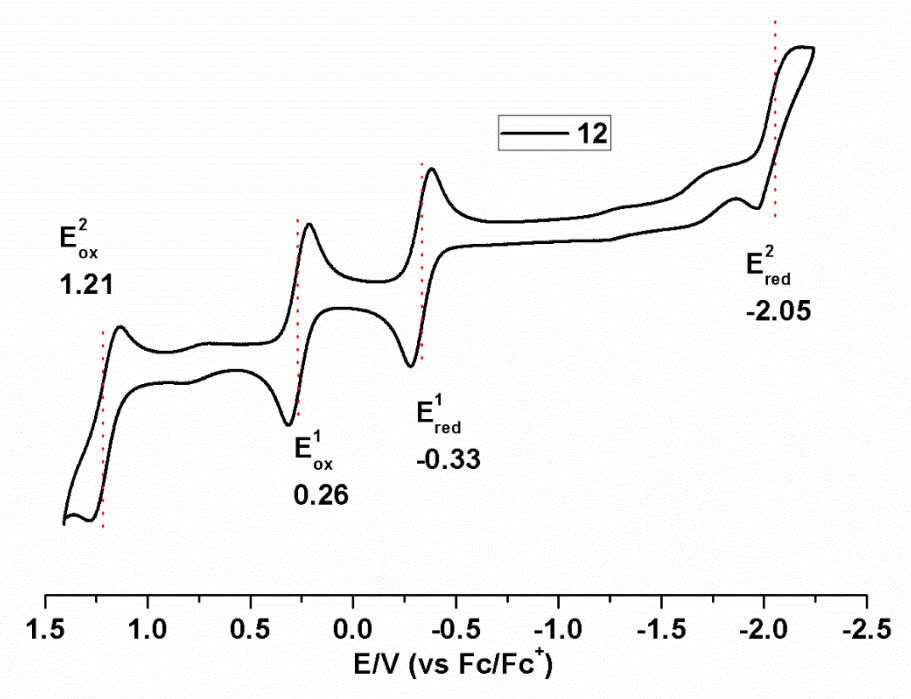

Figure S66: Cyclic voltammogram of **12** in CH_2Cl_2 (scan rate: 0.05 V/s, supporting electrolyte: 0.1 M $^nBu_4NPF_6$, working electrode: Pt, counter electrode: Pt wire, reference electrode: Ag/0.01 M $AgClO_4$).

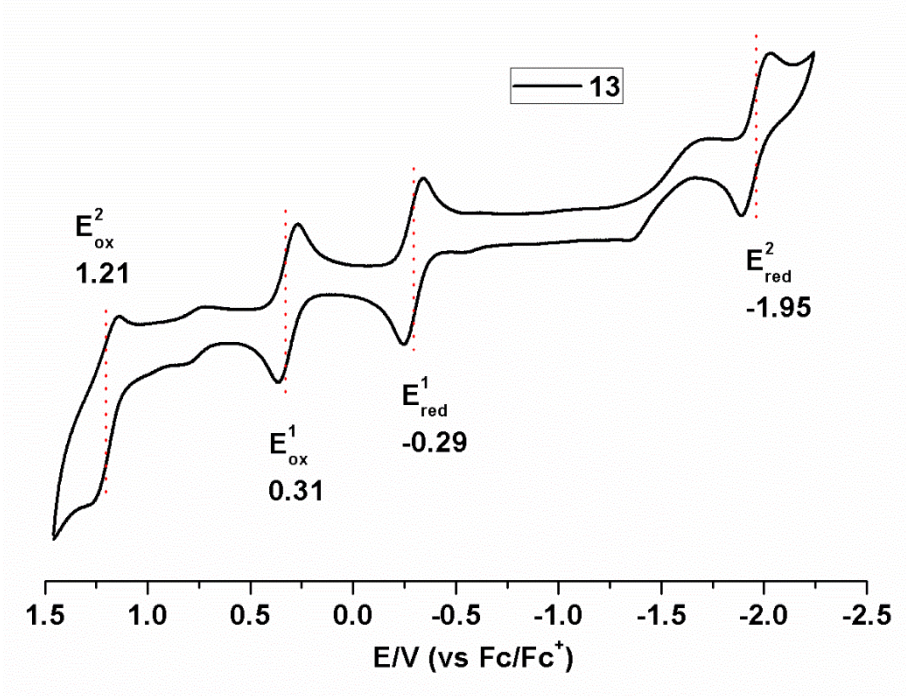

Figure S67: Cyclic voltammogram of **13** in CH_2Cl_2 (scan rate: 0.05 V/s, supporting electrolyte: 0.1 M $^nBu_4NPF_6$, working electrode: Pt, counter electrode: Pt wire, reference electrode: Ag/0.01 M $AgClO_4$).

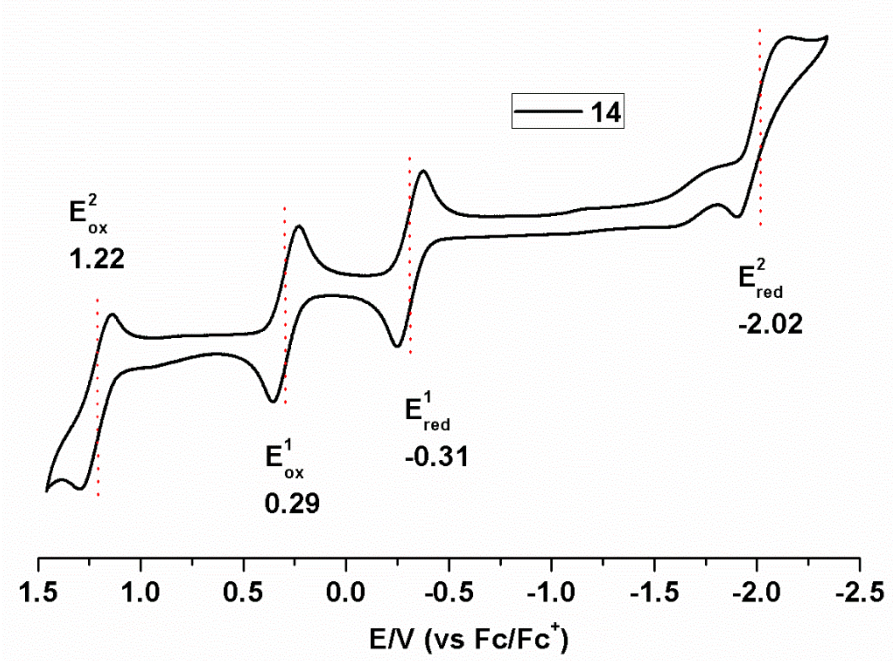

Figure S68: Cyclic voltammogram of **14** in CH_2Cl_2 (scan rate: 0.05 V/s, supporting electrolyte: 0.1 M $^nBu_4NPF_6$, working electrode: Pt, counter electrode: Pt wire, reference electrode: Ag/0.01 M $AgClO_4$).

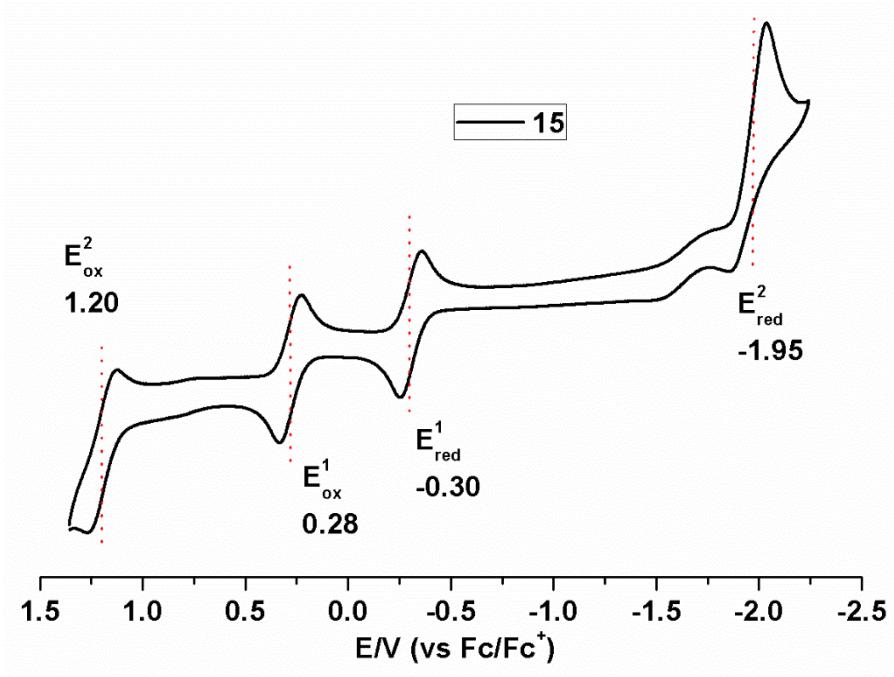

Figure S69: Cyclic voltammogram of **15** in CH_2Cl_2 (scan rate: 0.05 V/s, supporting electrolyte: 0.1 M $^nBu_4NPF_6$, working electrode: Pt, counter electrode: Pt wire, reference electrode: Ag/0.01 M $AgClO_4$).

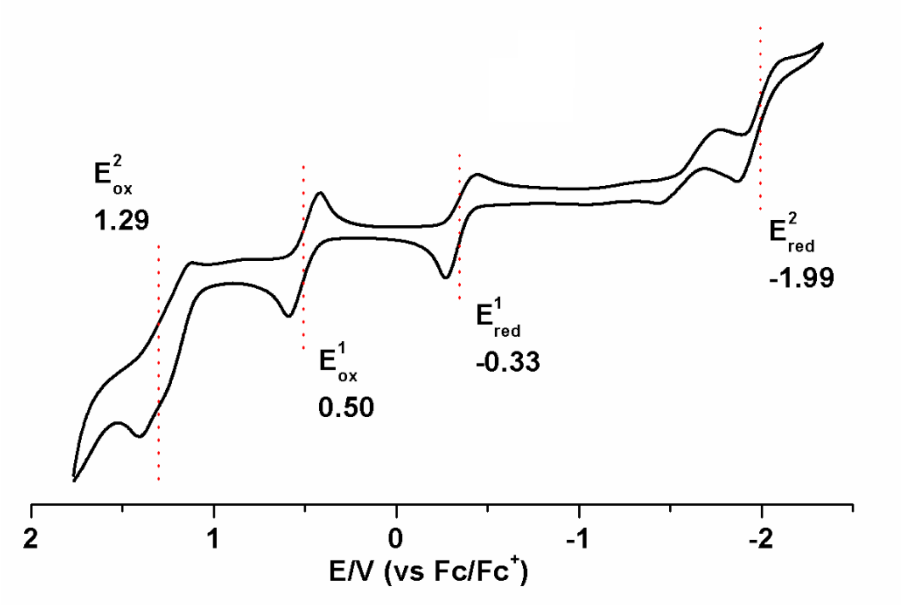

Figure S70: Cyclic voltammogram of **(24)$_2$** in CH_2Cl_2 (scan rate: 0.05 V/s, supporting electrolyte: 0.1 M $^nBu_4NPF_6$, working electrode: Pt, counter electrode: Pt wire, reference electrode: Ag/0.01 M $AgClO_4$).

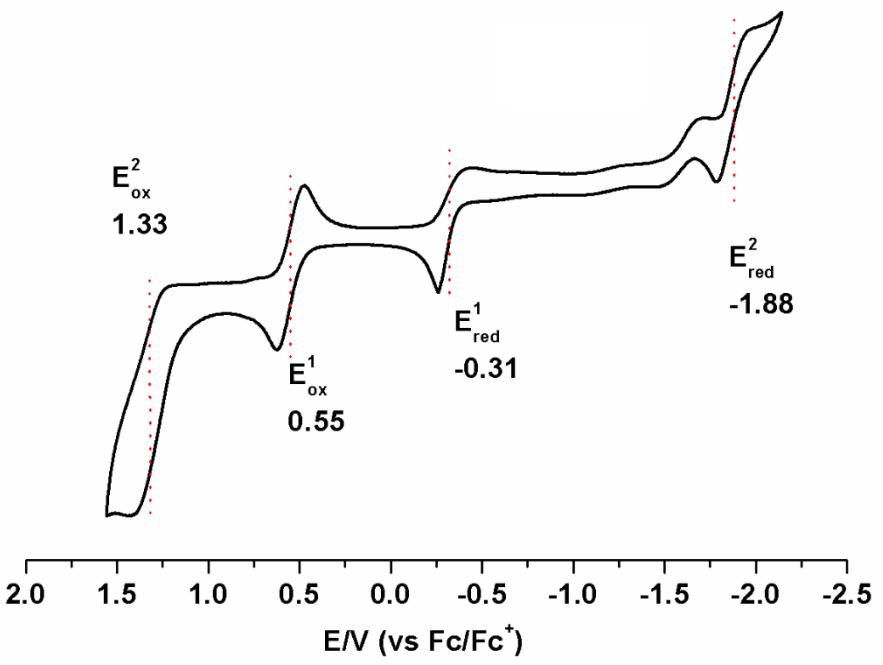

Figure S71: Cyclic voltammogram of **(25)$_2$** in CH_2Cl_2 (scan rate: 0.05 V/s, supporting electrolyte: 0.1 M $^nBu_4NPF_6$, working electrode: Pt, counter electrode: Pt wire, reference electrode: Ag/0.01 M $AgClO_4$).

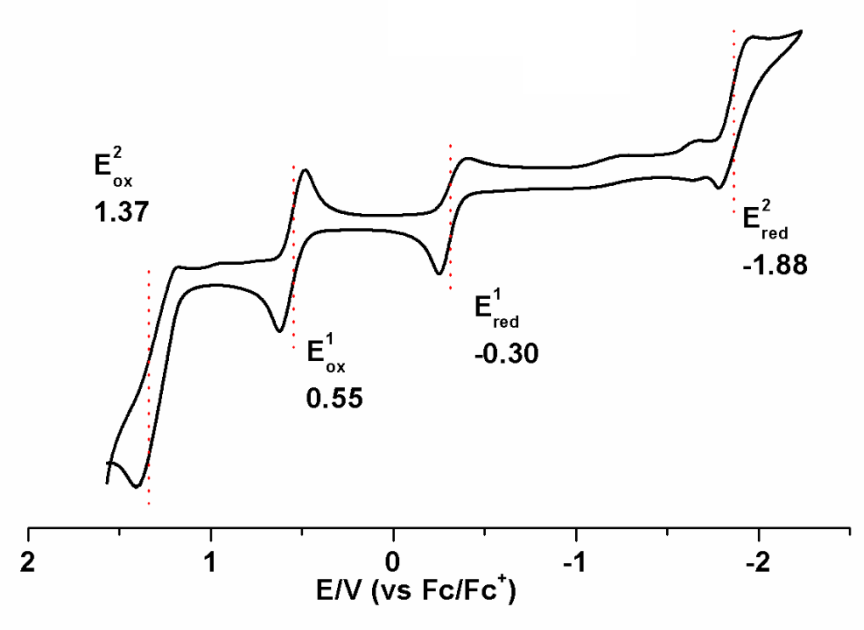

Figure S72: Cyclic voltammogram of **(26)$_2$** in CH_2Cl_2 (scan rate: 0.05 V/s, supporting electrolyte: 0.1 M $^nBu_4NPF_6$, working electrode: Pt, counter electrode: Pt wire, reference electrode: Ag/0.01 M $AgClO_4$). (* represents either impurity or radical formation).

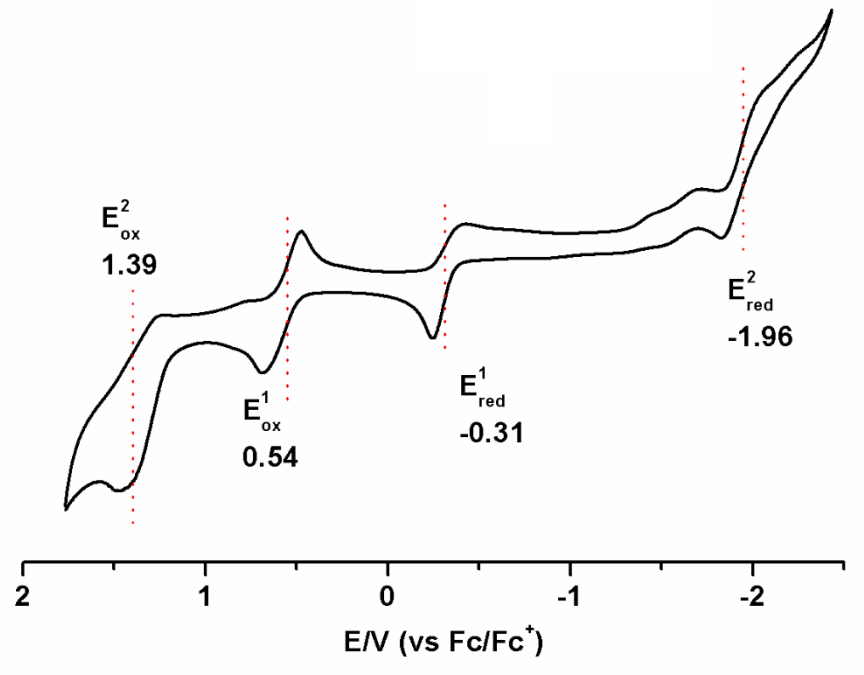

Figure S73: Cyclic voltammogram of **(27)$_2$** in CH_2Cl_2 (scan rate: 0.05 V/s, supporting electrolyte: 0.1 M $^nBu_4NPF_6$, working electrode: Pt, counter electrode: Pt wire, reference electrode: Ag/0.01 M $AgClO_4$). (* represents either impurity or radical formation).

Table S3: **Redox potentials of 12-15 and $(24)_2$-$(27)_2$:**

Compd.	$E_1^{1/2}{}_{OX1}/V$	$E_2^{1/2}{}_{OX2}/V$	$E_1^{1/2}{}_{RED1}/V$	$E_2^{1/2}{}_{RED2}/V$	$\Delta E_{HL}(eV)$
12	0.26	1.21	-0.33	-2.05	0.59
13	0.31	1.21	-0.29	-1.95	0.60
14	0.29	1.22	-0.31	-2.02	0.60
15	0.28	1.20	-0.30	-1.95	0.58
$(24)_2$	0.50	1.29	-0.33	-1.99	0.83
$(25)_2$	0.55	1.33	-0.31	-1.88	0.86
$(26)_2$	0.55	1.37	-0.30	-1.88	0.85
$(27)_2$	0.54	1.39	-0.31	-1.96	0.85

10. DFT calculations:

All calculations were carried out using the Gaussian 09 program.[S4] The calculations were performed by the density functional theory (DFT) method with UB3LYP level, employing a basis set 6-311G(d). *tert*-Butyl groups were replaced by hydrogen atoms to simplify calculations.

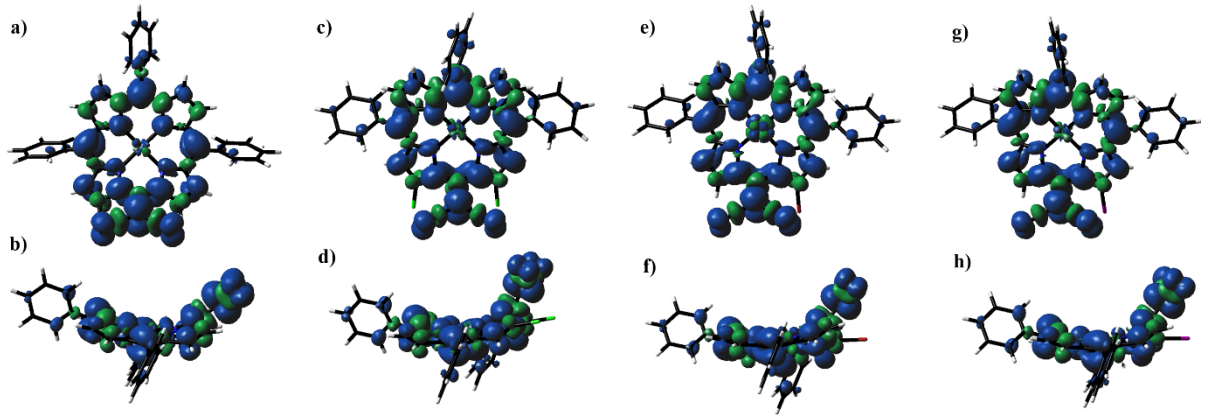

Figure S74. Spin density distribution plots of **12** (a,b), **13** (c,d), **14** (e,f) and **15** (g,h) calculated at the UB3LYP/6-311G* level (isovalue: 0.001).

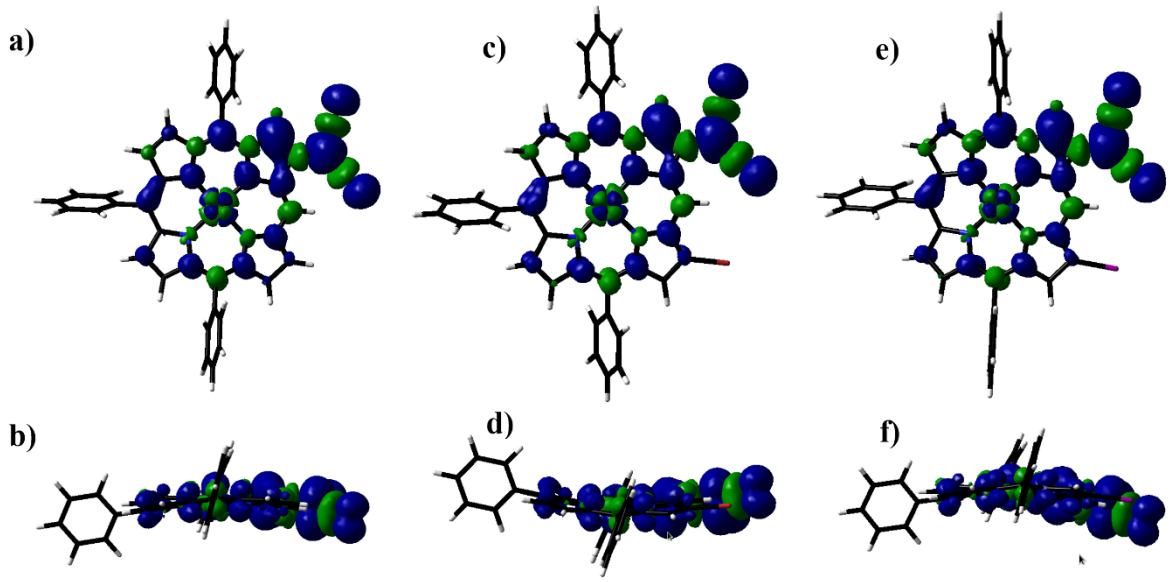

Figure S75. Spin density distribution plots of *β*-dicyanomethyl monomer radicals (a,b) **24**, (c,d) **25** and (e,f) **26**, calculated at the UB3LYP/6-311G* level (isovalue: 0.001).

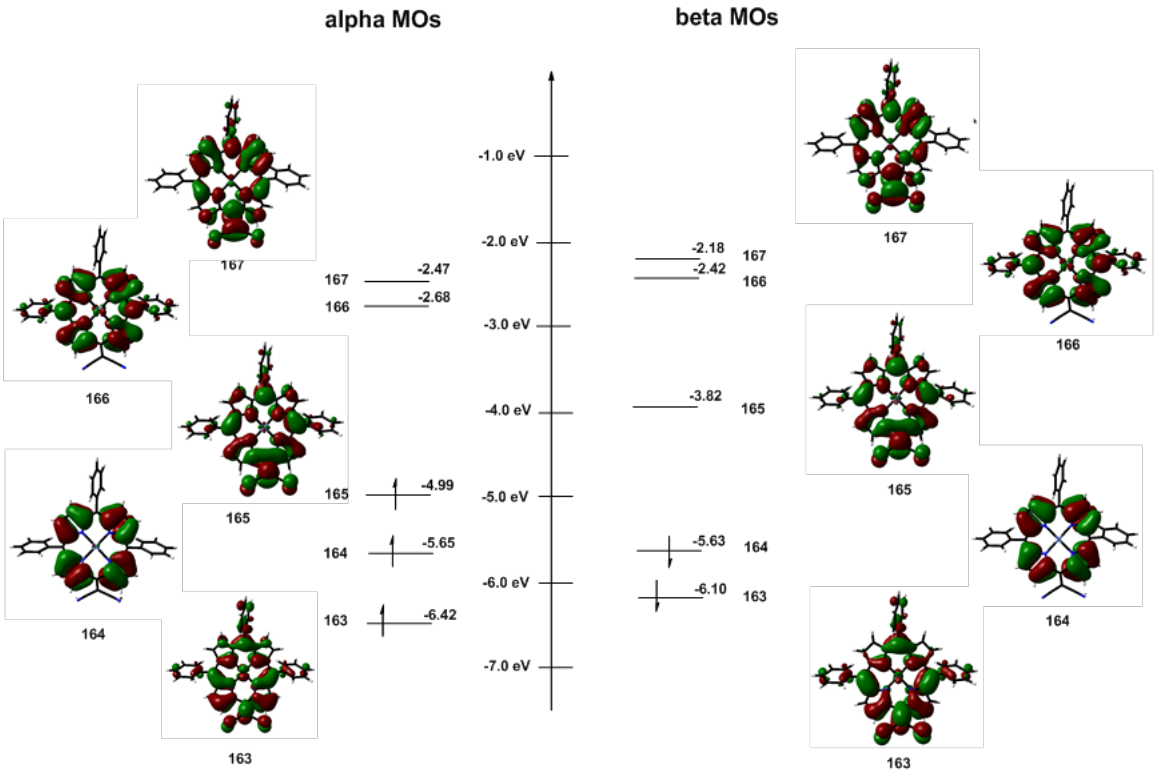

***Figure S76*:** Selected molecular orbitals of **12** calculated at UB3LYP/6-311G(d) .

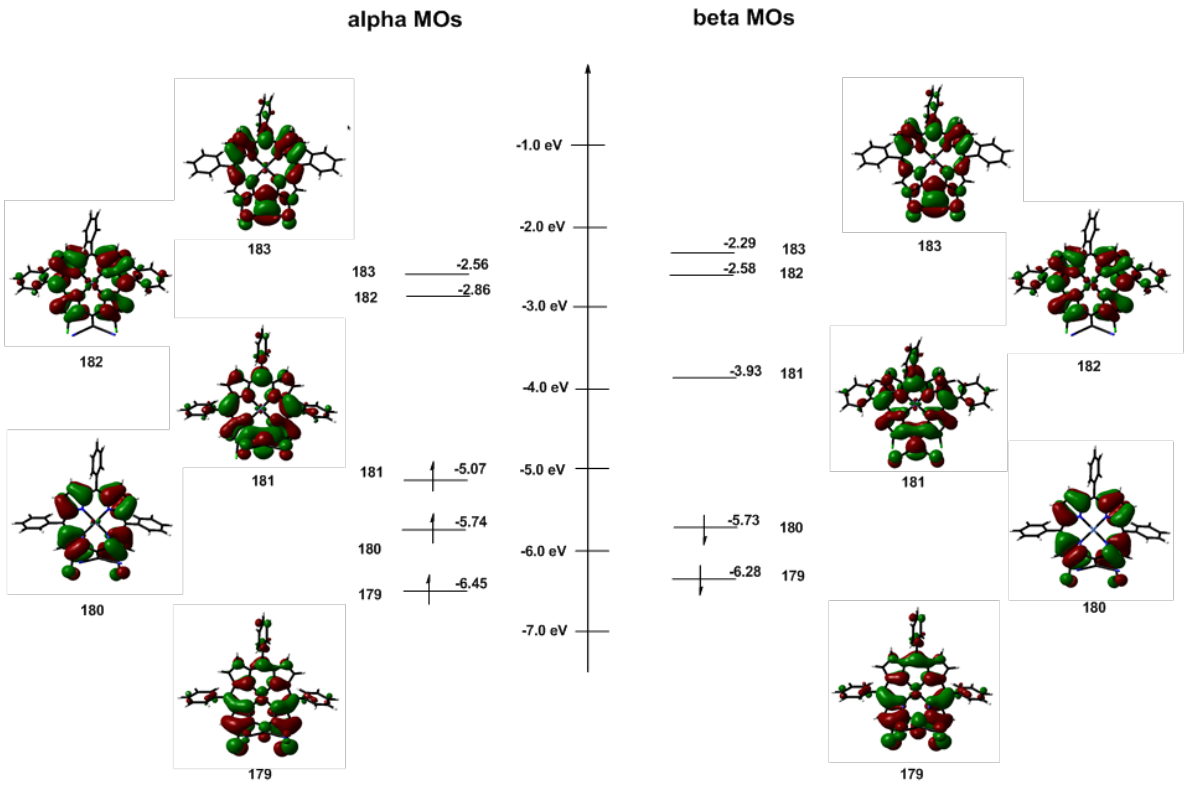

***Figure S77*:** Selected molecular orbitals of **13** calculated at UB3LYP/6-311G(d) .

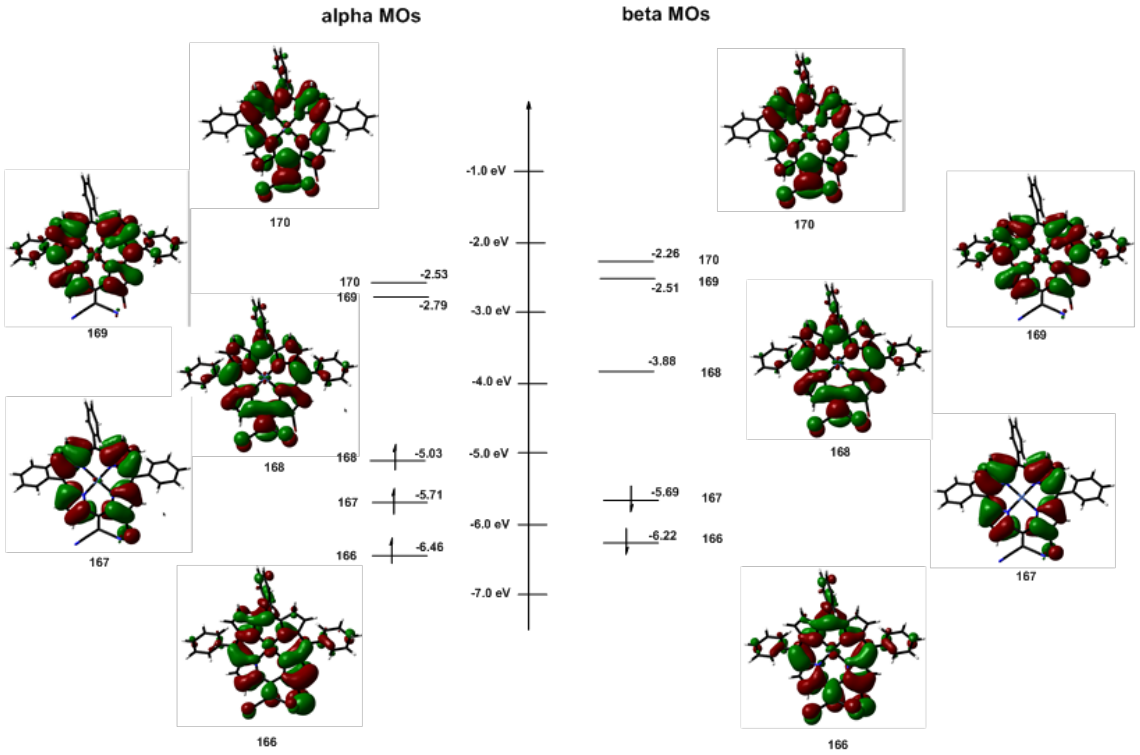

***Figure S78*:** Selected molecular orbitals of **14** calculated at UB3LYP/6-311G(d) .

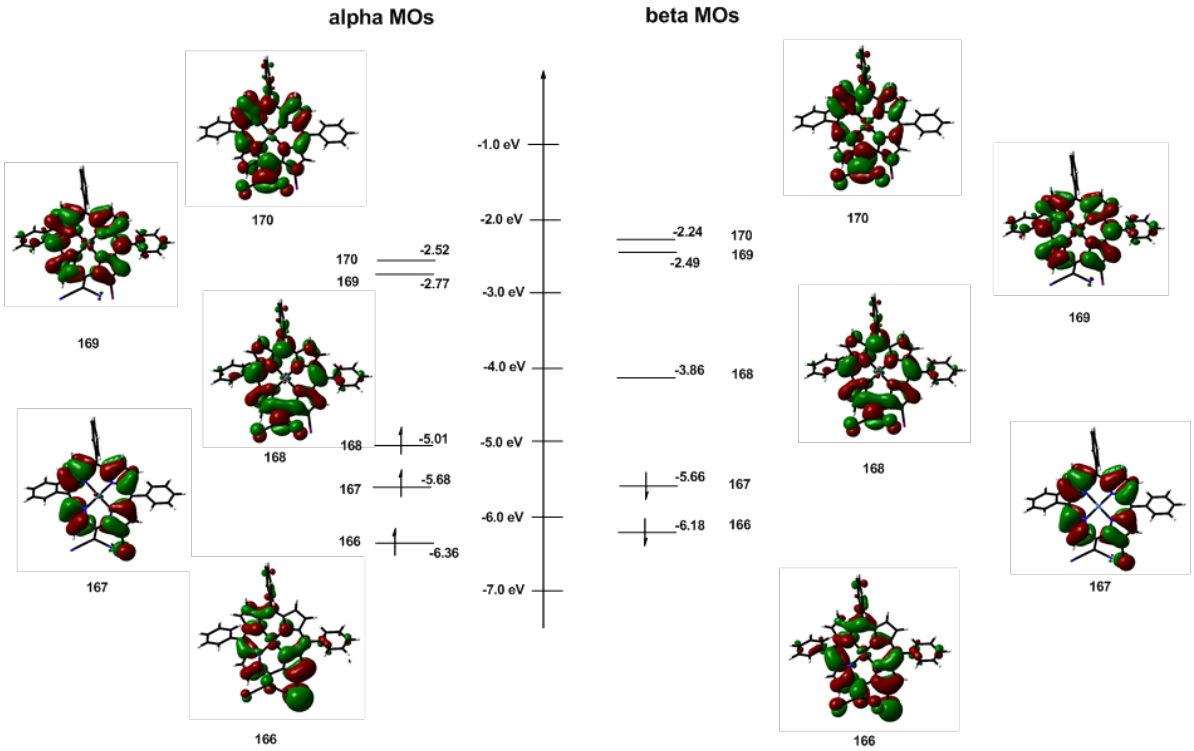

***Figure S79*:** Selected molecular orbitals of **15** calculated at UB3LYP/6-311G(d) .

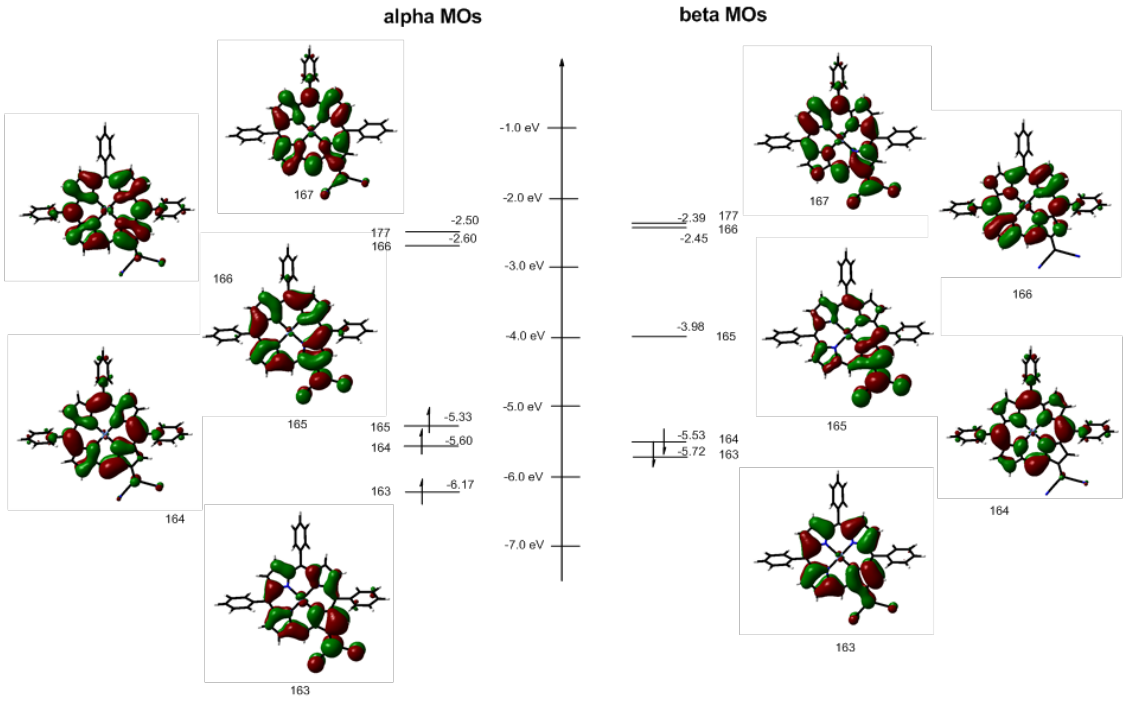

***Figure S80*:** Selected molecular orbitals of **24-monomer** radical calculated at UB3LYP/6-311G(d)

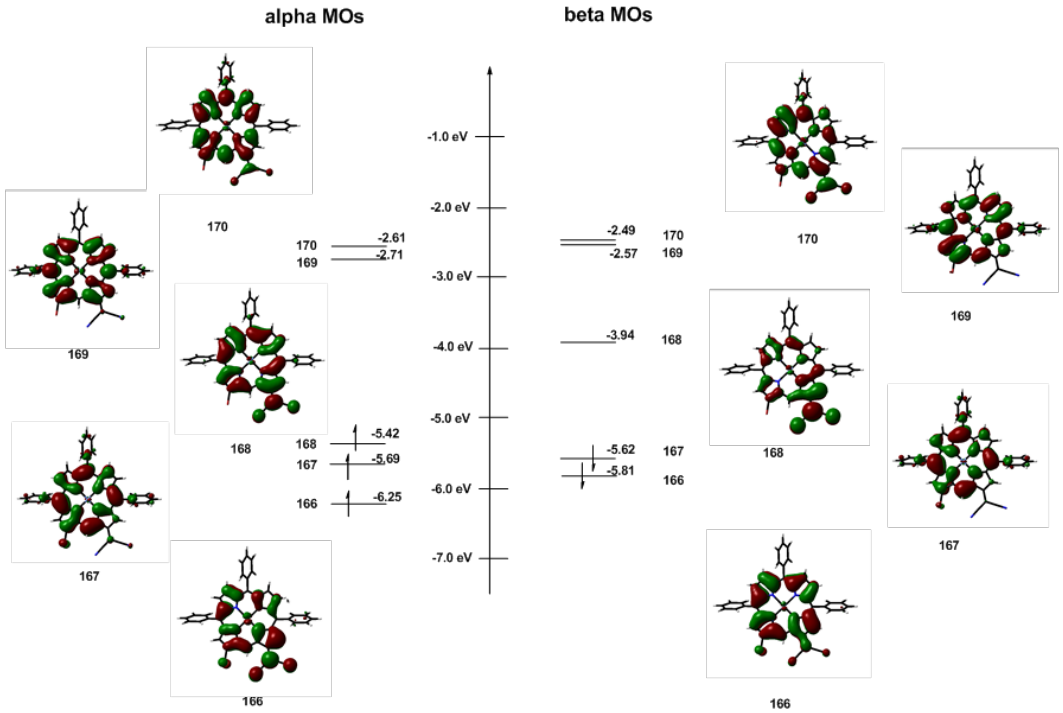

***Figure S81*:** Selected molecular orbitals of **25-monomer** radical calculated at UB3LYP/6-311G(d).

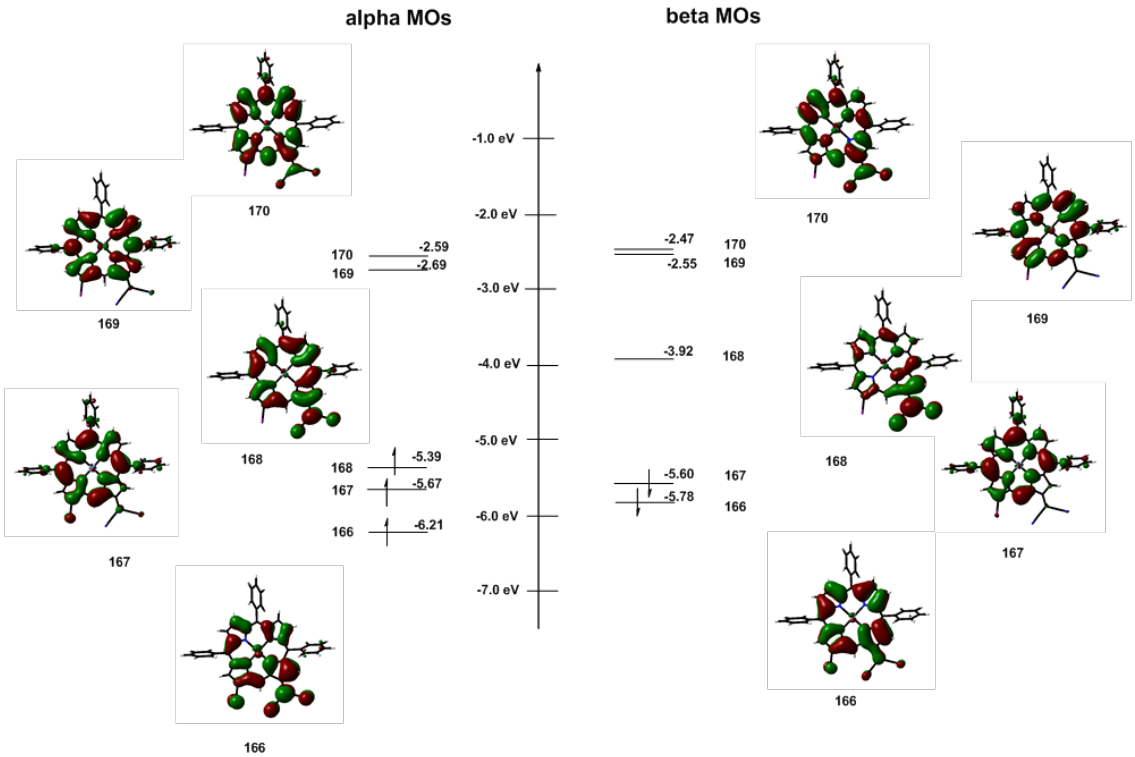

***Figure S82*:** Selected molecular orbitals of **26-monomer** radical calculated at UB3LYP/6-311G(d) .

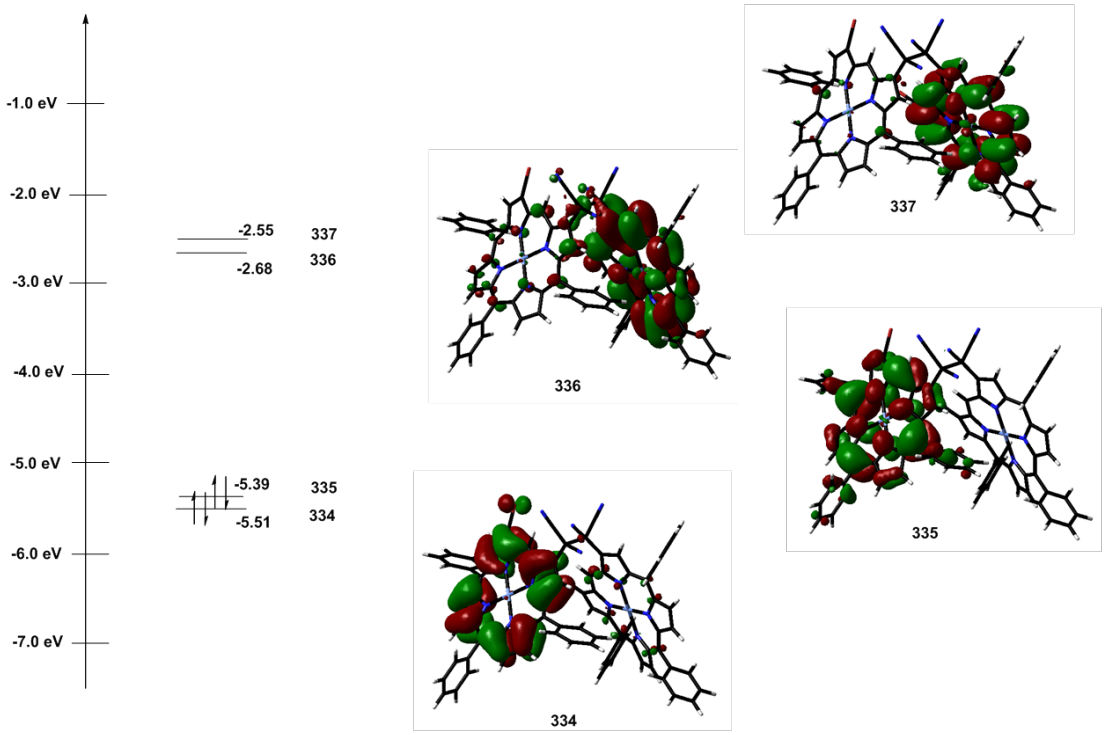

***Figure S83*:** Selected molecular orbitals of **(24)$_2$** calculated at UB3LYP/6-311G(d) .

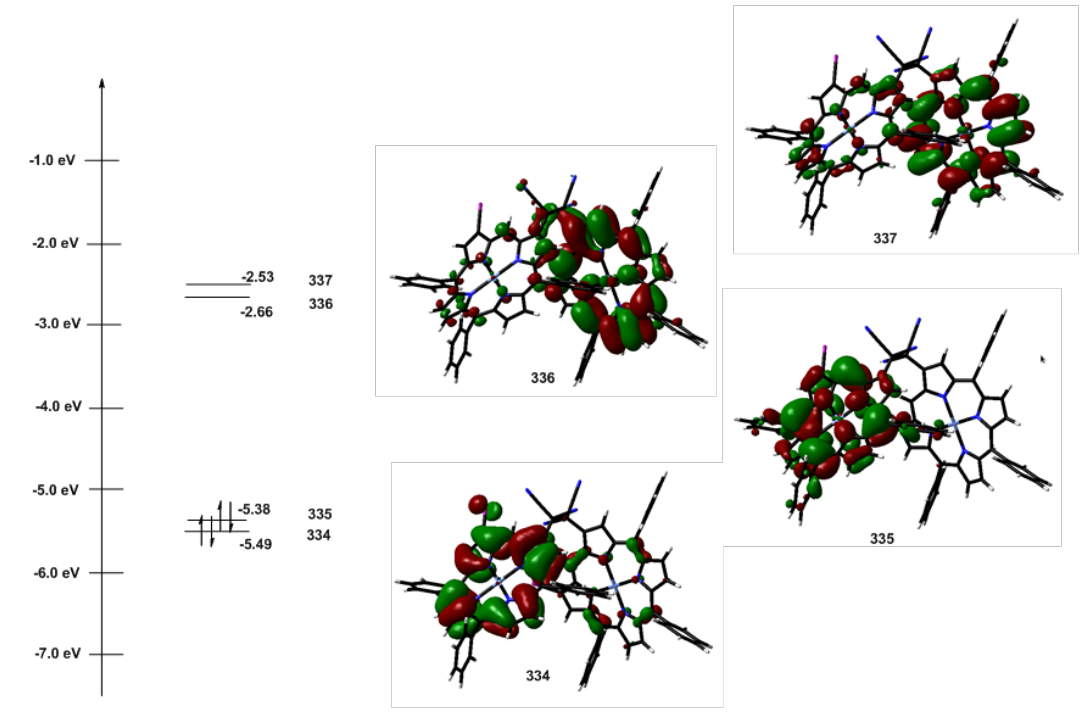

***Figure S84*:** Selected molecular orbitals of **(25)$_2$** calculated at UB3LYP/6-311G(d) .

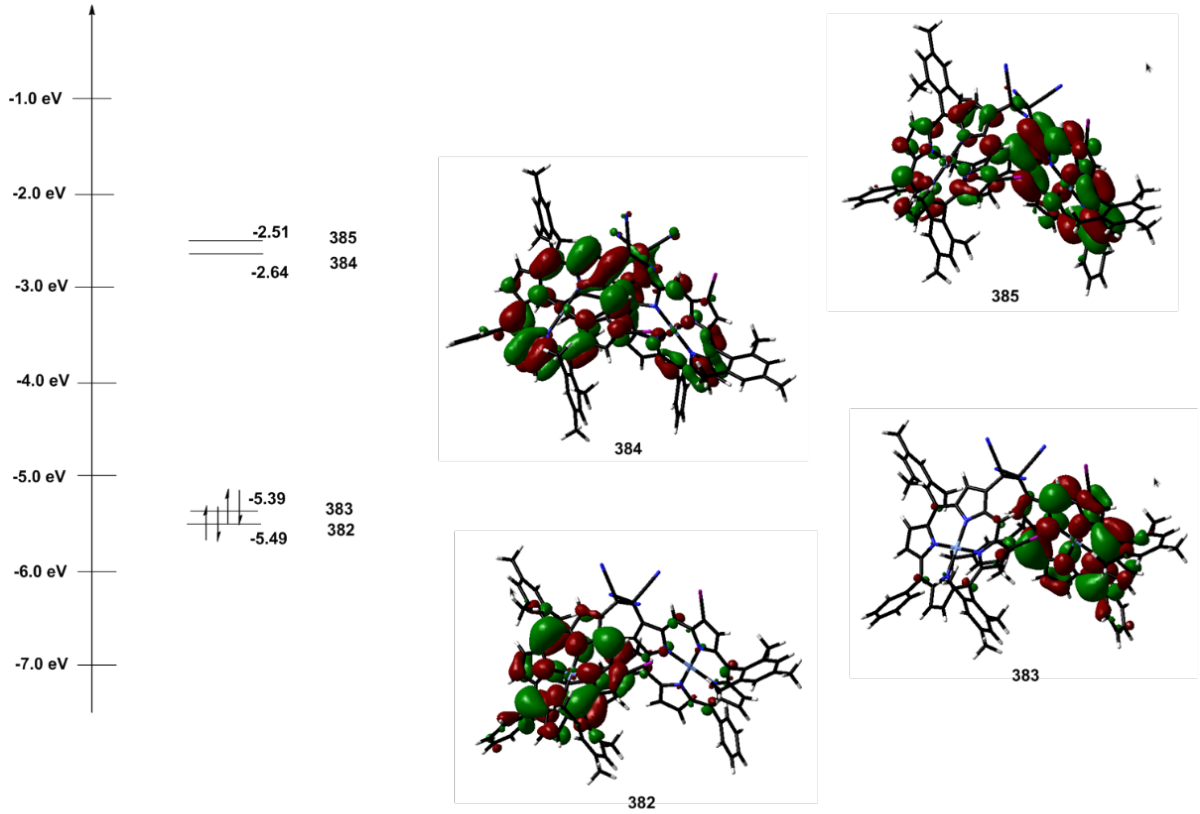

***Figure S85*:** Selected molecular orbitals of **(27)$_2$** calculated at UB3LYP/6-311G(d) .

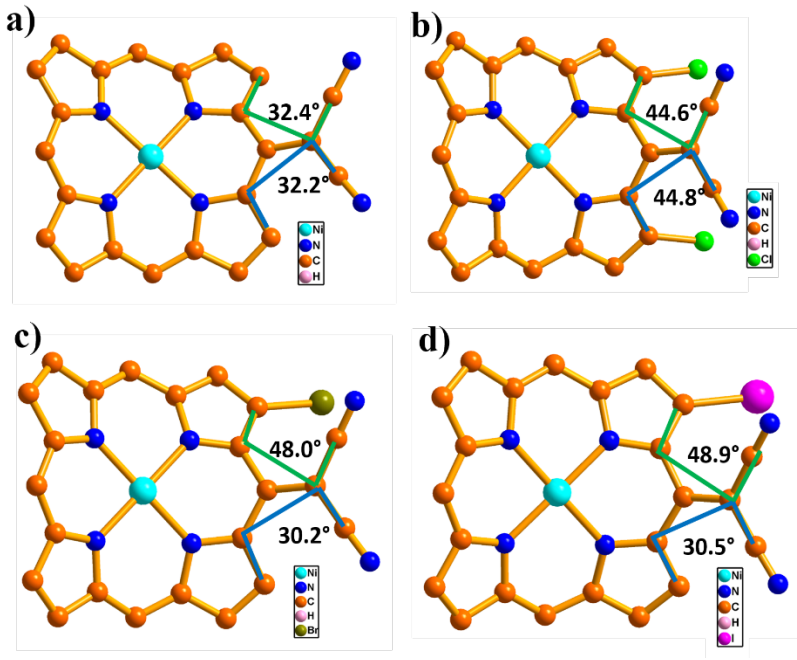

***Figure S86*:** Torsion angles of optimized structure of a) **12**, b) **13**, c) **14** and d) **15** (in deg.) calculated at UB3LYP/6-311G(d). The *meso*-aryl groups and the peripheral hydrogen atoms in a)-d) are omitted for clarity.

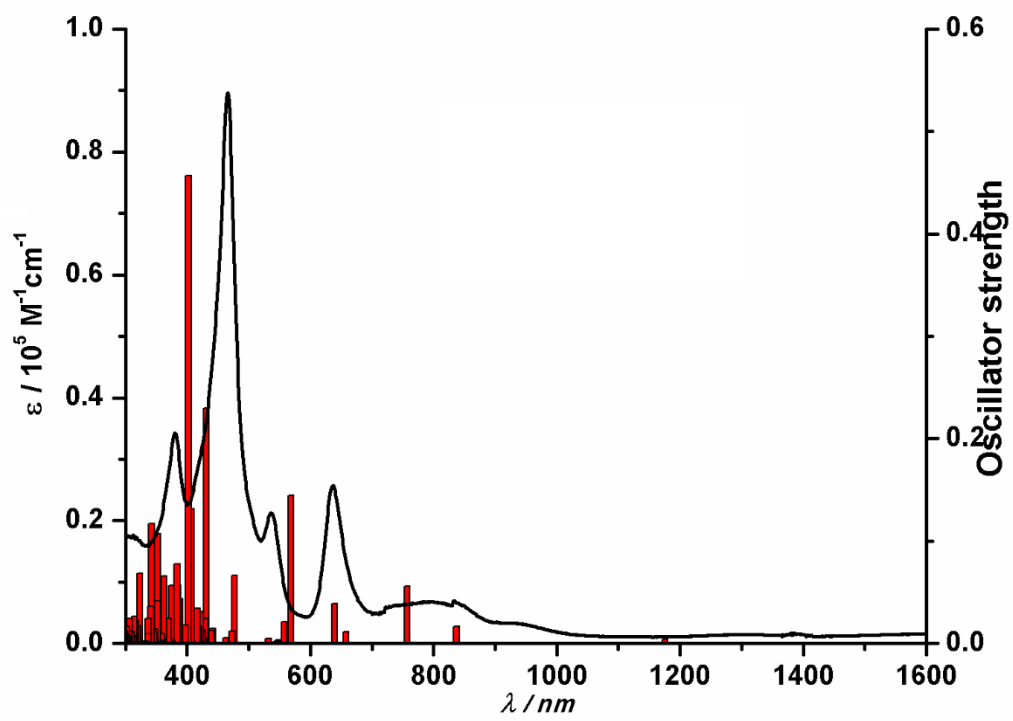

***Figure S87*:** The comparison between observed absorption spectrum in CH_2Cl_2 (line) of **12** *vs* calculated absorption spectrum on the basis of optimized structures (bar).

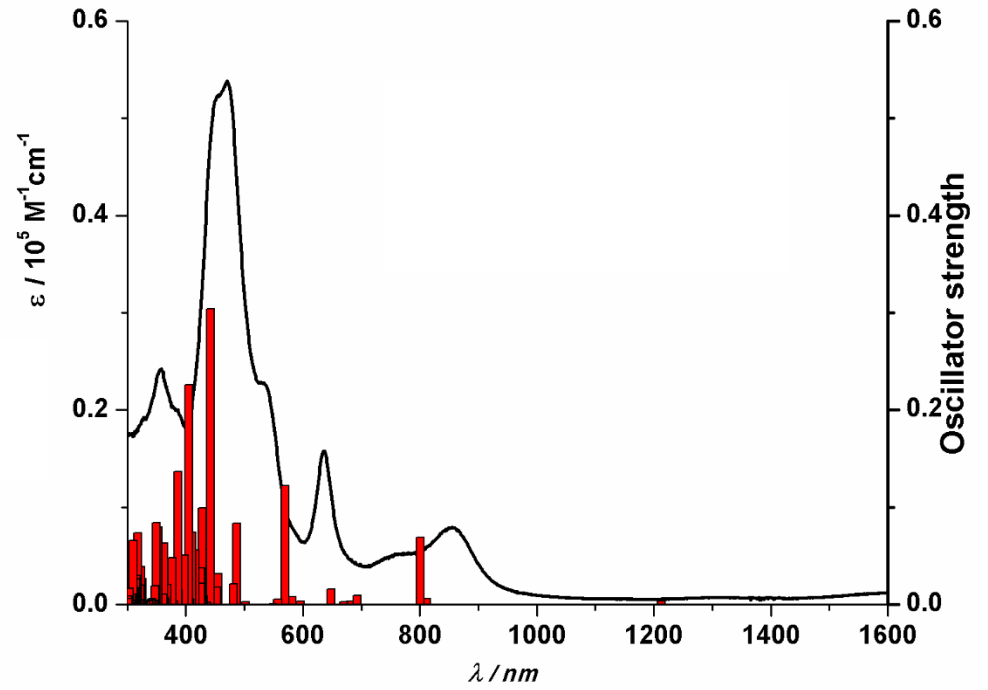

***Figure S88*:** The comparison between observed absorption spectrum in CH_2Cl_2 (line) of **13** *vs* calculated absorption spectrum on the basis of optimized structures (bar).

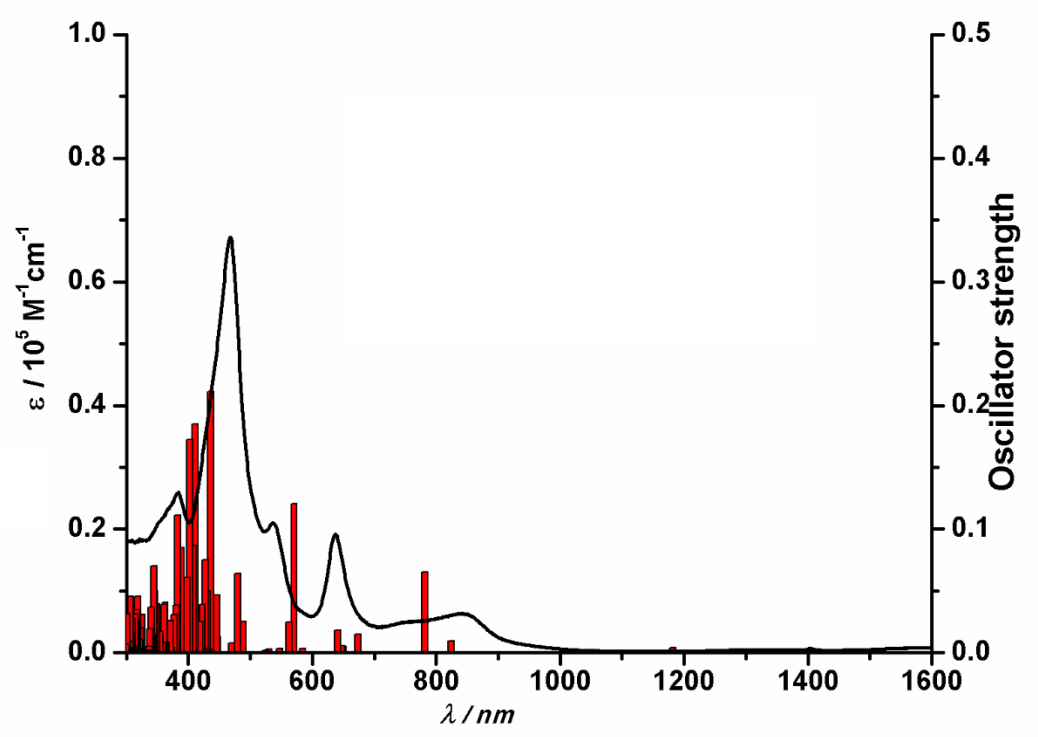

***Figure S89*:** The comparison between observed absorption spectrum in CH_2Cl_2 (line) of **14** *vs* calculated absorption spectrum on the basis of optimized structures (bar).

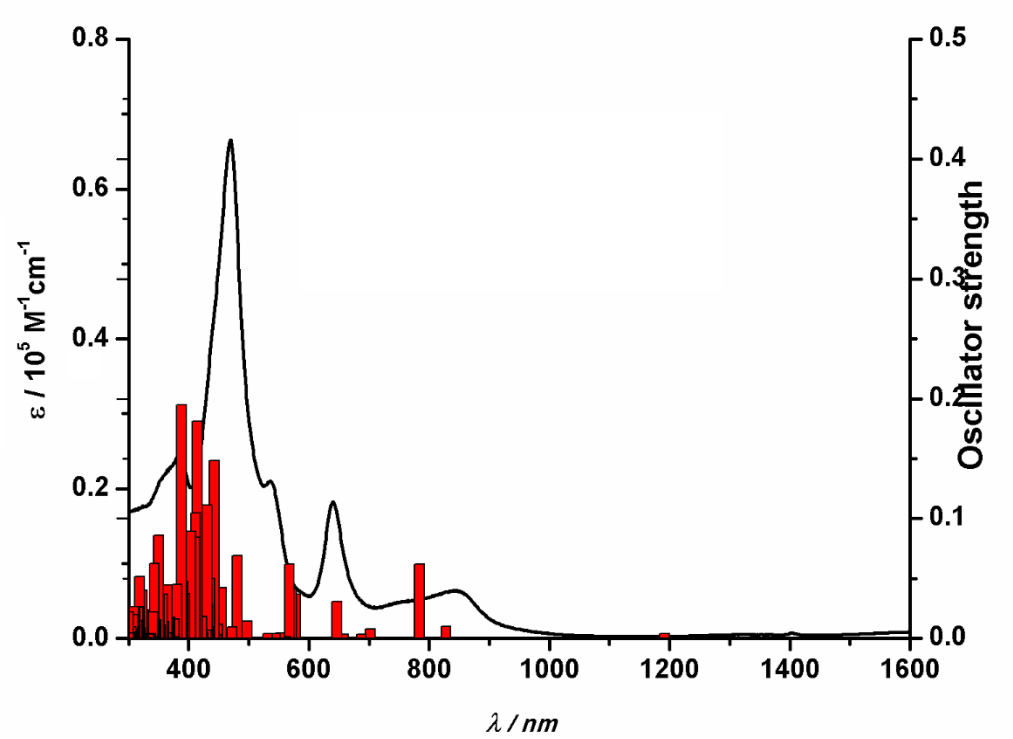

***Figure S90*:** The comparison between observed absorption spectrum in CH_2Cl_2 (line) of **15** *vs* calculated absorption spectrum on the basis of optimized structures (bar).

Supporting references:

S1. (a) Q. Chen, Y.-Z. Zhu, Q.-J. Fan, S.-C. Zhang, J.-Y. Zheng, *Org. Lett.,* 2014, **16**, 1590; (b) L.-M. Jin, L. Chen, J.-J. Yin, J.-M. Zhou, C.-C. Guo, Q.-Y. Chen, *J. Org. Chem.,* 2006, **71**, 527.

S2. (a) K. Fujimoto, H. Yorimitsu, A. Osuka, *Org. Lett.,* 2014, **16**, 972; (b) K.-i. Yamashita, S. Sakamoto, A. Suzuki, K.-i. Sugiura, *Chem. Asian J.,* 2016, **11**, 1004; (c) H. Hata, H. Shinokubo, A. Osuka, *J. Am. Chem. Soc.,* 2005, **127**, 8264; (d) N. Fukui, H. Yorimitsu, A. Osuka, *Angew. Chem. Int. Ed.,* 2015, **54**, 6311.

S3. (a) G. M. Sheldrick, *Acta Cryst. A,* 2008, **64**, 112; (b) G. M. Sheldrick, *Acta Cryst. C,* 2015, **71**, 3.

S4. Gaussian 09, Revision E.01, M. J. Frisch, G. W. Trucks, H. B. Schlegel, G. E. Scuseria, M. A. Robb, J. R. Cheeseman, G. Scalmani, V. Barone, G. A. Petersson, H. Nakatsuji, X. Li, M. Caricato, A. Marenich, J. Bloino, B. G. Janesko, R. Gomperts, B. Mennucci, H. P. Hratchian, J. V. Ortiz, A. F. Izmaylov, J. L. Sonnenberg, D. Williams-Young, F. Ding, F. Lipparini, F. Egidi, J. Goings, B. Peng, A. Petrone, T. Henderson, D. Ranasinghe, V. G. Zakrzewski, J. Gao, N. Rega, G. Zheng, W. Liang, M. Hada, M. Ehara, K. Toyota, R. Fukuda, J. Hasegawa, M. Ishida, T. Nakajima, Y. Honda, O. Kitao, H. Nakai, T. Vreven, K. Throssell, J. A. Montgomery, Jr., J. E. Peralta, F. Ogliaro, M.Bearpark, J. J. Heyd, E. Brothers, K. N. Kudin, V. N. Staroverov, T. Keith, R. Kobayashi, J. Normand, K. Raghavachari, A. Rendell, J. C. Burant, S. S. Iyengar, J. Tomasi, M. Cossi, J. M. Millam, M. Klene, C. Adamo, R. Cammi, J. W. Ochterski, R. L. Martin, K. Morokuma, O. Farkas, J. B. Foresman, and D. J. Fox, Gaussian, Inc., Wallingford CT, 2016.